# DESIGN AND IMPLEMENTATION OF A MICROCONTROLLER BASED MAXIMUM POWER POINT TRACKING SOLAR CHARGE CONTROLLER

By
MD. ROKONUZZAMAN
STUDENT NO./ID - 1013160025 (F)
SESSION: 2013-2014

**A Thesis Submitted in Partial Fulfillment of the Requirements for the Degree of**

MASTER OF SCIENCE IN ELECTRICAL, ELECTRONIC AND COMMUNICATION ENGINEERING



**Department of Electrical, Electronic and Communication Engineering**

**MILITARY INSTITUTE OF SCIENCE AND TECHNOLOGY**

**MIRPUR CANTONMENT, DHAKA-1216, BANGLADESH**
**DECEMBER 2016**

# APPROVAL CERTIFICATE

The thesis titled **"DESIGN AND IMPLEMENTATION OF A MICROCONTROLLER BASED MAXIMUM POWER POINT TRACKING SOLAR CHARGE CONTROLLER"** submitted by Md. Rokonuzzaman, Student no - 1013160025 (F), Session Oct/2013 has been accepted as satisfactory in partial fulfillment of the requirements for the degree of Master of Science in Electrical, Electronic and Communication Engineering on 29 December 2016.
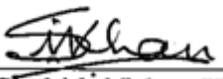
## BOARD OF EXAMINERS

1. _____

   Gp Capt Md Hossam-E-Haider, PhD, BAF
   Professor and Head
   Dept. of EECE, MIST, Dhaka - 1216

   Chairman
   (Supervisor)

2. _____

   Gp Capt Md Hossam-E-Haider, PhD, BAF
   Professor and Head
   Dept. of EECE, MIST, Dhaka - 1216

   Member
   (Ex-officio)

3. _____

   Maj Hussain Md. Abu Nyeem, PhD, EME
   Associate Professor
   Dept. of EECE, MIST, Dhaka - 1216

   Member

4. _____

   Dr. Shahidul Islam Khan
   Professor
   Dept. of EEE, BUET, Dhaka - 1000

   Member
   (External)

# CANDIDATE'S DECLARATION

I do hereby declare that this thesis is based on the results found by myself. Materials of work found by other researchers are mentioned in reference. This thesis, neither in whole nor in part, has been previously submitted elsewhere for the award of any degree or diploma.

Signature of the Candidate

_____

 Md. Rokonuzzaman

# DEDICATION

*To My Parents and Family*

# ACKNOWLEDGEMENT

# ABSTRACT

Photovoltaic (PV) system is one of the revolutionary renewable sources that are grabbing place rapidly instead of traditional energy sources. Industries are now designing solar roof, solar tree leaves, solar roadways, solar vehicles and even flexible solar cells for clothing. In the meantime, The International Energy Agency (IEA) reports that, last year, renewable overtook coal as the world's largest source of new power capacity. Yet, effective power generation or power extraction from renewable sources remain relatively low, and this must rise fast, as people transition to a more green and environment-friendly energy future. The demand or future work is looking for high efficiency, more reliable and low economical price of every components used in a PV system. PV charge controller (CC) is one of the most important parts of a PV system. CC circuit is used to extract the power of a solar panel during its less than optimum conditions. Under reduced incident solar radiation, due to the cloudy weather the low power level supplied by the solar cell normally would not be adequate to operating a load and charging up the storage or battery, but with the presence of the controller circuit, the low power generated by the solar panel would be accumulated to a high enough level to overcome the energy barrier of the battery or the load. In this research, a solar charge controller is designed based on Maximum Power Point Tracking (MPPT) technique. Microcontroller PIC 16F877A integrated circuit (IC) works as control unit, which reduced complexity in the number of electronic components and increased monitoring and regulative functions. The benefit of this charge controller is maximum power tracking capability from the solar panel, as well as customized programmable control unit, remote control and monitoring facility interfacing with smart phone or laptop applications, external device charging unit, Liquid Crystal Display (LCD) for displaying the system status including both of panel and battery voltage, current, power, charging state of battery in percentage and load status. Experimental results demonstrate that proposed MPPT charge controller increase 11% efficiency of 85W, 12V standalone PV systems. Estimated total cost of the CC is BDT 2047 (approximate USD 26).

# TABLE OF CONTENTS

# LIST OF FIGURES

# LIST OF TABLES

# LIST OF ABBREVIATIONS

| | |
|---|---|
| PV | Photovoltaic |
| SHS | Solar Home System |
| CC | Charge Controller |
| MPPT | Maximum Power Point Tracking |
| PWM | Pulse Width Modulation |
| LCD | Liquid Crystal Display |
| P&O | Perturb & Observe |
| INC | Incremental Conductance |
| CV | Constant Voltage |
| FLC | Fuzzy Logic Control |
| ANN | Artificial Neural Network |
| MPP | Maximum Power Point |
| Li-ion | Lithium-ion |
| LED | Light Emitting Diode |
| PIC | Peripheral Interface Controller |
| PCB | Printed Circuit Board |
| CC | Charge Controller |
| LVD | Low Voltage Disconnect |
| HVD | High Voltage Disconnect |
| SOC | State of Charge |
| IC | Integrated Circuit |
| CCM | Continuous Conduction Mode |
| DCM | Discontinuous Conduction Mode |
| ICD | In Circuit Debugger |
| A/D | Analog to Digital |
| $I^2C$ | Inter Integrated Circuit |
| USART | Universal Asynchronous Receiver Transmitter |
| LPF | Low Pass Filter |
| Wi-Fi | Wireless Fidelity |

| | |
|---|---|
| USB | Universal Serial Bus |
| MOSFET | Metal Oxide Semiconductor Field Effect Transistor |
| ESR | Equivalent Series Resistance |
| STC | Standard Test Condition |
| NOCT | Nominal Operating Cell Temperature |
| AGM | Absorbed Glass Mat |
| BDT | Bangladeshi Taka |
| USD | US Dollar |

# LIST OF SYMBOLS

$I_{sc}$    Current Source

$I_o$    Diode Saturation Current

m    Diode Ideality Constant

$V_T$    Thermal Voltage of Array

$N_s$    Cell Connected in Series

T    Temperature of PN Junction

K    Boltzmann Constant

q    Electron Charge

$R_S$    Equivalent Series Resistant of the Array

$R_p$    Equivalent Parallel Resistant of the Array

$i_{sa}$    Net Current

$V_{sa}$    Voltage Source

$V_{oc}$    Open Circuit Voltage

$i_L$    Inductor Current

$i_{L_{avg}}$    Average Inductor Current

$i_{L_{max}}$    Maximum Inductor Current

$i_{L_{min}}$    Minimum Inductor Current

$f_{pwm}$    Commutation Frequency

$i_c$    Capacitor Current

$M_V$    Voltage Factor

$\tau$    Time Constant

E    Internal Battery Voltage

$V_0$    Constant Voltage

# CHAPTER 1

# INTRODUCTION

## 1.1 Introduction

Photovoltaic (PV) system is one of the renewable energy resources that recently have become broader in energy sectors. The demand or future work is looking for high efficiency, more reliable and economical price PV charge controller which is come in portable size has become very popular in PV system. PV charge controller is very important in PV system. This thesis proposed a controller circuit that is used to extract the power of a solar cell during its less than optimum conditions. Under reduced incident solar radiation, due to the cloudy weather the low power level supplied by the solar cell normally would not be adequate to operating a load and charging up the storage or battery, but with the presence of the controller or power extractor circuit, the low power generated by the solar panel would be accumulated to a high enough level to overcome the energy barrier of the battery or the load. In this research work, a Photovoltaic (PV) Maximum Power Point Tracking (MPPT) charge controller is designed based on microcontroller PIC 16F877A, which reduced complexity in the number of electronic components and increased monitoring and regulative functions. This project used dc-dc buck converter circuit which has been simulated using software of MATLAB SIMULINK. Pulse width modulation (PWM) will be implemented on the PIC 16F877A to control duty cycle, voltage and current in the PV system and is programmed using software of microC. Bluetooth device is used to remote monitoring using smart phone or laptop apps. Liquid Crystal Display (LCD) is used to display the voltage and current from rechargeable battery. The benefit of this thesis is an improvement of efficiency depend on duty cycle and voltage change. Experimental results proof that proposed MPPT charge controller increase 11% efficiency of an 85 W, 12 V PV standalone systems and prevents high power level to component failure during the normal operation of the solar cell. This charge controller or power extractor circuit can also be used in other power sources to utilize the portion of power which normally would have been lost.

## 1.2 Background of the Thesis

Solar power is one of the clean and renewable sources of energy that have mass market appeal among the others being wind, geothermal steam, biomass, and hydroelectric etc. Solar power uses energy from the sun to provide passive heating, lighting, hot water, and active production of electricity through photovoltaic (PV) solar cells. PV's are the most promising of active solar power which directly convert sunlight into electricity. However, PV panels are very expensive, in terms of high production cost and low efficiency. Significant works have been done to improve the efficiency of the photovoltaic array. One of the earliest improvements is the addition of a battery. Without the battery, the photovoltaic array can supply electrical power directly to a load. The major drawback of this configuration is the uneven distribution of solar energy: during daylight operation, the photovoltaic array can produce excess power while during night time or periods of reduced sun light, there is no power supplied from the photovoltaic array. With the addition of a battery, the battery can be charged by the photovoltaic array during periods of excessive solar radiation, e.g. daylight, and the energy stored in the battery can then be used to supply electrical power during nighttime. The theorem known as the maximum power theorem (Jacobi's Law) states: "Maximum power is transferred when the internal resistance of the source equals the resistance of the load, when the external resistance can be varied, and the internal resistance is constant."

Single solar cell normally produces voltage and current much less than the typical requirement of a load. A photovoltaic cell typically provides $0.2 \sim 1.4$ V and $0.1 \sim 5$ A, depending on the photovoltaic cell and its operating conditions, e.g. direct sun light, cloudy, etc., while the load might need about $5 \sim 48$ V, $0.1 \sim 20$ A. Thus a number of photovoltaic cells are arranged in series to provide the needed voltage requirement, and arranged in parallel to provide the needed current requirement. These arrangements are critical since if there is a weak cell in the formation, the voltage or current will drop and the solar cell array will not be functioning properly. Thus for example, it is normal to see a photovoltaic array arranged for 17V to provide 12V to a battery. The additional 5V provides a safety margin for the variation in solar cell

manufacturing and solar cell operation, e.g. reduced sun light conditions. Since the current produced by these photovoltaic cell arrays is constant, in the best of lighting condition, the photovoltaic array loses efficiency due to the fixed voltage of the battery. Different techniques are available to reduce the losses, among the techniques Maximum Power Point tracking (MPPT) method performs better in this arena, where the PV voltage is tracked and converted it to the battery level voltage by a Buck-boost converter. This MPPT method can recover the 30% power loss and the power consumed by the MPPT circuitry is not excessive. Together with MPPT technique, various methods and circuits have been developed to improve the efficiency and applications of solar cell array. However, the basic assumption of all these methods and circuits is always that the photovoltaic array can produce at least the necessary power to operate the battery or the load. So far, no charge controller has been designed based on microcontroller to capture the power of a solar cell during the reduced sunlight conditions.

## 1.3 Literature Review

Renewable energy is generally defined as energy that comes from resources which are naturally replenished and regenerated after a regular time cycle. In its various forms, it derives directly from the sun, or from heat generated deep within the earth. Included in the definition is electricity and heat generated from solar, wind, ocean, hydro power, biomass, geothermal resources, and bio-fuels and hydrogen derived from renewable resources.

As people are much concerned with the fossil fuel exhaustion and the environmental problems caused by the conventional power generation, renewable energy sources are taking full concentration in this regards. And among them photovoltaic panels and wind-generators are now widely used. Photo voltaic (PV) sources are used today in many applications such as battery charging [1], lighting [2], water pumping [3], satellite power systems [4], irrigation etc. They have the advantage of being maintenance and pollution free but their main drawbacks are high fabrication cost, low energy conversion efficiency, and nonlinear characteristics. PV modules still

have relatively low conversion efficiency. High efficiency power trackers can be significantly improve the conversion efficiency which is designed to extract the maximum possible power from the PV module [5]. Energy extraction process from renewable sources like solar, wind, speed breaker [6] etc. has become more difficult. Some techniques are vastly used to extract energy from PV systems. Particularly, perturb and observe (P&O) [7], incremental conductance (INC) [8], constant voltage (CV) [9], short current pulse [10], fuzzy logic control (FLC) [11]-[12], artificial neural network (ANN) [13] and some other techniques [14] offer an efficient energy extraction process. Proposed controller has designed based on perturb & observe method. Different MPPT techniques have been developed and implemented [14]-[16]. Literature review evident that none of those have employed a microcontroller based MPPT technique. These proposed methods ensure a safe and fast battery charging process. Which can be significantly improved the system at the point of simplicity, highest efficiency and high flexibility. In short, real time measurements of panel open circuit voltage are used to detect the maximum power point of the solar panel.

Due to high energy densities and long life times, Lithium-ion (Li-ion) batteries are increasingly used in systems such as portable electronics, electric vehicles among others. The optimization designs of these batteries have been built in order to study its internal dynamics [17]-[19]. To minimize the cost of total system lead-acid battery is used. In this thesis a simple dynamic model based on capacitor/resistor networks is implemented in MATLAB SIMULINK environment in order to predict the charging time and optimize the use of the battery [20]. Battery charge rate is continuously adjusted in a way that the system operating point is forced near the detected maximum power point of the solar panel. Theoretical and experimental analyses are used to demonstrate the reliability and validity of the proposed technique.

## 1.4 Problem Statement

With the advancement of renewable energy, energy extraction process from renewable sources has not become more efficient. The efficiency of an energy

extraction process can further be improved considering the Current-Voltage (I-V) characteristic of a solar cell. I-V characteristic of a solar cell is nonlinear and varies with irradiation and temperature [14]-[16]. There is a unique point on the I-V or Power-Voltage (P-V) curve of the solar array called Maximum power point (MPP) at which the entire PV system operates with maximum efficiency and produces its maximum output power. When a PV array is directly connected to a load, the systems operating point will be at the intersection of the I-V curves of the PV array. However, under most conditions this operating point is not at the MPP [15]. Therefore it is desirable to ensure that the load line passes through the MPP to continuously deliver the maximum power to the output.

For example, a photovoltaic array rated 85 W, 19.7 V will have a maximum current of 85/19.7=4.31 A. During direct sunlight, the photovoltaic array produces 19.7 V and 4.31A, but since the battery is rated at 12V, the power transferred is only 12*4.31=51.78W, Power loss, 85W-51.78W=33.22W for a loss of about 39%. This is a significant power loss; however, it is not desirable to reduce the maximum possible voltage provided by the photovoltaic array because in the reduced sunlight condition, the current and voltage produced by the photovoltaic array will drop due to low electron generation, and thus might not able to charge the battery.

In order to reduce the power losses and improve the efficiency of the photovoltaic array, a method of Maximum Power Point Tracking (MPPT) is introduced where the voltage provided by the photovoltaic array is tracked and converted to the battery voltage by a DC-to-DC converter before the power is supplied to the battery. 30% power loss can recover utilizing these MPPT techniques. Most of the PV charge controller nowadays just uses LED to indicate the operating status of the rechargeable battery. It is hard to know the values of the rechargeable battery that have been used such as voltage, current and others. Besides most of PV charge controller is expensive depends on the total cost of PV system that has been used.

Literature review evident that none of those have employed a microcontroller based MPPT technique. These proposed methods ensure a safe and fast battery charging with different control and protection topologies. Which can be significantly improved the system at the point of simplicity, highest efficiency and high flexibility. In short, real time measurements of panel open circuit voltage are used to detect the maximum power point of the solar panel. Simulation has been executed with the MATLAB SIMULINK environment.

## 1.5 PV System and Charge Controller (CC)

Both rural and urban electrification through solar PV technology is becoming more popular day by day in the whole world. Every single PV system or stand-alone PV system is known as solar home systems (SHS). SHS are highly decentralized and particularly suitable for remote, inaccessible areas. Solar program mainly targets those areas, which have no access to conventional electricity and little chance of getting connected to the grid. SHS's can be used to light up homes, shops, fishing boats, high ways, office, school-colleges etc. It can also be used to charge cellular phones, run televisions (TV), radios and cassette players. SHSs have become increasingly popular among users because of offering an attractive alternative to conventional electricity. It also facilitates to avoid monthly bills, fuel cost, negligible repair and maintenance costs, easy installation at anywhere etc.

Globally SHS provide power to hundreds of thousands of households in remote locations where electrification by the grid is not feasible. SHS usually operate at a rated voltage of 12V DC or 24V DC. Provide power for low power DC appliances such as light, fan, radio and TV for about three to five hours a day. Furthermore appliances such as cables, switches, mounts, structural parts, power conditioners and inverters may also used. Inverter is used to invert 12V or 24V DC power to 240V AC power. A SHS typically includes one or more PV modules consisting of solar panels, a charge controller which distributes power and protects the batteries and appliances from damage and at least one battery to store energy for use when the sun is not shining. Fig. 1.1 shows a solar home system. Solar panel, battery and loads are

connected through the charge controller (CC). CC is an electronic device, used to control the operation of battery, load and solar panel of any PV system. PV modules produces energy from sunlight, CC extract this energy from panel and distribute to the load and store in the battery in most efficient and effective manner.
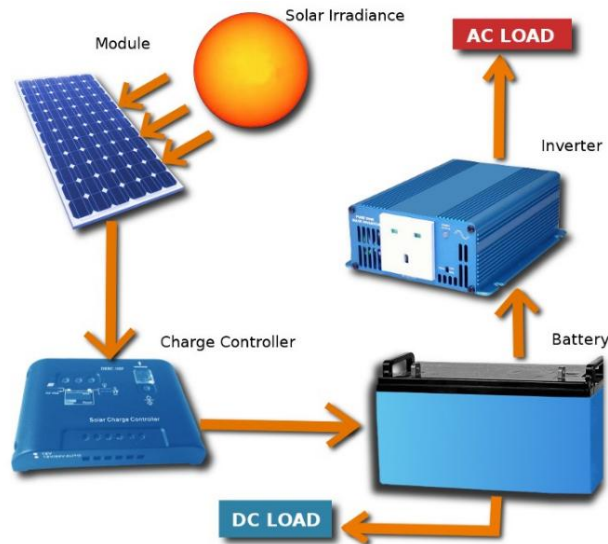


Fig. 1.1 A solar home system (SHS)

It is used to control the storage of electricity in the battery. This stored electricity can be used in later specially at night to for household purpose. Main function of charge controller is to prevent the battery from being overcharged. In addition, it can perform some other functions such as disconnecting the load at low voltage, giving indication to show state of charge, battery voltage, amount of current flowing, fault condition etc. Battery is used for back up of power. Inverter can be used to convert DC voltage to AC voltage.

## 1.6 Significance of this Thesis

Solar home system or standalone PV system come with a rechargeable battery, under the cloudy weather conditions that do not allow the solar cell array to produce adequate power to charge the battery. In this research, to extract maximum power in any types of weather condition, Microcontroller based MPPT charge controller has been designed. This controller can significantly reduce the power losses and improve 11% efficiency. In this proposed system of 85W, 12V PV system used for

performance test of the charge controller and theoretical losses of this standalone system is 39.08%, where using this controller circuit it has been reduced to 28.14%. The proposed study intends using the mathematical models and MATLAB SIMULINK environment to simulation in combination with experimental data to determine the maximum power extracting capability of the proposed controller of solar cells.

## 1.7 Scope of the Thesis

Solar charge controller is the heart of solar home system. Using low quality charge controllers greatly diminishes the efficiency of solar PV system. Infrastructure Development Company Limited (IDCOL) has specified some standards which should be followed by all the charge controller manufacturers. Technical appraisal and analysis of the available charge controllers in the market is highly necessary. In this thesis, a microcontroller based solar charge controller is designed that follow maximum power point tracking techniques (MPPT). MPPT techniques were well known for increasing the output of a solar panel. Using MPPT in the charge controllers is a great way of increasing the efficiency of solar home system. In this thesis, four MPPT algorithms were studied and modeled. Comparative analysis of their efficiency were made using MATLAB/SIMULINK.

## 1.8 Objective of the Thesis

The main goal of this thesis is to design a microcontroller based maximum power point tracker (MPPT) for off-grid standalone PV system, which is basically known as solar MPPT charge controller. Another purpose of this thesis is to develop an efficient controller circuit that can extract maximum power from Photovoltaic (PV) or solar panel. This will assist to recover power losses by increasing the efficiency with low price. Analyzing and evaluating the results of the experimental data with that from existing techniques, mathematical models and simulation packages used to validate the proposed charge controlling technique. Specific objectives of the thesis are:

a.  To design MPPT charge controller by using PIC microcontroller.

b.  To improve existing charge controller models including some additional features like data logging, external device charging unit, liquid crystal display (LCD) display for monitoring voltage and current status.

c.  To evaluate proposed design of charge controller both software and hardware performance test will validate for a complete PV system.

## 1.9 Outline of Methodology

A substantial number of literature/papers have been reviewed pertaining to different MPPT methods published for solar PV system. This review is intended to design and establish a MPPT technique base on microcontroller. Necessary experimental setup has been prepared in a laboratory of MIST. Key points of the proposed research are summarized below:

a.  A design layout including circuit diagram has developed for the proposed MPPT system followed by its implementation and performance analysis with necessary testing and developments. Thereby a prototype of solar charge controller have been developed and validated.

b.  Additionally, attractive features like, A LCD display will continuously show the system status. A charging unit for direct charging of smart phones or gadgets will be used. A Bluetooth module added, which could be helpful in getting data continuously from the PV system using a smart phone or laptop have been added to make the system smarter than existing controllers.

c.  A final version of the MPPT controller circuit designed on Printed Circuit Board (PCB) using Sprint-Layout and Proteus software utilizing experimented experience on prototype.

## 1.10  Organization of the Thesis

Chapter 1 gives a brief description of the total research work and basically is an introduction of the thesis. A typical solar home system and the role of charge controller are introduced. This chapter provides the background of the thesis,

objectives, scope of the research, problem statement, and brief evolution of charge controller and the thesis outline.

Chapter 2 deals with different features of a charge controller. Specifically charge controller design, switching mechanisms, different set points, operating characteristics are discussed in this chapter.

Chapter 3 presents a clear concept of solar charge controller. Description in details about the solar charge controller including the operating principle, classification, switching mechanisms and the different charge regulation set points are demonstrates well. Selection of a charge controller, PWM and MPPT techniques are also discussed.

Chapter 4 mainly focused on methodologies for the development of charge controller. Details on the progress of the simulation and hardware design are explained in this chapter. Full simulation has been executed by MATLAB SIMULINK environment.

Chapter 5 presents the experimental results obtained from the hardware and the limitation of the project. All discussions are concentrating on the field test result and performance of photovoltaic charge controller.

Chapter 6 includes the conclusion of the thesis. Obstacle faced and recommendation for future work also discussed in this chapter. Additionally, brief concept for industrialization is discussed here.

# CHAPTER 2

# PHOTOVOLTAIC SYSTEM

## 2.1 Introduction

Solar photovoltaic system are where the electricity gets generated, but are only one of the many parts in a complete photovoltaic (PV) system. In order for the generated electricity to be useful in a home or business, a number of other technologies must be in place. Sometimes, charge controllers are called as the brain of a PV system. Solar PV charge controllers, also known as solar charge regulators, are used in solar PV and wind energy systems to protect the battery from being overcharged and over-discharged. Either condition will damage a lead acid battery. The controller is a very important part of any energy system, as the latest technologies are equipped with some highly effective battery charging routines. An advanced charging routine ensures that the battery is charged as quickly as possible whilst ensuring the battery is not damaged by overcharging. The charge controller can also provide charging information to the user, often using a small digital display. Some units record the charging data over time and many offer a variety of electrical protection features such as surge protection.

## 2.2 Photovoltaic (PV) System

A PV system consists of four subsystems, each with its own function. These four subsystems are connected in accordance with the block diagram presented in Fig. 2.1. The first subsystem is a solar panel, consists of one polycrystalline PV module from KYOCERA, Module Products SM-85KSM. This PV module has a rated power of 85 Watt and is formed by 36 photovoltaic cells connected in series. The Charger Unit is the second subsystem includes a DC/DC converter controlled by a Pulse width modulation (PWM) signal. DC/DC converter is formed by two switches and an input and output filter. PWM signal is computed from the control unit, programmed in Micro C on PlC16F877A micro controller. The control unit is third subsystem of the proposed system consists of one Programmable Interface Circuit or Peripheral

Interface Controller (PIC) microcontroller, model PlC16F877A, and an Integrated Circuit (IC) SG3524. PIC microcontroller is a high performance 8-bit Reduced Instruction Set Code (RISC) architecture, operates from 2V to 5.5V belonging to 40 pins family and IC is a 16 pin PWM switching regulator circuit. The fourth subsystem consists of a rechargeable 12 Volt, 100Ah Lead-acid battery.
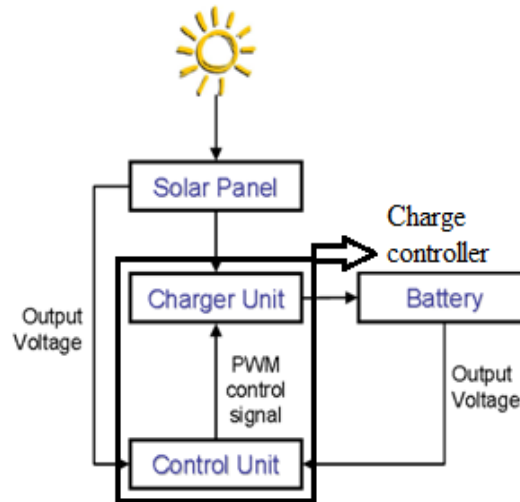


Fig. 2.1 Block diagram of standalone PV system.

## 2.3 Classifications of PV System

Photovoltaic power systems are generally classified according to their functional and operational requirements, their component configurations, and how the equipment is connected to other power sources and electrical loads [21]. There are four different configurations of PV system. These are:

a. Standalone or off-grid,
b. Grid-tie or on-grid,
c. Grid-tie with power backup or grid interactive and
d. Grid fallback.

### 2.3.1 Standalone or Off-grid

An off-grid or standalone PV system is not connected to the utility grid. These systems will generally have a battery bank in order to store the electricity for use when needed. Worldwide, stand-alone solar PV installations are the most popular

type of solar installation there is. It is what solar PV was originally created for to provide power at a location where there is no other source easily available. Whether it is powering a shed light, providing power for a pocket calculator or powering a complete off-grid home, stand-alone systems fundamentally all work in the same way, the solar panel generates power, the energy is stored in a battery and then used as required. In general, stand-alone systems are comparatively small systems, typically with a peak power generation of less than one kilowatt.
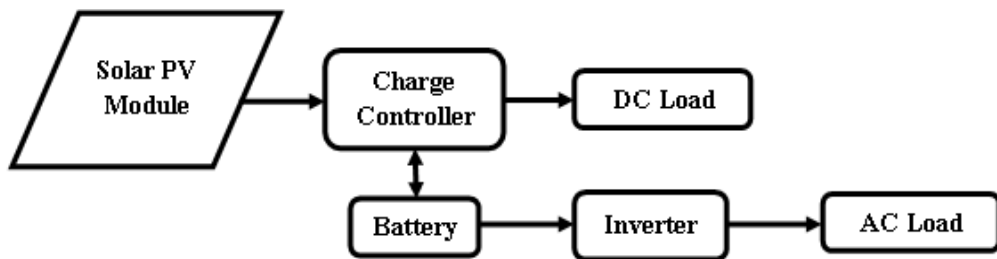
Fig. 2.2 Block diagram of standalone PV system

### 2.3.2 Grid-tie

Grid-tied solar electric systems connect directly into the electricity grid. When the sun is shining during the day, excess electricity feeds into the grid. During the evening and night, when the solar panels are not providing sufficient power, electricity is taken from the grid as required.
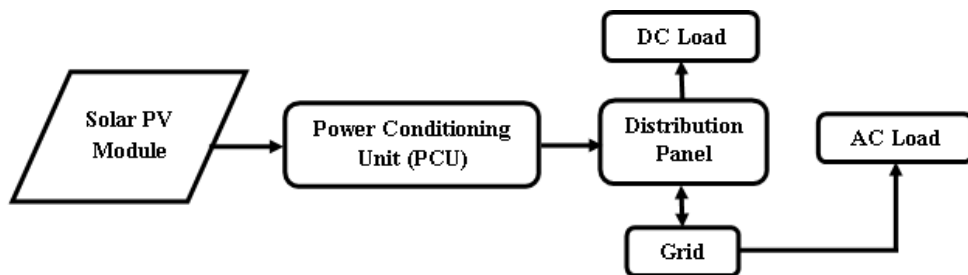
Fig. 2.3  Block diagram of grid-tie PV system

### 2.3.3  Grid-tie with Power Backup or Grid Interactive

Grid-tie with power backup also known as a grid interactive system combines a grid-tie installation with a bank of batteries. The cost of a grid-tie system with power backup is higher than a standard grid-tie system, because of the additional cost of

batteries and battery controllers. Typically, having power backup will add 12~20% of additional costs over a standard grid-tie system.

### 2.3.4 Grid Fallback

Grid fallback is a lesser-known system that makes a lot of sense for smaller household solar power systems. With a grid fallback system, the solar array generates power, which in turn charges a battery bank. Energy is taken from the battery and run through an inverter to power one or more circuits from the distribution panel in the house. When the batteries run flat, the system automatically switches back to the grid power supply. The solar array then recharges the batteries and the system switches back to solar power [21].

### 2.3.5 Grid-tie and Standalone Systems

Generally, standalone and smaller grid fallback systems run at low voltages, typically between 12 and 48 volts. This is because batteries are low-voltage units and so building a stand-alone system at a low voltage is a simple, flexible and safe approach. Grid-tie systems tend to be larger installations, often generating several kilowatts of electricity each hour. As the electricity is required as a high-voltage supply, it is more efficient to connect multiple solar panels together to produce a high voltage circuit, rather than use an inverter to step up the voltage. This high-voltage DC power is then converted into an AC current by a suitable grid-tie inverter.

Grid-tie systems either link multiple solar panels together to produce a solar array voltage of several hundred volts before running to the inverter, or have a small inverter connected to each solar panel to create a high-voltage AC supply from each panel. The benefit of this high voltage is efficiency. There is less power loss running high-voltage, low-current electricity through cables from the solar array. For standalone battery-based systems, low-voltage is the best solution, as the battery banks tend to work better as low-voltage energy stores. For grid-tie systems where the energy is not being stored in a battery bank, the higher-voltage systems are the best solution.

## 2.4 Photovoltaic Cells and PV Panels

The heart of a solar electric system is the solar cells itself. A PV module or solar panel is a packaged, connect assembly of typically 6×10 solar cells. There are various types of solar panel. Solar panel generates electricity from the sunlight. PV cell receives light from the sun and directly converts it to energy. The PV cell is nonlinear power source whereas most sources of electrical power are constant voltage sources, such as a battery, a PV cell is a constant current source. The PV cell only displays this constant current characteristic up to a limiting voltage where the current collapses. For an ideal PV module the voltage where the current collapses would be at the open circuit voltage, $V_{oc}$.

In reality the I-V characteristics for a PV cell do not look like Fig. 2.4 but exhibit the following characteristics shown in Fig. 2.5. The slight current drop between points M and A is a result of some of the current passing through the internal resistance of the PV cell. Between points A and S the load resistance increases forcing some of the current to flow through the diode resulting in the fast drop in current to the load. This continues until point *S* where all the current flows through the diode and the internal resistance.
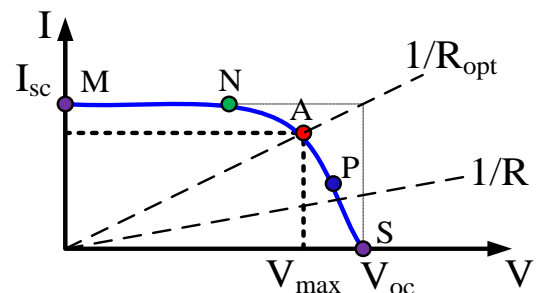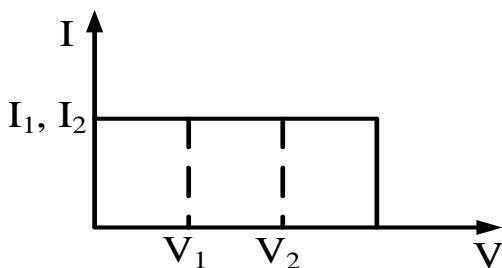


Fig. 2.4 Ideal I-V Curve for a PV cell        Fig. 2.5 Typical current-voltage (I-V) curve

Where the PV operates on this I-V curve is greatly determined by the insolation, array voltage, cell temperature and the load connected to the array. Altering the amount of sun light that is available to the PV module the current that the module can produce is also altered [22]. The current and power output of the used solar panel is approximately proportional to illumination intensity (irradiance). At a given

intensity, the module voltage is determined by the characteristics of the load. The effect of temperature on the current of a PV cell is only small. By increasing the temperature a slightly higher current is produced, however this increase in temperature has a negative effect on the cell voltage [23]. Increasing the temperature forces the diode to conduct at a lower voltage therefore reducing the PV voltage where the curve collapses and greatly reducing the output power. The effect of varying the load on the PV operating point can be explained using ohms law:

$$I = \frac{V}{R} \tag{2.1}$$

Fig. 2.5 shows the load lines for different load resistances. The slopes of these load lines are given by $1/R$. So, lower resistances result in steeper load lines and higher resistances result in flatter load lines. The operating point of the PV connected to these loads is restricted to the intersection of the load line and I-V curve. Therefore for a given irradiance there is only one load resistance that will produce maximum power and if the irradiance changes then the resistance required for operation at MPP also changes. The irradiance is not constant and will change throughout the day therefore maximum power point trackers are needed to match the operating point to the load resistance.
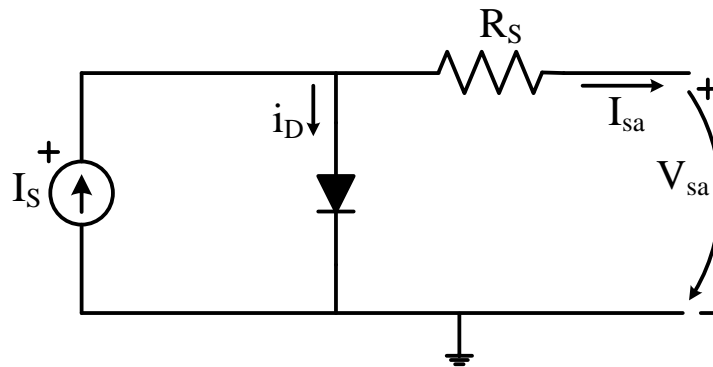


Fig. 2.6 Solar cell electrical equivalent model

## 2.5 Electric Model of Photovoltaic Cell

During darkness, the solar cell is not an active device, it works like a normal diode, i.e. a p-n junction. It produces neither a current nor a voltage. However, if it is connected to an external supply current $I_S$ , diode current, $I_D$ will be present. A solar

cell is usually represented by an electrical equivalent one-diode model with a series resistance, $R_S$ as shown in Fig. 2.6. The model contains a current source $I_s$, one diode and a resistor $R_S$. The net current is the Difference between the photocurrent $I_{sc}$ and the normal diode current $I_D$. The diode current is given as

$$I_D = I_0 \times \left[ e^{\frac{V_{sa} + (R_S \times i_{sa})}{mV_T}} - 1 \right] \tag{2.2}$$

Where,

$I_{sc} = Current\ Source$

$I_o = Diode\ saturation\ current$

$m = Diode\ ideality\ constant$

And,

$$V_T = \frac{N_s KT}{q} = Thermal\ voltage\ of\ array \tag{2.3}$$

Where,

$N_s = Cell\ connected\ in\ series$

$K = Boltzman\ constant = 1.38 \times 10^{-23}\ J/K$

$T = Temparature\ of\ the\ pn\ junction = 0°C = 273.16\ K$

$q = Electron\ charge = 1.6 \times 10^{-19}\ C$

$R_S = Equivalent\ series\ resistance\ of\ the\ array$

$R_p = Equivalent\ parallel\ resistance\ of\ the\ array$

The net current, $i_{sa}$ is given as

$$i_{sa} = I_s - I_0 \times \left[ e^{\frac{V_{sa} + (R_S \times i_{sa})}{mV_T}} - 1 \right] \tag{2.4}$$

Taking into account the model for a single solar cell, it is possible to determine the *I-V* characteristic of *M* cells in parallel and *N* cells in series:

$$V_{sa} = \gamma \times V_T \times ln\left[ \frac{I_s - i_{sa}}{M \times I_0} + 1 \right] - (R_s \times i_{sa}) \tag{2.5}$$

Where,

$\gamma = m \times N$. For the used solar panel *M* = 1, *N* = 36 and it is assumed *m* = 1.

In short, a real solar cell can be characterized by the following fundamental parameters:

**Short circuit current,** $I_{sc}$ is the greatest value of the current generated by a cell. It is produced under short circuit conditions: $V_{sa} = 0$

**Open Circuit Voltage,** $V_{oc}$ Corresponds to the voltage drop across the diode (p-n junction) when it is traversed by the photocurrent $I_s$, namely when the generated current is $i_{sa} = 0$. It can be mathematically expressed as:

$$V_{oc} = \gamma \times V_T \times ln\left[\frac{I_s}{M \times I_0} + 1\right] \qquad (2.6)$$

**Table 2.1 Electrical Specifications SM-85KSM**

| Parameter | Rating |
|---|---|
| Maximum power | 85W |
| Maximum voltage | 17.35V |
| Maximum current | 5.20A |
| Open circuit voltage, $V_{oc}$ | 19.7V |
| Short circuit current, $I_{sc}$ | 5.90A |
| Operating temperature | -40 $°C$ to +85 $°C$ |

**Maximum Power Point** – is the operating point A in Fig. 2.5, at which the power dissipated in the resistive load is maximum. Therefore for a given irradiance there is only one load resistance that will produce maximum power. From the datasheet of used solar module products KYOCERA: SM-85KSM, main characteristics are shown in Table 2.1.
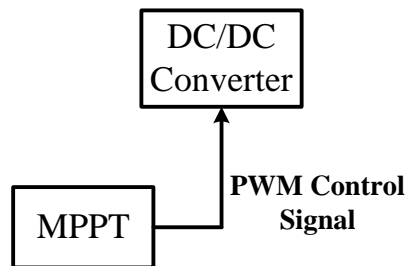


Fig. 2.7 Block diagram of the charging unit

## 2.6 Charger Unit

The charger unit is a global block that includes the Maximum Power Point Tracking allied to a DC/DC converter with buck-boost topology. Fig. 2.7 illustrates a general description of the charging unit block.

## 2.7 DC/DC Converter

A DC/DC converter consists of a number of storage elements and switches that are connected in a topology such that the periodic switching controls the dynamic transfer of power from the input to the output, in order to produce the desired DC conversion. The storage elements are connected in such a way that they form a low pass filter to yield low output ripple voltage. In the designed system, there is also an input storage element that will allow the input ripple voltage to be less than 3%. The two fundamental topologies of DC/DC converters are the buck and the boost converter. There are many other topologies, most of which are derived from either the buck or the boost. The purpose of the DC/DC converter is to transform a DC voltage from one level to another. This is done by varying the duty cycle, $\delta$. The duty cycle is defined as the ratio of the "ON" duration to the switching time period. By varying $\delta$ the width of the pulses is varied and the concept of pulse width modulation (PWM) is realized. DC/DC converters have two distinct operating modes, Continuous Conduction Mode (CCM) and Discontinuous Conduction Mode (DCM). The converter can operate in either of these modes and each mode has significantly different characteristics. The DC/DC converter serves the purpose of transferring power from the solar PV module to the load and acts as an interface between the load and the module. On this thesis the DC/DC converter is always working in CCM.
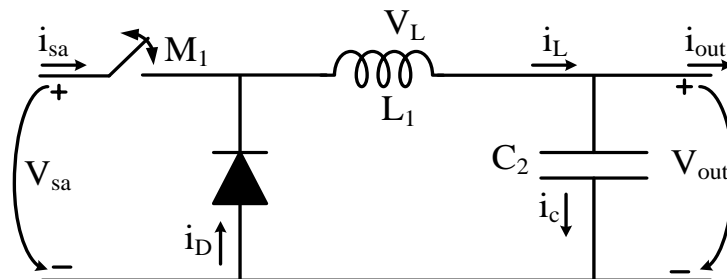


Fig. 2.8 Electrical model – DC/DC converter (buck topology)

## 2.7.1 Converter Topology

The ideal buck converter has the basic five components, namely a power semiconductor switch, a diode, an inductor, a capacitor and a PWM controller. The buck converter topology is shown in Fig. 2.8.

## 2.7.2 Theory of Operation

The DC/DC converter will connect or disconnect conveniently the solar panel from the battery based on PWM signals. Taking in account the idealized buck converter shown in Fig. 2.8 and in order to simplify the results shown bellow, it is assumed that input voltage $V_{sa}$ is ripple free. The capacitor $C_2$ is assumed to be large enough such that $V_{out}$ has a ripple of less than 3% and therefore essentially ripples free. Current $i_{out}$ is also assumed to be ripple free. Assuming continuous conduction (e.g. $i_L$ is always greater than zero), the circuit has two topologies. One topology is switch $M_1$ closed and another is switch $M_1$ open.
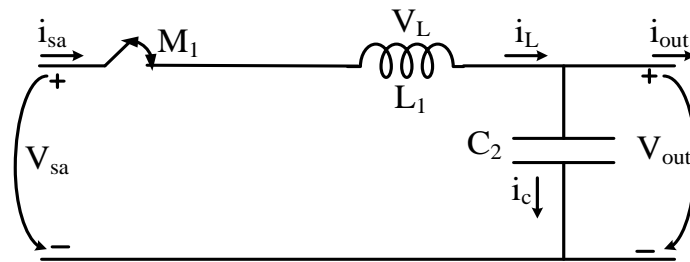


a) Switch M1 closed
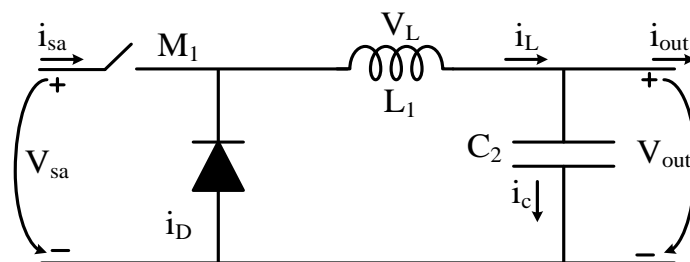


b) Switch M1 open

Fig. 2.9 Switch operation – DC/DC converter

These steady states are shown in Fig. 2.9. In Fig. 2.9 (a), when switch $M_1$ is closed, the power of the voltage source $V_{sa}$ is delivered to the load through inductor $L_1$. The diode is reverse biased and opens, and the current $i_L$ increases at the rate of equation 2.7.

$$\frac{di_L}{dt} = \frac{V_L}{L_1} = \frac{V_{sa} - V_{out}}{L_1}, \qquad 0 \le t \le \delta T \tag{2.7}$$

In this case the inductor $L_1$ is charging. In Fig. 2.9 (b), when the switch is open, current $i_L$ continues to circulate through the diode, and this component is forward biased, and $i_L$ decreases at the rate of equation 2.8, and the inductor $L_1$ is discharging.

$$\frac{di_L}{dt} = \frac{V_L}{L_1} = \frac{-V_{out}}{L_1}, \qquad \delta T \le t \le T \tag{2.8}$$

If the parameters of the circuit are well dimensioned such that the current $i_L$ does not go to complete zero, the diode remains in conduction until the switch closes and the diode is reverse biased and opens. Due to the steady state inductor principle, the average voltage $V_L$ across $L_1$ is zero. Since $V_L$ have two states, both having constant voltage, the average value is given as

Therefore,

$$Vout = \frac{1}{T} \int_0^T Vout(t)dt = \frac{1}{T} \int_0^{\delta T} Vsa(t) = Vsa\delta \tag{2.9}$$

$$Vout = Vsa\delta \tag{2.10}$$

This relationship is very important because describes the operation of the buck converter. $\delta$, is the duty cycle and varies between 1 and 0. Therefore the output voltage will always be less then the input voltage.

### 2.7.3   Sizing of the Output Filter

Equations 2.7 and 2.8 give the rate of rise and fall for current $i_L$. The average value of $i_L$ is found by examining the node at the top of capacitor in Fig. 2.8. Applying

Kirchoffs Current Law (KCL) in the average sense, and recognizing that the average current through a capacitor operating state is zero, it is obvious that:

$$i_{Lav} = i_{out} \tag{2.11}$$

Equations 2.7, 2.8 and 2.11 provide the necessary information to draw a graph of current $i_L$, as shown in Fig. 2.10.
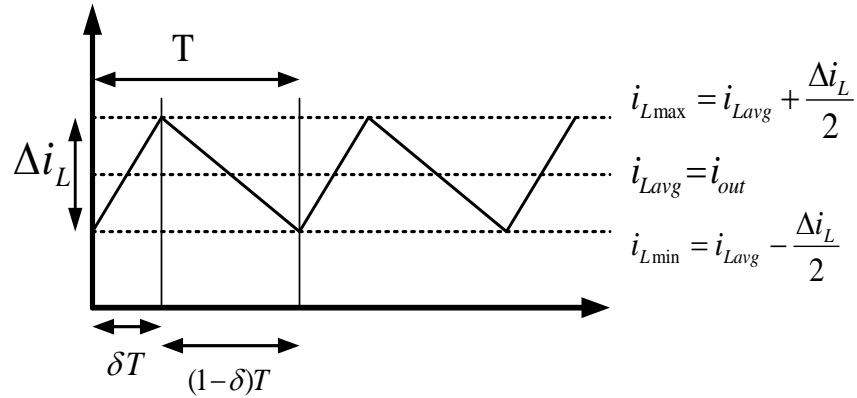


Fig. 2.10 Inductor Current Waveform of Output Filter

### 2.7.4  Value of the Inductor, L

Since the inductor current consists on straight line segments, it is possible to write the following expression:

$$\begin{cases} i_{L_{avg}} = \frac{i_{Lmax} + i_{Lmin}}{2}, \\ i_{L_{max}} = i_{L_{avg}} + \frac{\Delta i_L}{2} \\ i_{L_{min}} = I_{L_{avg}} - \frac{\Delta i_L}{2} \end{cases} \tag{2.12}$$

From equation 2.7 we have

$$\frac{di_L}{dt} = \frac{V_{sa} - V_{out}}{L_1} = \frac{\Delta i_L}{\delta T} \tag{2.13}$$

So that,

$$\Delta i_L = \frac{V_{sa} - V_{out}}{L_1} \times \delta T = \frac{V_{sa} - \delta V_{sa}}{L_1} \times \delta T = \frac{V_{sa}\delta(1-\delta)}{L_1 f_{pwm}} \tag{2.14}$$

Where,

$f_{pwm}$ is the commutation frequency. In the limit of the CCM,

$$\Delta i_L = 2i_{L_{avg}} = 2i_{out},$$

$$\frac{V_{out}}{L_{max}}(1-\delta)T = 2i_{out} \iff L_{max} = \frac{V_{out}\ (1-\delta)}{2i_{out}\ \times f_{pwm}} \qquad (2.15)$$

The maximum value occurs when, $\rightarrow 0$. Therefore

$$L_{max} > \frac{V_{out}}{2i_{out}\ \times f_{pwm}} \qquad (2.16)$$

This guarantees a continuous conduction for any value of duty cycle. $V_{out}$ and $i_{out}$ are the converter output voltage and current at the maximum input power and $f_{pwm}$ is the switching frequency.
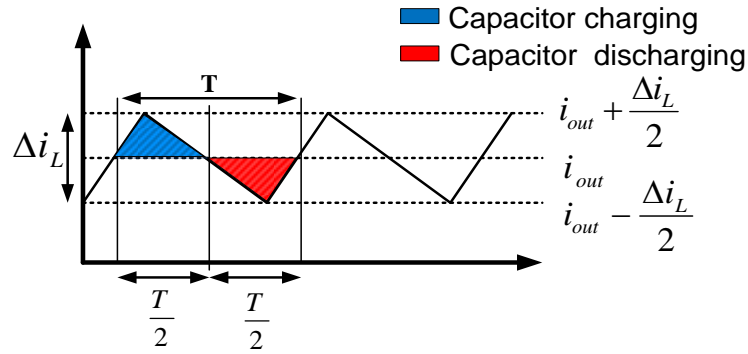


Fig. 2.11 Inductor current waveform used to illustrate capacitor charging

### 2.7.5  Value of the Capacitor, C

The capacitor current, $i_c$ is given by the difference between the current in the inductor and the load current $i_{out}$ as

$$i_c = i_L - i_{out} \qquad (2.17)$$

Looking at Fig. 2.11, it can be seen that each charging and discharging process is given by an equal area where it spends half of the period value $\left(\frac{T}{2}\right)$, and where each area represents a charge increment $\Delta Q$ of the capacitor.

$\Delta V$ is the output ripple voltage and the relation can express as

$$V = \frac{\Delta Q}{C} \qquad (2.18)$$

From Fig. 2.11 we have

$$\Delta V = \frac{\Delta Q}{C} = \frac{1}{C} \times \frac{1}{2} \times \frac{T}{2} \times \frac{\Delta i_L}{2} = \frac{T \times \Delta i_L}{8 \times C} \qquad (2.19)$$

In the worst case, $\Delta i_L = 2 \times i_{out}$ and therefore

$$C_2 = \frac{i_{out}}{4 \times \Delta V \times f_{pwm}} \qquad (2.20)$$

Where,

$i_{out}$ = converter output current at maximum input power,

$\Delta V$ = voltage ripple and

$f_{pwm}$ = switching frequency.

## 2.8 Maximum Voltage Output for Duty Cycle Ratio Control

Less usual in the literature is the buck topology on Fig. 2.12. It is intended to minimize the voltage ripple $V_{sa}$, similar to voltage $v_{c1}$, since voltage $V_{out}$ is supposed to be constant. Fig. 2.12 presents the case where the load is a battery or a resistor-capacitor (R-C) network with ripple free.
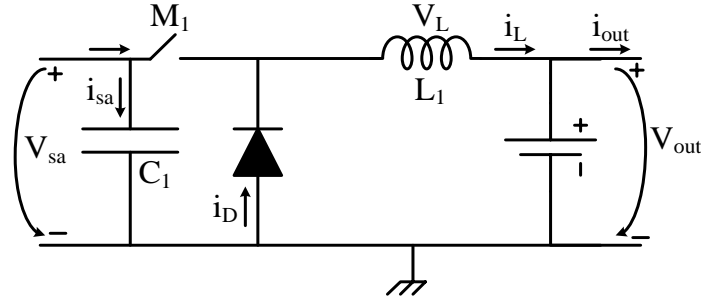


Fig. 2.12 Switching operation of DC/DC converter

When switch $M_1$ is closed, the diode is reverse biased and it can be written as

$$\frac{di_L}{dt} = \frac{V_L}{L} = \frac{V_{sa} - V_{out}}{L}, \qquad 0 \leq t \leq \delta T \qquad (2.21)$$

$$\frac{dv_{c1}}{dt} = \frac{i_{in} - i_L}{C_1}, \qquad 0 \leq t \leq \delta T \qquad (2.22)$$

When switch $M_1$ is open, current $i_L$ continues to circulate through the diode and capacitor being charged by current $i_{in}$. Now, equation 2.21 and 2.22 can be rewrite as

$$\frac{di_L}{dt} = \frac{V_L}{L} = \frac{-V_{out}}{L}, \qquad \delta T \leq t \leq T \qquad (2.23)$$

$$\frac{dv_{c1}}{dt} = \frac{i_{in}}{C_1}, \qquad\qquad \delta T \leq t \leq T \qquad\qquad (2.24)$$

Assuming that all currents and voltages across the circuit are ripple free, when compared to the respective average values and due to the condition of permanent state applied to inductor $L_1$ and capacitor $C_1$, then

$$(V_{sa} - V_{out})\delta T - V_{out}(1 - \delta)T = 0 \rightarrow v_{outavg} = \delta v_{saavg} \qquad (2.25)$$

$$(i_{in} - i_L)\delta T + i_{in}(1 - \delta)T = 0 \rightarrow i_{Lavg} = \frac{i_{inavg}}{\delta} \qquad (2.26)$$

In the same conditions it is possible to see that the ripple voltage for capacitor $C_1$, when it is being charging by the current $i_{in}$.

$$\Delta C_{C1} = C_1 i_{in}(1 - \delta)T \qquad (2.27)$$

The previous deductions keep their validity even for cases where less restrictive conditions are stated. Fig. 2.13 presents the inductor current waveform where is represented the current ripple.
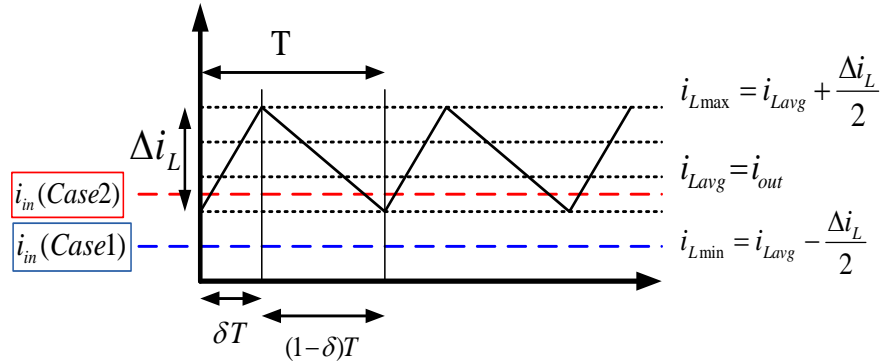


Fig. 2.13 Inductor current waveform

Current $i_{in}$ is presented in two different situations. In the first situation $i_{in}$ (blue dash line) is always lower than $i_L$ and secondly (red dash line), although is average value is still lower than the average value of $i_L$, this behaviour is not constantly identified for all the period of time $\delta T$. In the first case equation 2.26 is still valid. In the second case the process is not equal. On the last situation, the capacitor charging process happens not only on the period of time $(1 - \delta)T$ but also partially in $\delta T$. This

behaviour is not compatible with the duty cycle ratio control that is implemented. In the limit, for the duty cycle control:

$$\Delta i_L = 2\left(i_{Lavg} - i_{in}\right) \tag{2.28}$$

Replacing equation 2.28 in equation 2.21 and taking into account equation 2.25 and equation 2.26 it is possible to write the maximum value for voltage $V_{out}$ that allows the circuit to be in permanent control.

$$V_{out} = \sqrt{2 \times i_{in} \times V_{sa} \times L_1 \times f_{pwm}} \tag{2.29}$$

Where,

$i_{in} = Input\ current$

$V_{sa} = Input\ voltage$

$L_1 = Inductance$

$f_{pwm} = Switching\ frequency$

## 2.9 Maximum Power Point Tracking (MPPT)

A Maximum Power Point Tracker is an electronic DC/DC converter that optimizes the match between the PV module and the load. Maximum Power Point trackers maximize the PV module output power despite of the ambient temperature and insulation levels. As seen in the I-V curve of typical PV modules in Fig. 2.5 there is a single maximum of power. This means that there is a peak power corresponding to a particular voltage and current. Knowing that efficiency of the solar panel is low it is desirable to operate the module at the peak power point so that the maximum power can be delivered to the load. There are several studies of MPPT techniques such as the perturbation and observation, the constant current method, the constant voltage method and the incremental conductance method [24] - [25]. Due to the non-linear I-V characteristics of a PV cell, a different maximum power point can be found for each irradiance condition on the solar cell. To fit the demand of a low power algorithm, a simplified 75% perturb and observe (P&O) method was used to deduce the maximum power point. Instead of finding the maximum via derivative, and employ numerical methods to show a linear dependency between cell voltages

correspond to maximum power and cell open circuit voltages it is assumed that a maximum power point of the used solar PV module lies at about 0.75 times the open circuit voltage of the module. The MPPT can be found at 75% of the open circuit voltage according to equation 2.30. Therefore, by measuring the open circuit voltage of the solar panel, $V_{oc}$ , a reference voltage, $V_{MP}$ can be generated and a duty cycle control scheme can be implemented in order to bring the solar PV module voltage to the maximum power point.

$$V_{MP} = M_V \times V_{OC} \tag{2.30}$$

Where,

$$M_V = Voltage\ factor$$

In order to use this voltage factor value an analysis to the solar panel main characteristics was done. With the help of the solar panel datasheet and looking at the maximum voltage under load it is possible to state that the chosen value for the voltage factor, $M_V = 0.75$ characterizes the main idea of the voltage-based maximum power point tracking technique. This method is very simple and has a high efficiency compared to other MPPT methods. In reality $M_V$ is not constant and is affected by temperature and irradiance levels. Another limitation of this technique is the open circuit voltage of the module, it varies with the temperature. Therefore, as the temperature increases the module open circuit voltage changes and it is required to measure the open circuit voltage of the module very often.

## 2.10   Control Unit

The brain of the control unit is a microcontroller PIC16F877A integrated circuit (IC). Fig. 2.14 shows a microcontroller IC that is used to process measured voltage (from the solar panel output) and to compute the required signal for control of the system. IC is also employed to generate the required PWM command that will control the switch gate of the DC/DC converter.
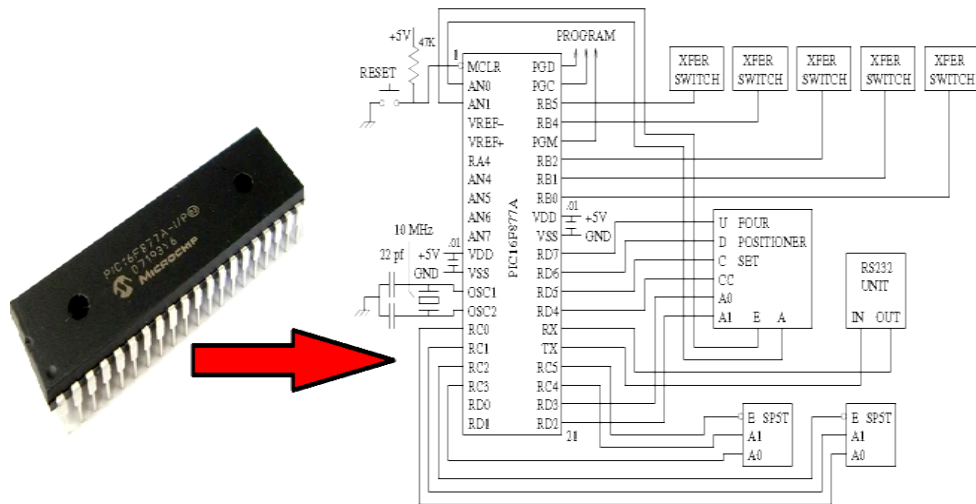
Fig. 2.14 Schematic diagram of microcontroller connections that it controls [26]

### 2.10.1 Microcontroller PIC16F877A

A microcontroller is a type of microprocessor furnished in a single integrated circuit. Its principal nature is self-sufficiency and low cost. Fig. 2.14 shows the schematic diagram of PIC16F877A microcontroller that includes a central processor, input and output doors, memory for program and data storage. It also has an internal clock and more than one peripheral device such as: timers, counters, analog-to-digital converters and serial communication facilities. This powerful (200 nanosecond instruction execution) yet easy-to-program CMOS FLASH-based 8-bit microcontroller packs Microchip's powerful PIC® architecture into 40 pin packages. The PIC16F877A features 256 bytes of EEPROM data memory, self programming, an In-Circuit Debugger (ICD), 2 Comparators, 8 channels of 10-bit Analog-to-Digital (A/D) converter, 2 capture/compare/PWM functions, the synchronous serial port can be configured as either 3-wire Serial Peripheral Interface (SPI™) or the 2-wire Inter-Integrated Circuit (I²C™) bus and a Universal Asynchronous Receiver Transmitter (UART). All of these features make it ideal for more advanced level A/D applications in automotive, industrial, appliances and consumer applications. These PIC microcontrollers can be programmed in high-level languages or in their native machine language (Assembly). The use of the microprocessor allows capturing the

28

voltage value from the solar panel. In order to reach the MPPT algorithm the PIC16F877A will:

- Capture analog voltage value from the solar panel output
- Proceed to an Analog / Digital (A/D) conversion
- Apply the VMPPT algorithm
- Send to the Integrated Circuit the correspondent voltage signal $\left(V_{ref}\right)$ in a way to allow the control of the PWM duty cycle.

After the PWM signal has been generated from the microcontroller there is a need to "transform" it into an average value. An easy and inexpensive way to implement this functionality is by passing the signal into a low pass filter. This PWM signal is fixed, but the pulse width is variable, depending on the operation point of the solar panel. Fig. 2.15 is clarifying the description.
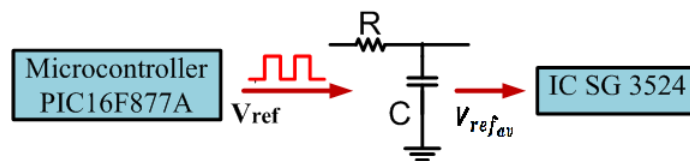


Fig. 2.15 Average value of PWM signal

## 2.10.2 Integrated Circuit SG3524

IC SG3524 is an improved version of a PWM controller that is used in this thesis in electrical model of Fig. 2.8 to set switch $M_1$. The IC SG3524 is responsible for the generation of an appropriate PWM signal, according to the values received from the microcontroller, in a way to correctly control the switch gate from the DC/DC converter.

## 2.11   Low Pass Filter

The low pass filter (LPF) mentioned in Fig. 2.15 is a simple RC filter where the capacitor is in parallel with the load. The capacitor exhibits reactance, and blocks low frequency signals, causing them to go through the load instead. At higher frequencies the reactance drops, and the capacitor functions as a short circuit. The combination of

resistance and capacitance gives the time constant of the filter, that can be represent as

$$\tau = RC \tag{2.31}$$

The cut off frequency is given as

$$f_c = \frac{1}{2\pi RC} \tag{2.32}$$

## 2.12  Battery

For large scale back-up systems like emergency lightning's, power sump pumps, house hold water pump, solar system, wind turbine and other renewable energy system storage purposes lead-acid battery is commonly used. Lead-acid batteries can draw a higher current, have a higher voltage and hold a charge much longer than other types of batteries. For these main reasons, the Lead-acid battery is chosen for the proposed solar charge controller. Fig. 2.16 shows basic construction of a Lead-acid battery. Lead $(Pb)$ as negative electrode and Lead oxide $(PbO_2)$ as positive electrode, Sulphuric acid $(H_2SO_4)$ as electrolyte.
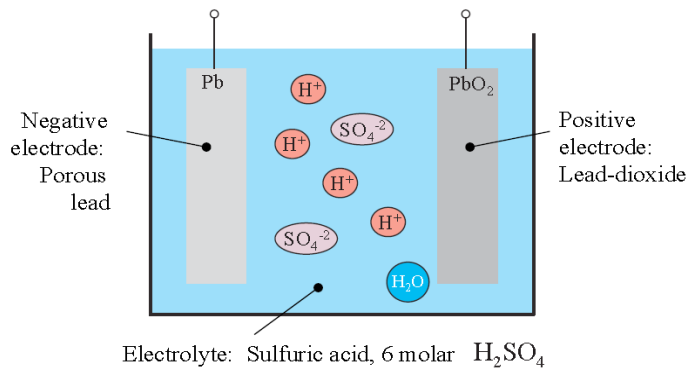


Fig. 2.16 Construction of Lead-acid battery

## 2.13  Conclusion

This chapter represents a brief description of PV system with their classification. Electrical models of a solar cell and its operation are clearly described here. Converter topology, mathematical model of determining the inductor, capacitor and low pass filter are discussed. MPPT technique, control unit and battery functions are also discussed here.

# CHAPTER 3
# SOLAR CHARGE CONTROLLER

## 3.1 Introduction

A solar charge controller (SCC) is a dc voltage regulator. A SCC is needed in virtually all solar power systems that utilize batteries. The function of the solar charge controller is to regulate the generating power from the solar panels and storing the power to the batteries. In a solar panel generally 16 to 21 volt is generated. But to charge the battery, the needed voltage is between 14V and 14.4V. A charge controller steps down the voltage. The basic function of a charge controller is to prevent battery overcharging. If battery is allowed to routinely overcharge, their life expectancy will be dramatically reduced. A charge controller will sense the battery voltage, and reduce or stop the charging current when the voltage gets high enough. This is especially important with sealed lead acid battery where we cannot replace the water that is lost during overcharging. There are some other functions that a charge controller performs such that preventing battery over-discharge, protecting from electrical overload, and maximum power tracking etc.
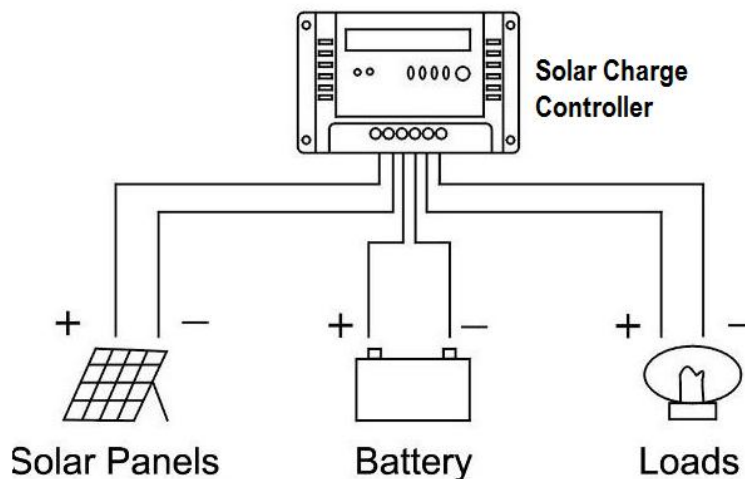


Fig. 3.1 Simple block diagram of a charge controller

## 3.2 Evolution of Solar Charge Controller

The design of charge controller was significantly developed with the huge use of solar panel. For the increasing demand of charge controllers in the market, special features like low voltage disconnect (LVD), battery voltage, state of charge (SOC), measurement of current, indication of fault etc are introduced. These features can be implemented with analog electronics. But with the improvement of components digital electronics are used more frequently. So the solid state controller is emerged. On-off charge controller was first introduced in 1992. The set points low voltage disconnect (LVD) and high voltage disconnect (HVD) were done by relay.
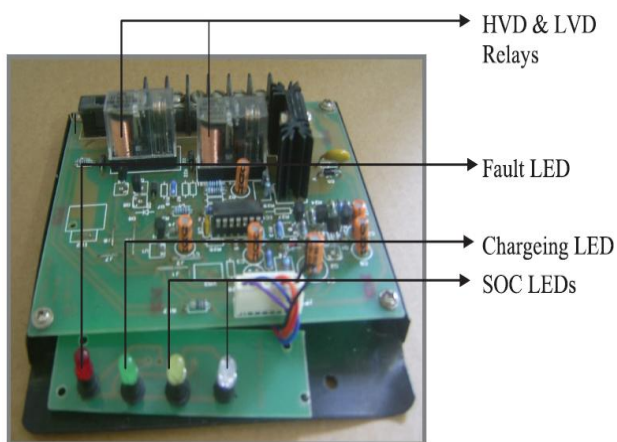


Fig. 3.2 On-off charge controller
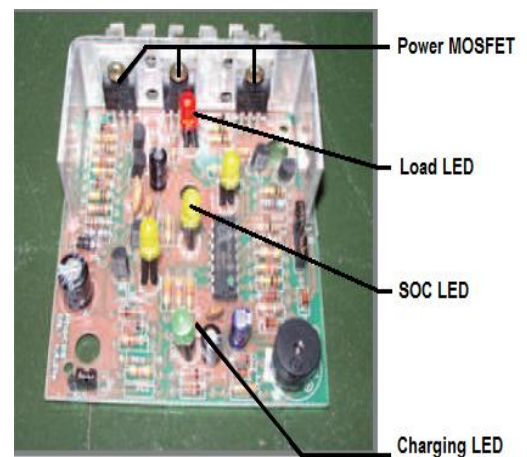


Fig. 3.3 Solid state series controller



Fig. 3.4 Micro-processor based series controller

The latest technology used in charge controller is micro-processor based. In this type of controllers, there is a data logger which is an extra-ordinary feature. This charge controller uses excess energy management and adaptive charging algorithm by which different data of solar home system can be stored and displayed by connecting with

computer. For the invention of special IC for solar PV, intelligent charge controllers are manufactured now-a-days. For uncontrolled use of electricity, life time of battery is reduced and load is detached frequently for low voltage. At present, intelligent controllers are found in low cost where LVD can be set at the first stage of operation and for the subsequent time, the controller itself fixes the ideal LVD by observing the charge and discharge of battery. This is the latest technology.

## 3.3 Operating Principle

Fig. 3.5 shows the operational block diagram of a solar charge controller. Current is stored in the battery from the photovoltaic array through the charge controller. Current is supplied to the DC load from the battery through the controller. For AC load an inverter is used to convert the DC voltage to AC voltage. In addition, there is a scope of remote telemetry for transmitting data, temperature compensation probe, lighting control etc. Generally buck converter is used which converts high voltage into low voltage. For this operation two types of switch are used.

- Relay type switch
- Solid state switch (power transistor or MOSFET)
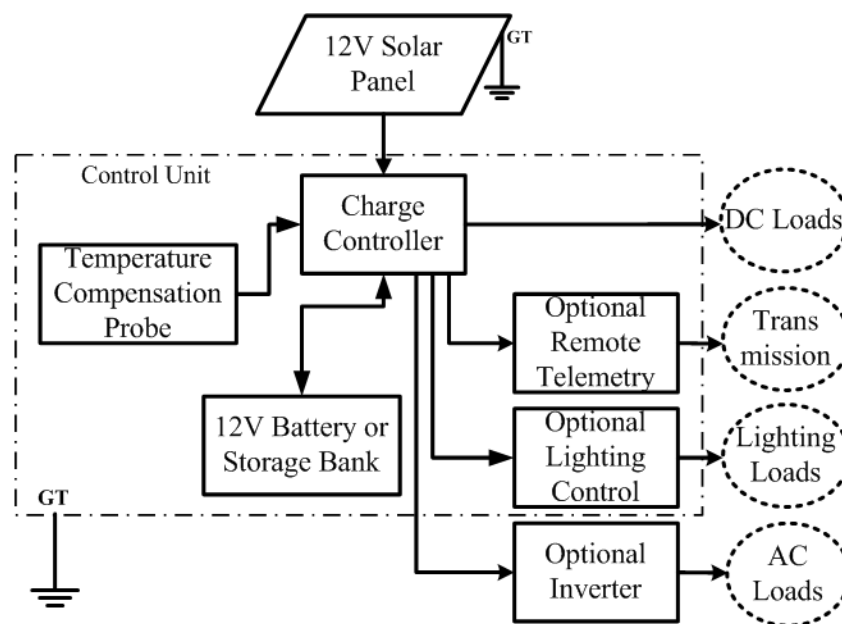


Fig. 3.5 Block diagram of operation of charge controller
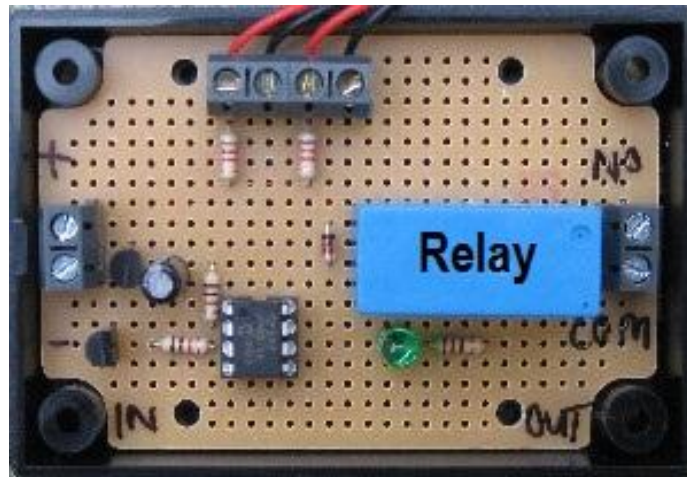
Fig. 3.6 Rely type switch used for solar charge controller

### 3.3.1 Relay Type Switch

It is the simplest type of switch. It has a very small resistance so the power loss is small. But it can be switched on-off for 100 thousands time. So its life time is not large enough for desired operation. Its advantage is low cost. An electromagnetic coil opens and closes a mechanical switch. This is called a relay. It switches off at night, to block reverse current. As it turns on and off, there is an audible clicking sound. A relay type switch used in a charge controller shown in Fig. 3.6

### 3.3.2 Solid State Switch

Now-a-days most of the charge controllers use solid state switch because of its long life time. But it has greater conduction loss specially at high current.
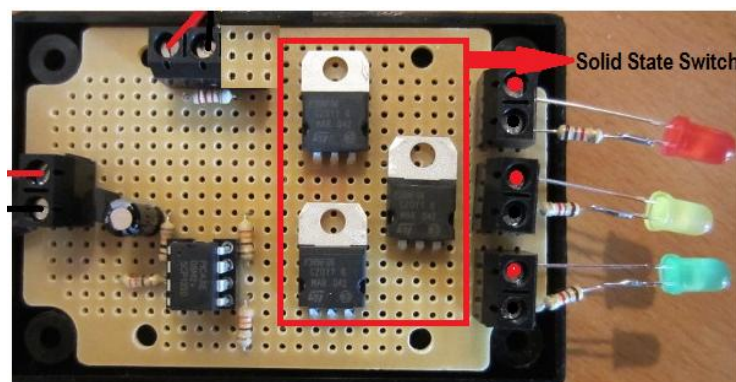


Fig. 3.7 Solid state switch for solar charge controller

Charge current passes through a semiconductor (a transistor) which acts like a valve to control the current. This semiconductor switch passes current in only one direction. It prevents reverse current without any extra effort or cost. Solid state switches are shown in Fig. 3.7

## 3.4 Charge Controller Types

According to connections there are two common types of photovoltaic charge controllers. Each has it benefits and limits; the choice of controller is best determined by the specific application or customer demand.

- Shunt Controller and
- Series Controller and
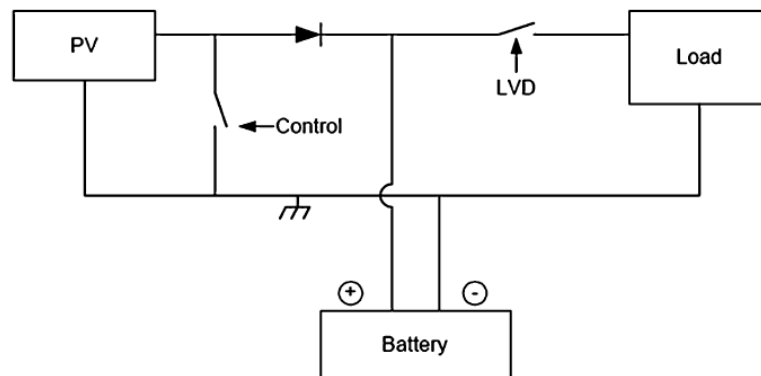


Fig. 3.8 Block diagram of a shunt charge controller

### 3.4.1 Shunt Controller

In a shunt controller, a blocking diode is used in series between the battery and the other element to prevent any short-circuiting or reverse voltage when the panel is regulating. Shunt controllers are limited to use in Solar PV systems with PV module currents less than 20A. A heat sink is required to dissipate the power because of the voltage drop between the module and controller. Fig. 3.8 shows the diagram of shunt controller. Shunt controller are of two types. LVD for low voltage disconnect, disconnects the system at the predefined low voltage set point.

a. **Shunt-Interrupting:** The shunt-interrupting controller completely disconnects the array current in an interrupting or on-off fashion when the battery reaches the voltage regulation set point. Controller set points are the battery voltage levels at which a charge controller performs control or switching functions.

b. **Shunt-Linear:** Once a battery becomes nearly fully charged, a shunt-linear controller maintains the battery at near a fixed voltage by gradually shunting the array through a semiconductor regulation element.

### 3.4.2 Series Controller

A solid-state switch or a relay is used to open the circuit between the module and the battery, in case of overcharging, deep discharging and short-circuiting. Fig. 3.9 presents the block diagram of a series controller. There are two types of series controller.

a. **Series-Interrupting:** In the simpler series interrupting design, the controller reconnects the module to the battery once the battery falls to the module reconnect voltage set point.

b. **Constant-Current:** Constant current design controller is similar to the series- interrupting type charge controller, however when the voltage regulation set point is reached, instead of totally interrupting the array current, limited constant current remains applied to the battery.
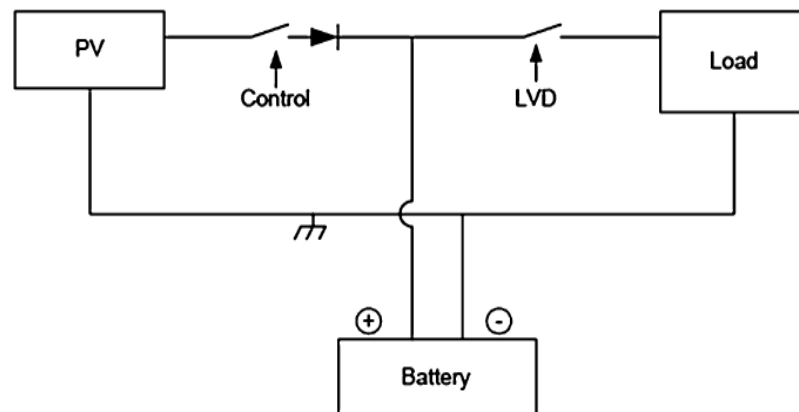


Fig. 3.9 Block diagram of a series charge controller

### 3.5 Switching Mechanism of Charge Controller

Proper operation of a charge controller should prevent overcharge or over discharge of a battery regardless of the system sizing/design and seasonal changes in the load profile and operating temperatures. The algorithm or control strategy of a battery charge controller determines the effectiveness of battery charging and PV array utilization, and ultimately the ability of the system to meet the load demands. Additional features such as temperature compensation, alarms, and special algorithms can enhance the ability of a charge controller to maintain the health, maximize capacity, and extend the lifetime of a battery. Moreover the controller protects against sulfation of a battery, overload and short circuit condition. Micro-processor based controllers measure the ampere-hour of the battery rather than state of charge of the battery to control the current supply.

Most importantly, the controller algorithm defines the way in which PV array power is applied to the battery in the system. In general, interrupting on-off type controllers require a higher regulation set point to bring batteries up to full state of charge than controllers that limit the array current in a gradual manner. Three switching mechanisms are well-liked to control the charge controller function.

- On-off
- Pulse width modulation (PWM)
- Maximum Power Point Tracking (MPPT)

### 3.5.1 On-Off Mechanism

Battery charging of a solar system is a complex process and challenging. In the old days, simple on-off regulators were used to limit battery out gassing when a solar panel produced excess energy. However, as solar systems matured it became clear how much these simple devices interfered with the charging process. The charge controllers which regulate the flow of charge to the battery by switching the current on fully ON or fully Off state are called On/Off control. The history for On-Off regulators has been early battery failures, increasing load disconnects, and growing

user dissatisfaction. PWM mechanism has recently surfaced as the first significant advance method to charging solar battery.
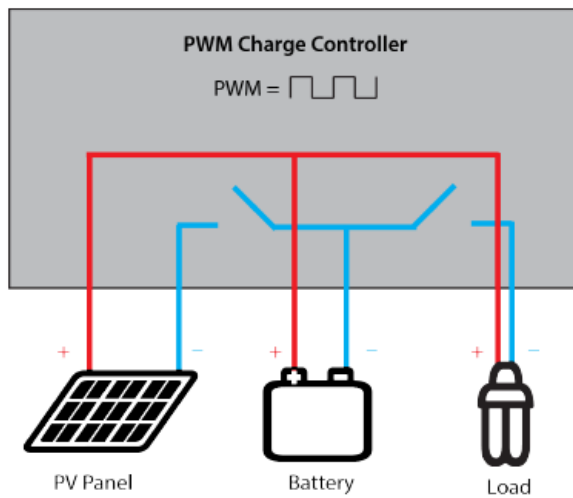


Fig. 3.10 Schematic diagram of PWM          Fig. 3.11 Schematic diagram of MPPT
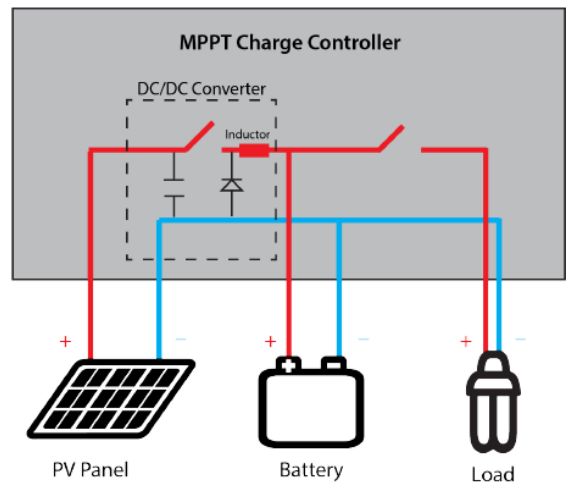
### 3.5.2 PWM

Pulse-Width Modulation (PWM) comes into play when the battery bank is full. During charging, the controller allows as much current as the PV panel/array can generate in order to reach the target voltage for the charge stage the controller is in. Once the battery approaches this target voltage, the charge controller quickly switches between connecting the battery bank to the panel array and disconnecting the battery bank, which regulates the battery voltage holding it constant. This quick switching is called PWM and it ensures the battery bank is efficiently charged while protecting it from being overcharged by the PV panel/array. Fig. 3.10 presents a schematic PWM diagram.

### 3.5.3 MPPT

Maximum Power Point Tracking features an indirect connection between the PV array and the battery bank. The indirect connection includes a DC/DC voltage converter that can take excess PV voltage and convert it into extra current at a lower voltage without losing power. MPPT controllers do this via an adaptive algorithm that follows the maximum power point of the PV array and then adjusts the incoming voltage to maintain the most efficient amount of power for the system. Over the past

decades many methods to find the MPP have been developed. These techniques differ in many aspects such as required sensors, complexity, cost, range of effectiveness, convergence speed, correct tracking when irradiation and temperature change, hardware needed for the implementation or popularity, among others. Some of the most popular MPPT techniques or algorithm is listed below [14].

- Perturb and observe (P&O).
- Incremental Conductance method.
- Fractional short circuit current.
- Fractional open circuit voltage.
- Fuzzy logic.
- Neural networks.
- Ripple Correlation Control
- Current Sweep.
- DC-link capacitor droop control.
- Load current or load voltage maximization.
- Voltage or current Feedback control.
- $\beta$ Method
- System Oscillation Method
- Constant Voltage Tracker
- Lookup Table Method

- Online MPP Search Algorithm
- Temperature method
- Three Point Weight Comparison
- PV Output Senseless Control
- Biological Swarm Chasing
- Variable Inductor
- Incremental Resistance (INR)
- Array Reconfiguration
- Linear Current Control
- IMPP and VMPP Computation
- One-cycle control Method
- Best Fixed Voltage algorithm
- Linear Reoriented Coordinates
- Slide Control
- Solid State Based MPPT

Among several techniques mentioned, the Perturb and Observe (P&O) method and the Incremental Conductance (InCond) algorithms are the most commonly applied algorithms. Other techniques based on different principles include fuzzy logic control, neural network, fractional open circuit voltage or short circuit current, current sweep, etc. Most of these methods yield a local maximum and some, like the fractional open circuit voltage or short circuit current, give an approximated MPP, rather than an exact output. In normal conditions the V-P curve has only one

maximum. However, if the PV array is partially shaded, there are multiple maxima in these curves. Both P&O and InCond algorithms are based on the hill-climbing principle, which consists of moving the operation point of the PV array in the direction in which the power increases. Hill-climbing techniques are the most popular MPPT methods due to their ease of implementation and good performance when the irradiation is constant. The advantages of both methods are simplicity and requirement of low computational power. The drawbacks are: oscillations occur around the MPP and they get lost and track the MPP in the wrong direction during rapidly changing atmospheric conditions. In this thesis, perturb and observe (P&O) algorithm is used to implement the solar charge controller.

### 3.5.3.1 Perturb & Observe (P&O) or Hill Climbing Method

Hill climbing involves a perturbation in the duty ratio of the power converter; P&O involves a perturbation in the operating voltage of the PV array. In the case of a PV array connected to a power converter, perturbing the duty ratio of power converter perturbs the PV array current, and consequently perturbs the PV array voltage; hill climbing and P&O methods are two different ways to perform the same fundamental method.
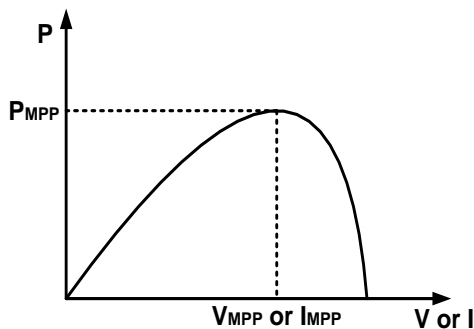


Fig. 3.12 Characteristic PV array power curve
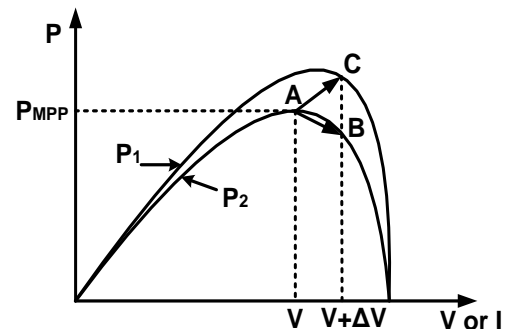
Fig. 3.13 Divergence of hill climbing/P&O from MPP [15]

Fig. 3.12 shows the characteristic power curve for a PV array. It can be seen from PV power curve that the increment, or decrement of the voltage increases, or decreases the power when the operating point is on the left of the MPP, and decreases, or

increases the power when being on the right of the MPP. The process is repeated periodically until the MPP is reached. The system then oscillates around the MPP. This oscillation can be minimized by reducing the perturbation step size [14]. However, a smaller perturbation size slows down the MPPT. A solution to this conflicting situation is to have a variable perturbation size that gets smaller towards the MPP. A two-stage algorithm is proposed that offers faster tracking in the first stage. Hill climbing and P&O methods can fail under rapidly changing atmospheric conditions as illustrated in Fig. 3.13 starting from an operating point A, i.e. $P_1$ curve is utilized, if atmospheric conditions stay approximately constant, a perturbation $\Delta V$ in the PV voltage V will bring the operating point to point B and consequently the perturbation will be reversed due to a decrease in power. However, if the irradiance increases and shifts the power curve from $P_1$ to $P_2$ within one sampling period, the operating point will move from point A to C. This represents an increase in power due to the new curve $P_2$, while the perturbation is kept the same. Consequently, the operating point diverges from the MPP and will keep diverging if the irradiance steadily increases, numerous number of researches apparel in the literature recently covering not only these two methods, but also outlining other MPPT techniques.
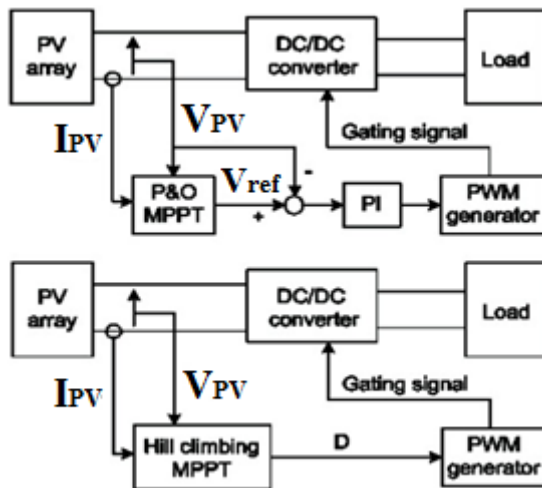


Fig. 3.14 Block diagram of the PV system using the hill climbing and P&O methods.
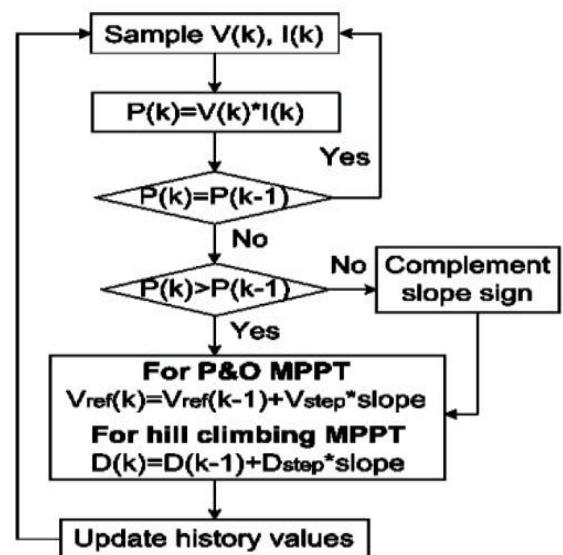
Fig. 3.15 The flowchart of P&O control technique.

Fig. 3.14 shows the block diagram of the PV system using the hill climbing and P&O methods, while Fig. 3.15 shows the algorithm flowchart of the technique [27].

## 3.6 Characteristics of MPPT

- **High Voltage Wire Runs** – smaller wire can be used and greater distances achieved using higher voltage PV input due to less voltage drop. A big advantage to having a higher voltage solar panel array is that we can use smaller gauge wiring to the charge controller. And since a solar panel array can sometimes be over a 100 feet away from the charge controller, keeping the cost of the wiring down to a minimum is usually an important financial goal for the whole project. When you double the voltage (e.g. from 12 to 24 volts), you will decrease the current going through the wires by half which means you use a quarter as much copper (or cable with half of the diameter).

- **Shading and Cloud Irradiance Effects** – Cloud edge effect can cause the module to exceed its rated wattage for a short time. Shading can cause tricky IV curve shapes. MPPT can follow both these changes to ensure maximum power during these conditions.

- **Low Battery Protection** – when the battery is very low, a high voltage difference between the $V_{mp}$ of PV and the battery voltage causes an even greater power boost. This can prevent an LVD at a time when the power is most needed.

- **Reduced Power Loss** – Another area that is enhanced by an MPPT charge controller is power loss. Lower voltage in the wires running from the solar panels to the charge controller results in higher energy loss in the wires than higher voltage. With a PWM charge controller used with 12V batteries, the voltage from the solar panel to the charge controller typically has to be 18V. Using an MPPT controller allows much higher voltages in the wires from the panels to the solar charge controller. The MPPT controller then converts the excess voltage into additional amps. By running higher voltage in the wires

from the solar panels to the charge controller, power loss in the wires is reduced significantly.

Table 3.1 is presents some specific pros and cons of both PWM and MPPT charge controllers.

**Table 3.1 Pros and Cons of Both Types of Controllers**

|  | **PWM Controller** | **MPPT Controller** |
|---|---|---|
| **Pros** | 1/3 − 1/2 the cost of a MPPT controller. | Highest charging efficiency (Especially in cool climates). |
|  | Longer expected lifespan due to fewer electronic components and less thermal stress. | Can be used with 60-cell panels. |
|  | Smaller size | Possibility to oversize array to ensure sufficient charging in Winter months. |
|  | Controller cost is low, it is less expensive | 30% more efficient than PWM |
| **Cons** | PV arrays and battery banks must be sized more carefully and may require more design experience. | 2-3 times more expensive than a comparable PWM controller. |
|  | Cannot be used efficiently with 60-cell panels. | Shorter expected lifespan due to more electronic components and greater thermal stress. |
|  | Higher wiring cost and less efficient than MPPT | Higher controller cost |
|  | PWM controller is used with off-grid modules. | higher frequency charge control and suitable for more than 200W solar panel |

## 3.7 Charge Controller Selection

Basically, to allow high rates of charging, solar charge controller are used. Selection of a charge controller in PV systems depends on some factors like to prevent battery overcharge, low voltage disconnect (LVD), high voltage disconnect (HVD), load regulation and control, control of backup energy sources and system monitoring. For specific application specific designs are needed. The charge controller must be able to handle expected peak or surge conditions besides the typical voltage and current control. It is important to be adequately sized for the intended application such as solar home system, solar irrigation system, solar power grid station etc. MPPT techniques allow operating the solar module in a maximum power generating mode. MPPT algorithms are used to obtain the maximum power from the solar array based on the variation in the irradiation and temperature. The voltage at which PV module can produce maximum power is called 'maximum power point' (or peak power voltage). Maximum power varies with solar radiation, ambient temperature and solar cell temperature.
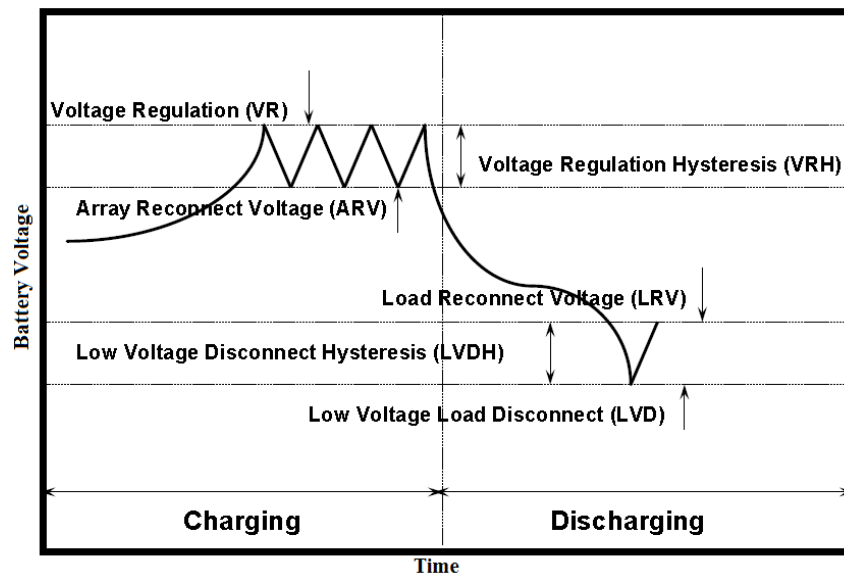


Fig. 3.16 Charge controller set points [29]

## 3.8 Charge Regulation Set Points

While the specific control method and algorithm vary among charge controllers, all have basic parameters and characteristics. Manufacturers' data generally provide the

limits of controller application such as PV and load currents, operating temperatures, losses, set points, and set point hysteresis values. In some cases the set points may be dependent upon the temperature of the battery and/or controller, and the magnitude of the battery current [28]. A discussion of the four basic charge controller set points present below and graphically shown in Fig. 3.16

### 3.8.1  Voltage Regulation (VR) Set Point

This set point is the maximum voltage a controller allows the battery to reach. At this point a controller will either discontinue battery charging or begin to regulate the amount of current delivered to the battery. Proper selection of this set point depends on the specific battery chemistry and operating temperature.

### 3.8.2  Voltage Regulation Hysteresis (VRH)

The set point is voltage span or difference between the VR set point and the voltage when the full array current is reapplied. The greater this voltage span, the longer the array current is interrupted from charging the battery. If the VRH is too small, then the control element will oscillate, inducing noise and possibly harming the switching element. The VRH is an important factor in determining the charging effectiveness of a controller.

### 3.8.3  Low Voltage Disconnect (LVD)

The set point is voltage at which the load is disconnected from the battery to prevent over discharge. The LVD defines the actual allowable maximum depth-of-discharge and available capacity of the battery. The available capacity must be carefully estimated in the system design and sizing process. Typically, the LVD does not need to be temperature compensated unless the batteries operate below 0°C on a frequent basis. The proper LVD set point will maintain good battery health while providing the maximum available battery capacity to the system.

### 3.8.4  Low Voltage Disconnect Hysteresis (LVDH)

This set point is the voltage span or difference between the LVD set point and the voltage at which the load is reconnected to the battery. If the LVDH is too small, the

load may cycle on and off rapidly at low battery state-of-charge, possibly damaging the load and/or controller. If the LVDH is too large, the load may remain off for extended periods until the array fully recharges the battery. With a large LVDH, battery health may be improved due to reduced battery cycling, but this will reduce load availability.

### 3.8.5 Effect of Duration of Load on Set Point

Due to 'On Load' at night, the charge controller will save the total current to the battery. Due to 'On Load' condition at daytime, charge controller will supply a portion of current from the solar panel to the load directly and save a portion of current to the battery according to the requirement.

### 3.8.6 Depth of Charge Effect

If the battery is used excessively, the voltage decreases to a low level. It can happen if the total ampere-hour is not used for certain duration of time. In that case, sulfation problem occurs. To return the battery in its normal condition, boost charging is necessary (2.50 or 2.58 volt/cell).

### 3.8.7 Temperature Effects on Battery

Normally, the set point of a controller is set for 25°C. Temperature compensation is necessary. For variation of temperature, the compensation factor is -5 mV/cell/°C.

### 3.9 Conclusion

The numbers of stand-alone PV systems are increasing incredibly every year. The success and acceptance of PV systems by the consumer is typically judged by the reliability and performance of these systems. Performance of the batteries in these systems is a key factor in their success. To maintain a wide acceptance and increasing demand for any PV systems and actual service life for the batteries a smart solar charge controller is must.

# CHAPTER 4
# MODELLING AND SIMULATION

## 4.1 Introduction

This chapter presents the mathematical models of the components of PV module, MPPT control unit, and Buck-boost converter, described in second chapter are implemented in MATLAB/SIMULINK v2008. MATLAB SIMULINK software and its facilities are used to design the proposed electric models of solar MPPT charge controller. With this software, it is possible to characterize the MPPT algorithm and to obtain an estimate charging time for the battery. SIMULINK is a simulation program, which provides a graphical interface to build the models as block diagrams. It offers the advantage of building hierarchical models, namely presenting the possibility to view the system at different levels. This presents the advantage that the models can easily be connected together in order to simulate a system. Such models are also very useful to optimize the components of the PV system. For practical use, the SIMULINK model blocks for each component of the PV system can be gathered in a library. In this thesis, the library contains model blocks for a PV module, a MPPT controller, a Buck-boost converter and a battery. A brief overview of the internal structure of other blocks of the SIMULINK library presented in Fig. 4.1 to Fig. 4.17 respectively. These figures contain the SIMULINK implementation of the mathematical models described in chapter 2.

## 4.2 PV Module Modeling

Each of the power electronic models represents subsystems within the simulation environment. These blocks have been developed so they can be interconnected in a consistent and simple manner for the construction of complex systems. The subsystems are masked, meaning that the user interface displays only the complete subsystem, and user prompts gather parameters for the entire subsystem. Relevant parameters can be set by double-clicking a mouse or pointer on each subsystem

block, then entering the appropriate values in the resulting dialogue window. In accordance with equation 2.5 deducted in second chapter,

$$V_{sa} = \gamma \times V_T \times ln\left[\frac{I_s - i_{sa}}{M \times I_0} + 1\right] - (R_s \times i_{sa}) \tag{4.1}$$
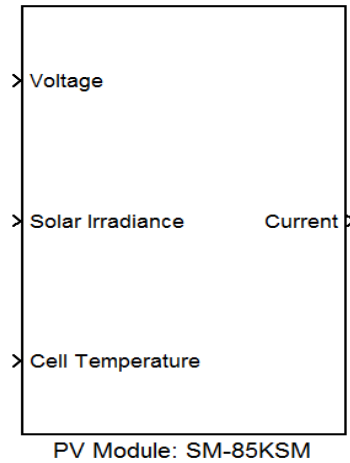


Fig. 4.1 Block of PV Module: SM-85KSM model
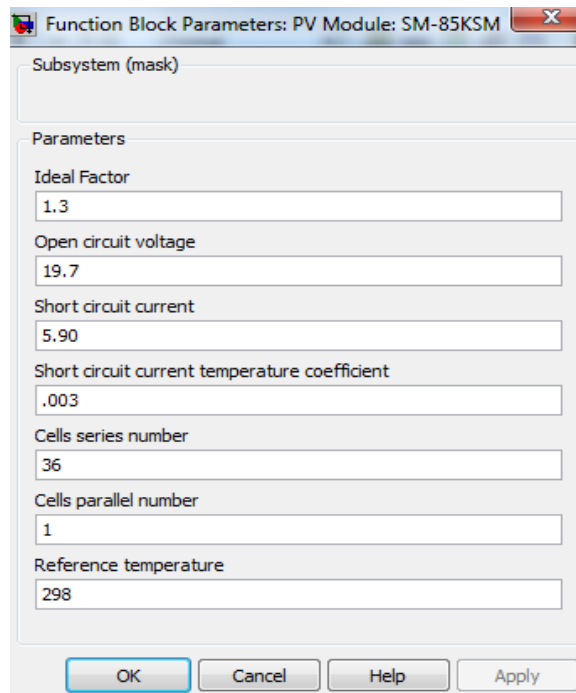


Fig. 4.2 Function block parameters of PV Module: SM-85KSM

It is possible to build the block of the solar panel. It represents the detailed SIMULINK implementation of the mathematical model of the PV module and allows

simulating the nonlinear I-V and P-V characteristic. The implicit function of the I-V characteristic of the solar module can be easily solved by this block. Fig. 4.1 represents the PV module blocks. This block has three inputs and one output. Voltage, solar irradiance and cell temperature are the inputs and current is the output of this block. Fig. 4.2 shows the function block parameter of the PV module blocks. Block set are used to design this module are described below.

### 4.2.1 Ideal Factor

From ideal diode equation,

$$I = I_L - I_0 \left[ \exp\left(\frac{qV}{nkT}\right) - 1 \right] \tag{4.2}$$

The ideality factor of a diode is a measure of how closely the diode follows the ideal diode equation. The derivation of the simple diode equation uses certain assumption about the cell. In practice, there are second order effects so that the diode does not follow the simple diode equation and the ideality factor provides a way of describing them. In this simulation inputted ideal factor is 1.3

### 4.2.2 Open Circuit Voltage

The open-circuit voltage $V_{oc}$ is the maximum voltage available from a solar cell, and this occurs at zero current. In this simulation the open-circuit voltage is 19.7V are taken from the specification sheet of KYOCERA PV Module: SM-85KSM Model.

### 4.2.3 Short Circuit Current

The short-circuit current $I_{sc}$ is the current through the solar cell when the voltage across the solar cell is zero (i.e., when the solar cell is short circuited). In this simulation the short-circuit current is 5.90A are taken from the solar panel specification sheet.

### 4.2.4 Short Circuit Current Temperature Coefficient

The short-circuit current, $I_{sc}$ increases slightly with temperature, since the band gap energy, $E_G$, decreases and more photons have enough energy to create E-h pairs.

However, this is a small effect and the temperature dependence of the short-circuit current from a silicon solar cell is,

$$\frac{1}{I_{sc}}\frac{dI_{sc}}{dT} \approx 0.0006 \; per \; °C \; for \; Silicon \tag{4.3}$$

In this simulation short circuit current coefficient 0.003 are taken.

### 4.2.5 Cells Series Number

A bulk silicon PV module consists of multiple individual solar cells connected, nearly always in series, to increase the power and voltage above that from a single solar cell. The voltage of a PV module is usually chosen to be compatible with a 12V battery. Taking into account an expected reduction in PV module voltage due to temperature and the fact that a battery may require voltages of 15V or more to charge, most modules contain 36 solar cells in series. This gives an open-circuit voltage of about 21V under standard test conditions, and an operating voltage at maximum power and operating temperature of about 17 or 18V. The remaining excess voltage is included to account for voltage drops caused by other elements of the PV system, including operation away from maximum power point and reductions in light intensity. In this simulation module, 36 cells are connected in series to produce a voltage sufficient to charge a 12V battery.

### 4.2.6 Cells Parallel Number

Modules are paralleled in large arrays so the mismatch usually applies at a module level rather than at a cell level. In small modules the cells are placed in series so parallel cell number is 1 (One). Connecting solar panels together in parallel is used to boost the total system current. When solar panels connected together in parallel, the total voltage output remains the same as it would for a single panel, but the output current becomes the sum of the output of each panel.

### 4.2.7 Reference Temperature

Most semiconductor modeling is done at 300°K since it is close to room temperature and a convenient number. However, solar cells are typically measured almost 2

degrees lower at 25°C (298.15°K). In most cases the difference is insignificant (only 4 mV of $V_{oc}$) and both are referred to as room temperature.

### 4.2.8 Subsystem of PV Module

Analyzing Fig. 4.3 it is possible to generate a transfer function. Saturation and delay functions are introduced to limit the fast response of the controlled voltage source, as well as to improve convergence. The other variables are directly obtain/calculated from the PV datasheet.
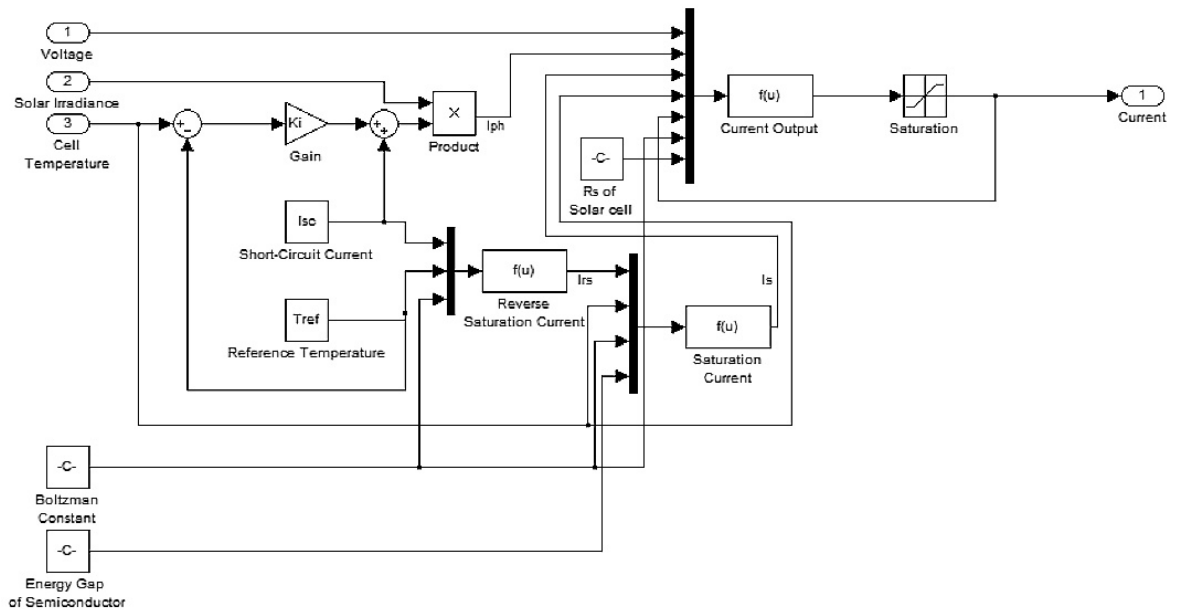


Fig. 4.3 Subsystem implementation of generalized PV Module: SM-85KSM

The value of $I_{sc}$ is imposed on this process in order to limit the complexity of this block, its value is taken from the PV datasheet and is equal to $I_{sc} = 5.90A$. Solar irradiance is taken maximum 1000 W/m$^2$, Boltzmann constant, $K = 1.38 \times 10^{-23} J/K$. Thus, applying equation (4.1), it is possible to obtain the voltage characteristic of the solar panel that allows the simulation.

### 4.3 Battery Modeling

Fig. 4.4 represents dialog box of a 12V, 100Ah Lead-Acid battery. Fig. 4.5 illustrates block parameters of this battery.
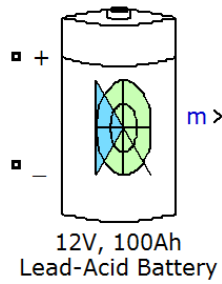
Fig. 4.4 Block of 12V, 100Ah lead-acid battery
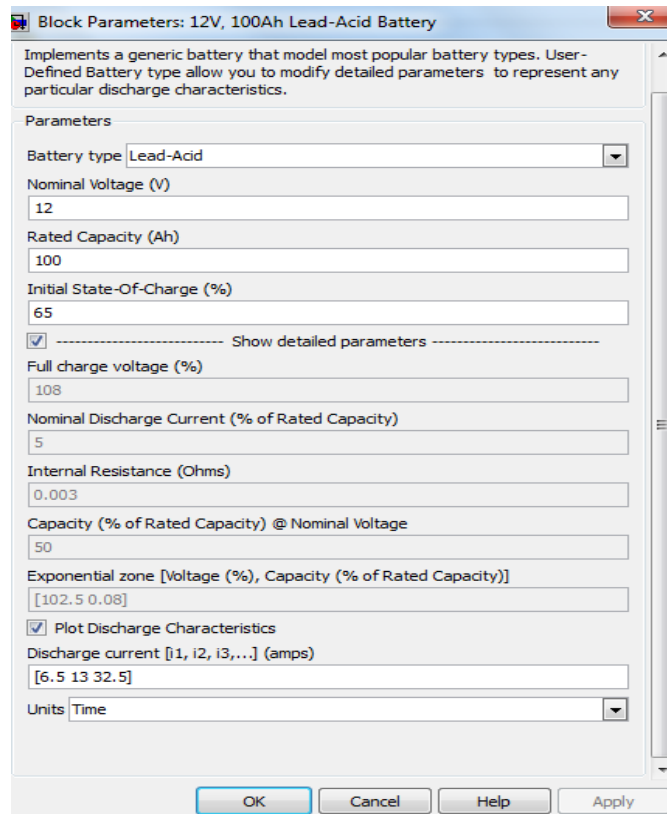


Fig. 4.5 Block parameters for lead-acid battery

### 4.3.1 Battery Type

In this section, a set of predetermined charge behavior for four types of battery such as Lead-Acid, Lithium-Ion, Nickel-Cadmium, and Nickel-Metal-Hydride are provided. Here, Lead-Acid is chosen.

### 4.3.2 Nominal Voltage (V)

The nominal voltage (V) of the battery represents the end of the linear zone of the discharge characteristics. Nominal voltage is 12V is selected.

### 4.3.3 Rated Capacity (Ah)

The rated capacity in ampere-hour is the minimum effective capacity of the battery. The maximum theoretical capacity (when the voltage crosses 0 volts) is generally equal to 105% of the rated capacity. The rated capacity of this battery is in 100 Ampere-hour (Ah).

### 4.3.4 Initial State-of-Charge (SOC)

This parameter is used as an initial condition for the simulation and does not affect the discharge curve. 100% indicates a fully charged battery and 0% indicates an empty battery. 65% means it will start charging from this charge level of battery.

### 4.3.5 Full Charge Voltage

The voltage factor (% of the nominal voltage) corresponding to the fully charged voltage, for a given nominal discharge current. Note that the fully charged voltage is not the no-load voltage.

### 4.3.6 Internal Resistance (Ohms)

When the model is used, a generic value is loaded, corresponding to the nominal voltage and the rated capacity of the battery. The resistance is supposed to be constant during the charge and the discharge cycles and does not vary with the amplitude of the current.

### 4.3.7 Capacity @ Nominal Voltage

The percentage of the rated capacity extracted from the battery until the voltage drops under the nominal voltage. This value should be in 0% to 100%.

### 4.3.8 Exponential Zone

The voltage and the capacity of the battery corresponding to the end of the exponential zone. The voltage should be between nominal voltage and full charged voltage.

### 4.3.9 Units

In this section, a set of predetermined unit is available for two types. One is Time and another is Ampere-hour.
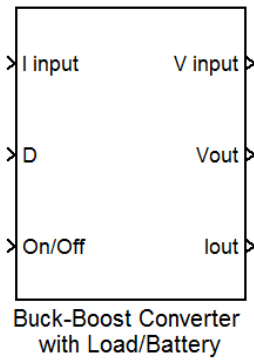
Fig. 4.6 Block of buck-boost converter model
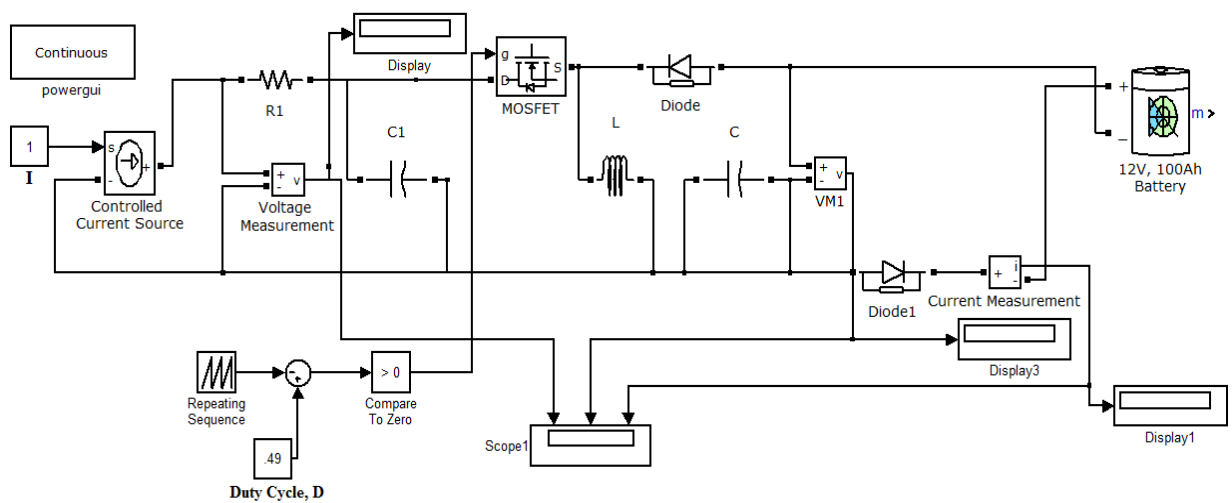


Fig. 4.7 Subsystem implementation of buck-boost converter

## 4.4 Buck-boost Converter Modeling

To facilitate the subsequent simulation analysis and feedback controller verification, the pulse-width-modulation signal to control the ideal switch can also be built into the masked subsystem shown in Fig. 4.6 and Fig. 4.7. For each converter to verity it's working in open loop configuration trigger pulses have been derived using a repeating sequence generator and duty cycle block. Function block compares the duty cycle and saw tooth from repeating sequence-derived trigger pulses are connected as an input to the switch control. Hence inputs for the masked subsystem are duty ratio and input voltage, and the outputs are chosen to be inductor current, capacitor voltage, and output voltage. When double-clicking the pointer on the masked subsystem in Fig. 4.6, one enters parameter values of the switching converter circuit in a subsystem of buck-boost converter in Fig. 4.7. In this simulation

SimPowerSystems library is used and created a buck-boost converter. The input of the subsystem is connected to the solar panel block and output to a battery. MOSFET used for switching operations.
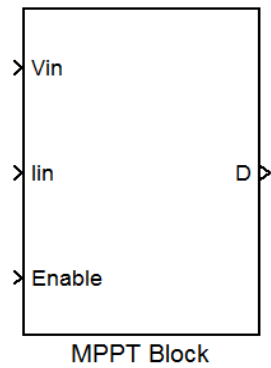


Fig. 4.8 Dialog box of MPPT block
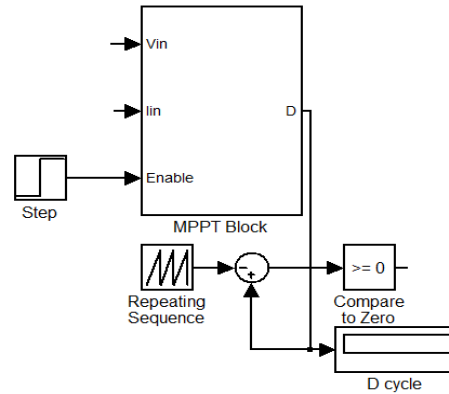
Fig. 4.9 MPPT unit of simulation
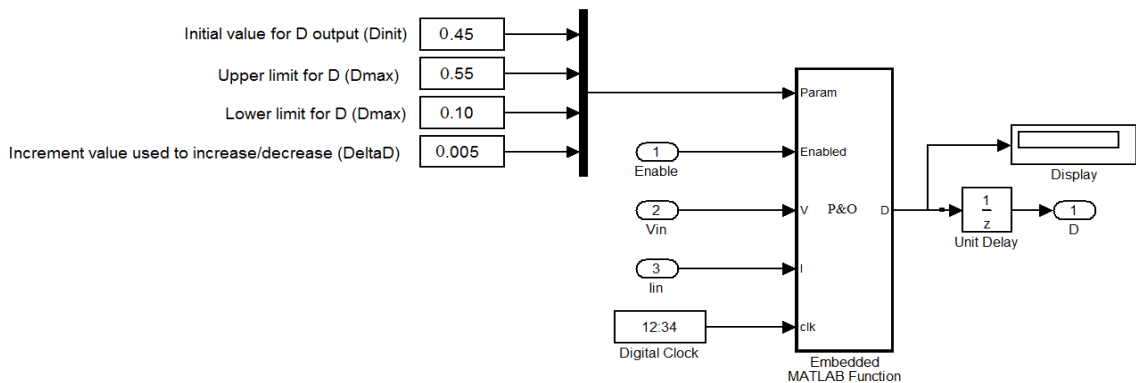


Fig. 4.10 Subsystem implementation of P&O MPPT block

## 4.5 MPPT Modeling

MPPT block is the most important part of the PV system. It controls the duty cycle of the Buck-Boost converter by using Perturb and Observe (P&O) algorithm to track the MPP of the solar panel. Duty cycle, D is calculated and converted to digital pulses using repeating sequence, sum and compare to zero block. The PWM frequency was selected to be 20 KHz. Fig. 4.8 shows the MPPT block, consisting three inputs and one output of duty cycle, D. Fig. 4.9 represents the MPPT unit with repeating sequence, sum, comparison block to zero and a duty cycle monitoring display. Fig. 4.10 shows the implemented subsystem for MPPT block. Embedded MATLAB

function unit designed based on perturb and observe (P&O) algorithm MPPT. Initial value of duty cycle is 0.45, Upper limit of D is 0.55 and changed value of duty cycle $\Delta D = 0.005$.
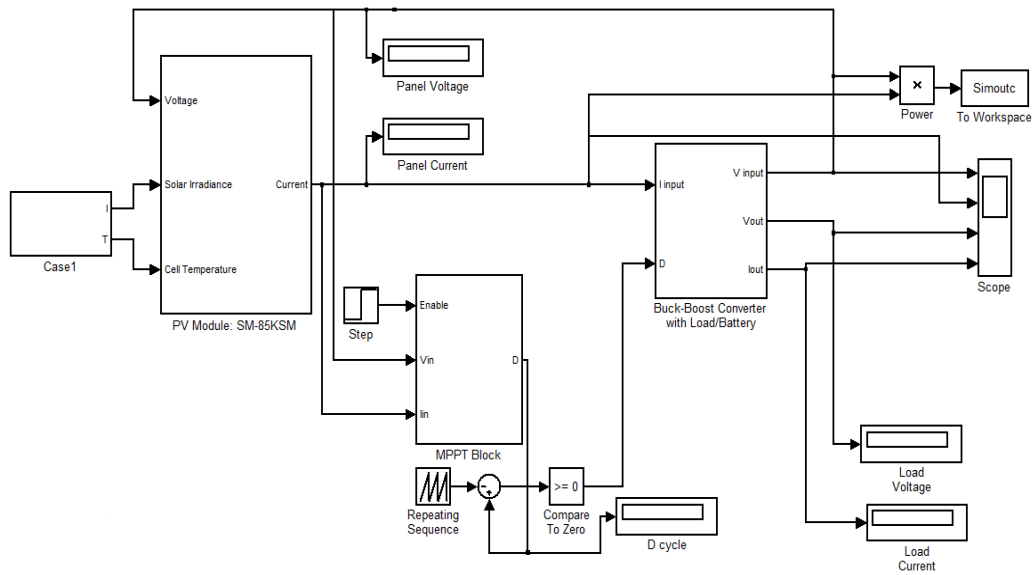


Fig. 4.11 MATLAB/SIMULINK based full solar MPPT system
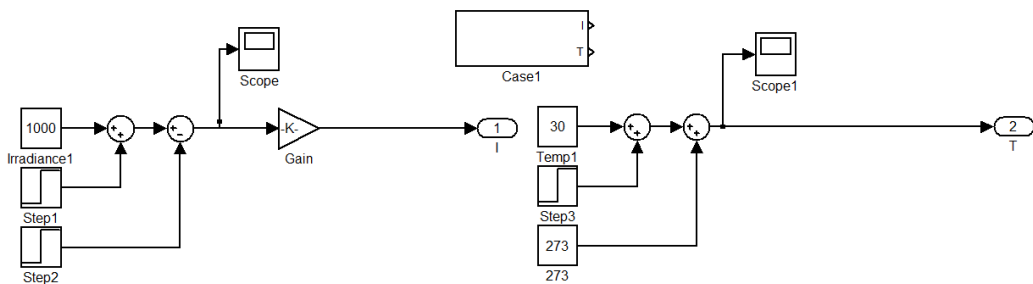


Fig. 4.12 Subsystem of case1

## 4.6 SIMULINK Model of Charge Controller

The complete circuit involving the PV array, charge controller and battery is illustrated in Fig. 4.11. All the blocks described above are connecting together to design full PV system. Fig. 4.11 shows the full PV system designed with SIMULINK. This system includes, PV module block, converter with battery block and MPPT block. The output of the solar panel block is the panel current and is connected to the input of the Buck-boost converter. The converter with battery block gives panel voltage ($V_{in}$), load voltage ($V_{out}$) and load current ($I_{out}$) as the output. Panel voltage ($V_{in}$) is input of the solar panel block. The MPPT block takes and as

the input and gives duty cycle, D as the output which controls the converter block. The solar irradiance and cell temperature profile are given as input to the solar panel. Case1 block consist Irradiance and Temperature subsystems. Fig. 4.12 shows the subsystem of Case1. Maximum power will generate when irradiance is maximum 1000 W/m$^2$.

## 4.7 Simulation Results

Fig. 4.13 shows scope waveforms of buck boost converter. First plot shows the output voltage of the converter. The performance of the system is measured with the time duration of 1 minute. The simulation output between the voltage multiplier output voltage in volts and the time in minutes. At the half of 0.1 second, output voltage of the converter reaches 17.6V. At the time of 0.1 second, the output voltage reaches 16V and attains the constant value. Second plot shows the output current. At the quarter of 0.1 second time the current was maximum, more than 3.5A and after passing of 0.1 second time current attains a constant value of 2.25A. Third plot shows the battery level charging voltage. The limit of high voltage disconnect is 13.5V and this converter is providing constant 13.4V to the battery as charging voltage. For lead-acid battery exponential area is very low. The second section represents the charge that can be extracted from the battery until the voltage drops below the battery nominal voltage. Finally, the third section represents the total discharge of the battery, when the voltage drops rapidly. Fig. 4.15 shows the output of MPPT charge controller as wave forms. First plot (V_out) shows the panel voltage, indicated as $V_{in}$. At the time of 0.01 second the voltage of the solar panel was 19.9V and this voltage decreases almost linearly to 17V at the time of 0.3 seconds. At the time period of 0.3 seconds to 0.38 seconds panel voltage was very non linear and some moments around 0.4 second panel provides stable voltage of 18V.
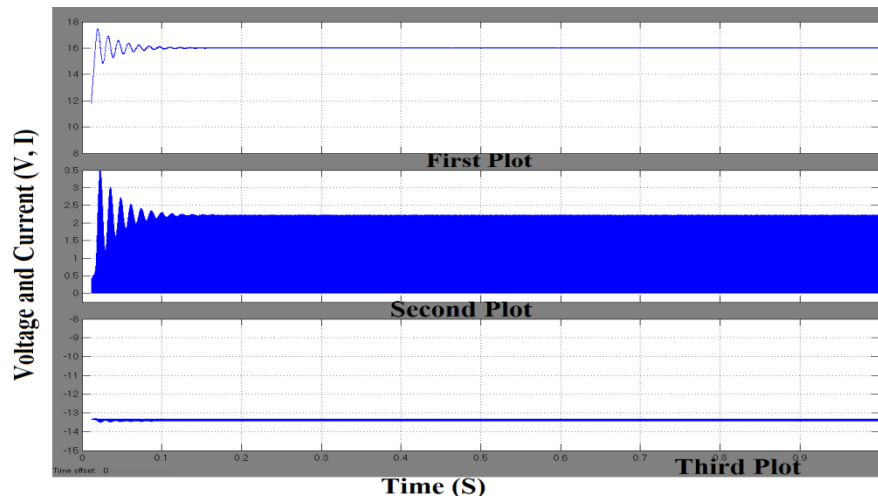
Fig. 4.13 Scope wave forms of buck-boost converter
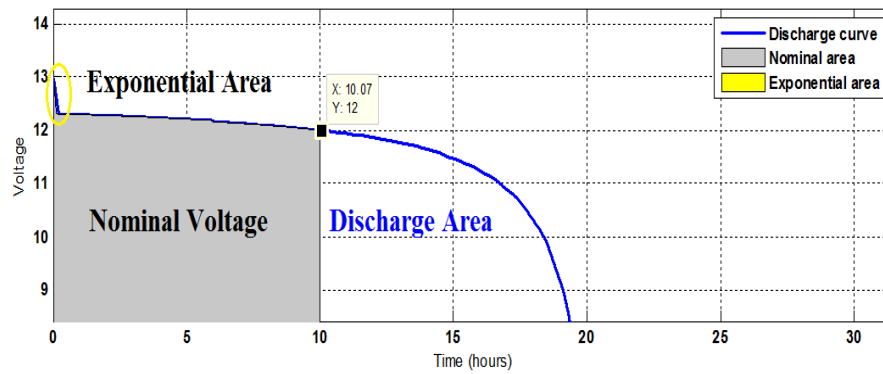


Fig. 4.14 Discharge characteristics of battery
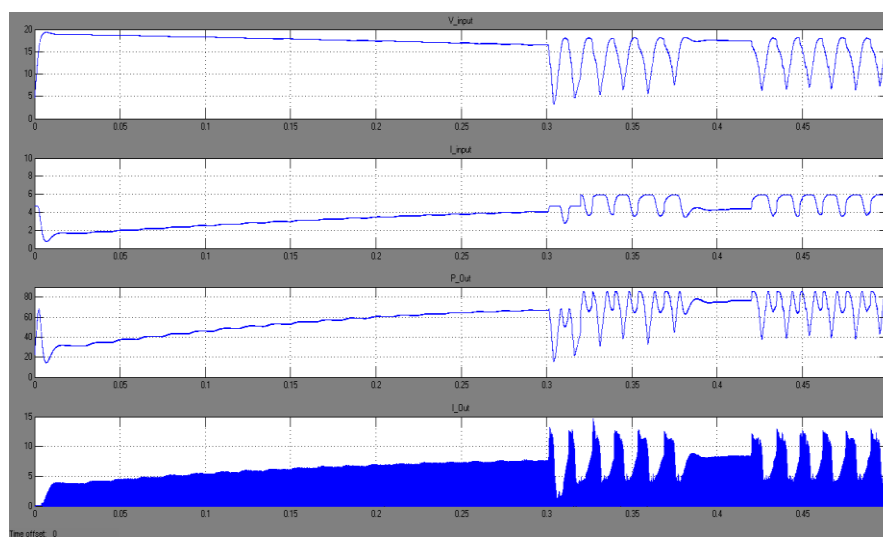


Fig. 4.15 Scope wave forms of complete circuit
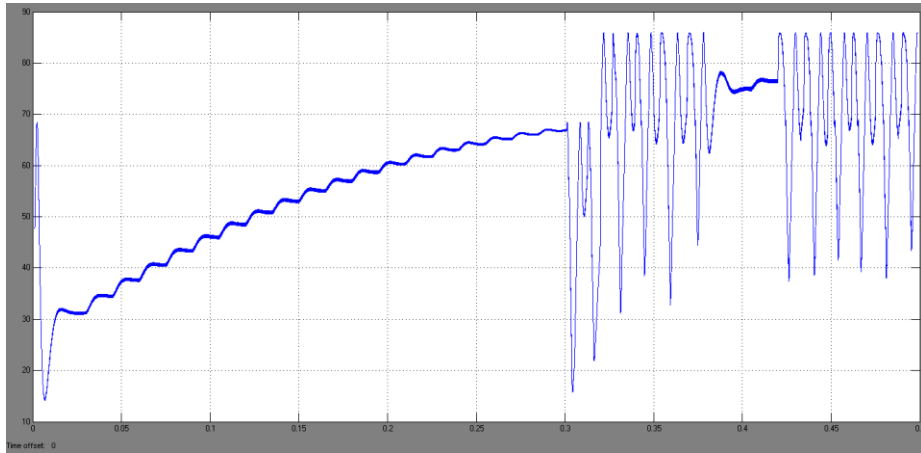
Fig. 4.16 Scope wave forms of extracting power from PV panel

At 0.43 seconds panel provides unstable voltages again. Second plot (I_inp) shows generated current from PV panel. This plot shows that current is proportionally increases or decreases with respect to the panel voltage. Third plot (P_out)shows the generated power from the panel using MPPT control method. Finally, fourth plot (I_out) shows the charging current of the battery. Comparing second and fourth plot, it's clear that charging current is higher than the input current. That means, MPPT techniques working efficiently and extracted maximum power from the panel. Fig. 4.16 shows the generating power after using MPPT control techniques. It shows that the maximum extracted power from the panel is 68W in a certain time of 0.3 m seconds. This simulation runs for 0.5 minutes.

## 4.8    Conclusion

Respecting the results achieved it is possible to conclude that, the PV simulation ensures that the theoretical assumptions, namely the voltage factor assumed, is a very approximate value of what can be expected in real implementation of the solar panel. The simulation using the Lead-acid battery model gives an ideal response of the system: the total time of battery charging (approximately seven hours). This is a very good charging average, knowing that the amount of time that the same Lead-acid battery takes to full charge using a DC power supplier is approximately three hours.

# CHAPTER 5

# HARDWARE DESIGN AND FIELD TEST

## 5.1 Introduction

The aim of the thesis is to design a stand-alone off-grid photovoltaic (PV) solar charge controller that utilizes maximum power point tracking (MPPT) to obtain the maximum efficiency. Due to the inherent losses that occur in photovoltaic systems, it is essential that the maximum power is extracted. The intent is to design an extremely efficient charge controller that will be able to monitor the power generated by the photovoltaic array and deliver the maximum amount to the battery bank during varying atmospheric conditions. The priority of the design will take place in the charge controller module of the system but will be integrated with the other parts to demonstrate a fully functional stand-alone system. The overall system will consist of a solar panel, MPPT charge controller, battery bank, and a distribution system to deliver usable power to the end user. The plan is to construct a product that is portable, easy to use, efficient, and inexpensive. In order to implement maximum power point tracking, data from several different sensors will be fed into a microcontroller. Here the MPPT algorithms will interpret the incoming current and voltage from the PV panel as well as the battery to calculate what amount of power should be used to charge the battery. The microcontroller can then physically change the voltage by driving the buck and boost DC-DC converter in the circuitry.

## 5.2 Hardware Implementation

In order to experimentally test the performance of the proposed MPPT solar charge controller, a prototype is designed and tested experimentally. Full system constructed using one polycrystalline 85 Watt PV module, one 12 V Lead-acid battery and as a load 36 (12*3) Watt DC Light. Individual representation of components that is used to construct the charge controller is listed in Table 5.1.

**Table 5.1 Component List**

| Sl. No. | Product | Model | Quantity |
|---|---|---|---|
| 01 | Microcontroller | PIC16F877A | 01 |
| 02 | Capacitor | 0.1 µF | 04 |
| | | 10 µF-50 V (Electrolyte) | 09 |
| | | 470 µF-50 V (Electrolyte) | 08 |
| | | 1000 µF-16 V (Electrolyte) | 01 |
| 03 | Inductor | 100 µH | 02 |
| 04 | MOSFET | IRFZ44N | 11 |
| 05 | MOSFET Driver | IR2104 | 01 |
| 06 | Voltage Regulator | LM7805 | 01 |
| | | LM7812 | 01 |
| 07 | Inverting Switching Regulator | MC34063A | 01 |
| 08 | Diode | 1N4917 | 07 |
| 09 | Current sensor | ACS712ELCTR-30A-T | 02 |
| 10 | LED | Green | 02 |
| | | Red | 01 |
| | | Blue | 01 |
| 11 | LCD Display | JHD204A | 01 |
| 12 | Bluetooth Module | JU-MCU | 01 |
| 13 | Opto-coupler | PC817 | 01 |
| 14 | Resistor | 220 Ω | 03 |
| | | 1 KΩ | 12 |
| | | 3.3 KΩ | 02 |
| | | 10 KΩ | 05 |
| | | 100 KΩ | 02 |
| 15 | Fuse | T8AL250 V | 02 |
| | | 25 A | 01 |
| 16 | Wire socket | - | 03 |
| 17 | USB port | - | 01 |

To implement this charge controller into hardware shapes and for simplicity total design process is divided into small sections. The sections are described below:

- Buck-boost converter circuit design
- Voltage and Current Measurements
- LCD display and LED indication
- Making the Enclosure
- Making the USB Charging Circuit
- Wi-Fi Data Logging
- MPPT algorithm and flow chart

## 5.2.1 Buck Converter Design

In this hardware design 85 Watt solar panel is used as input source and 12V lead acid battery as storage or load. For this system a buck converter is designed and that mainly consist of:

- Inductor
- Capacitor
- MOSFETS

To run the buck converter selection of frequency switching is most important part. The switching frequency is inversely proportional to the size of the inductor and capacitor and directly proportional to the switching losses in MOSFETs. So higher the frequency, lower the size of the inductor and capacitor but higher switching losses. So a mutual trade-off between cost of the components and efficiency is needed to select the appropriate switching frequency. Keeping these constraints in to consideration assumed selected frequency is 50 KHz.

## 5.2.1.1 Inductor Selection

Calculating the inductor value is most critical in designing a buck converter. Fig. 5.1 (a) shows the inductor designed for the charge controller. First, assume the converter is in continuous current mode (CCM). CCM implies that the inductor does not fully discharge during the switch-off time.

(a)                                                (b)

Fig. 5.1 a) 0.37 µH Inductor b) 470 µF Capacitor

To design a buck converter for 85 W, 12V solar systems the following calculations are made. The first step to calculate the switch current is to determine the duty cycle, D, for the maximum input voltage. The maximum input voltage is used because this leads to the maximum switch current. The efficiency, $\eta$ is added to the duty cycle calculation, because the converter also has to deliver the energy dissipated. This calculation gives a more realistic duty cycle than just the formula without the efficiency factor [31]. Use either an estimated factor, e.g., 90% (which is not unrealistic for a buck converter worst-case efficiency). From the PV panel datasheet,

Input voltage, $V_{in} = 19.7\ V$

Output Voltage, $V_{out} = 12\ V$

Output current, $I_{out} = \frac{85\ W}{12\ V} = 7.08\ A\ (approx)$

Switching Frequency, $F_{sw} = 50\ KHz$

Duty Cycle, $D = \frac{V_{out}}{V_{in} \times \eta}$

$= \frac{12\ V}{19.7\ V \times .9}$

$= 0.68\ or\ 68\%$

Where, $\eta = efficiency\ of\ the\ converter, e.g., estimated\ 90\%$

A good estimation for the inductor ripple current is 20% to 40% of the output current [31]. Therefore, Inductor Ripple Current,

$$\Delta I_L = 40\% \text{ of the output current} \times \text{inductor output current}$$

$$= 0.4 \times 7.08$$

$$= 2.83 \ (approx)$$

Therefore, The value of Inductance,

$$L = V_{in} - V_{out} \times D \times \left(\frac{1}{F_{sw}}\right) \times \left(\frac{1}{\Delta I_L}\right) \tag{5.1}$$

$$= (19.7 - 12) \times 0.68 \times \left(\frac{1}{50000}\right) \times \left(\frac{1}{2.83}\right)$$

$$= 0.37 \ \mu H$$

### 5.2.1.2 Inductor Peak Current

If $I_L = average\ inductor\ current$, then the inductor ripple current $\Delta I_L = 2 I_L$ [32].

Therefore, $Inductor\ Peak\ Current = I_{out} + \frac{\Delta I_L}{2}$

$$= 7.08 + \frac{2.83}{2}$$

$$= 8.5 \ A$$

### 5.2.1.2 Capacitor Selection

Output capacitance is required to minimize the voltage overshoot and ripple present at the output of a buck converter. Large overshoots are caused by insufficient output capacitance, and large voltage ripple is caused by insufficient capacitance as well as a high equivalent-series resistance (ESR) in the output capacitor. Thus, to meet the ripple specification for a buck converter circuit, an output capacitor with ample capacitance is must including low ESR.

Let,

    Inductor ripple current $\Delta I_L = 2.83$ A,

    Switching frequency $F_s = 50\ KHz$ and

    Output ripple voltage, $\Delta V_{out} = 20\ mV$ then the output capacitance,

$$C_{out} = \frac{\Delta I_L}{8 \times F_s \times \Delta V_{out}} \tag{5.2}$$

$$= \frac{2.83}{8 \times 50000 \times 0.02}$$

$$= 353.75 \ \mu F$$

By taking some margin, 470 $\mu F$ electrolytic capacitor are taken. Fig. 5.1 (b) shows the capacitor used for the device.
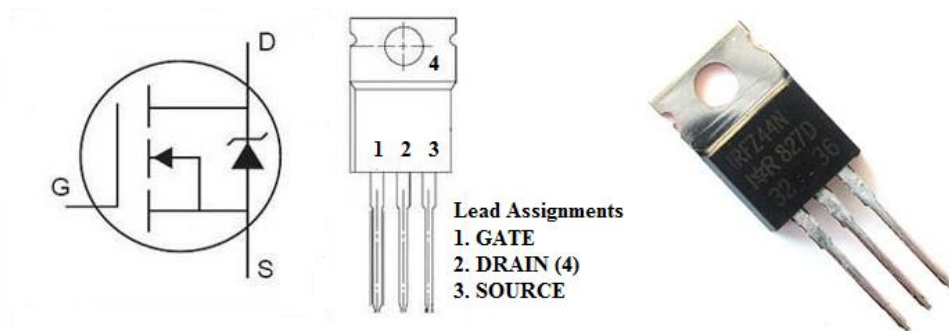


Fig. 5.2 IRFZ44N MOSFET

### 5.2.1.3 MOSFET Selection

The vital component of a buck converter is MOSFET. Fig. 5.2 shows the MOSFET used for this design. IRFZ44N MOSFET is used for better switching. Since it has very low amount of voltage drop it increases the total efficiency of the system. Voltage rating of this solid state device is greater than 20% of rated voltage. Current rating is greater than 20% of rated current. It has minimum conduction loss. IR2104 MOSFET driver is used that accept low power input from the microcontroller and produces a high current drive input for the gate of the MOSFETs. Few basic parameters for selecting right MOSFET are written below:

- **Voltage Rating:** $V_{ds}$ of MOSFET should be greater than 20% or more than the rated voltage.
- **Current Rating:** $I_{ds}$ of MOSFET should be greater than 20% or more than the rated current.
- **ON Resistance ($R_{ds}$ on):** Select a MOSFET with low ON Resistance ($R_{on}$)
- **Conduction Loss:** It depends on $R_{ds}$ (ON) and duty cycle. Keep the conduction loss minimum.
- **Switching Loss:** Switching loss occurs during the transition phase. It depends on switching frequency, voltage, current etc. Switching loss should be keep minimum.

| | | |
|---|---|---|
| 1 | $V_{CC}$ | $V_B$ | 8 |
| 2 | IN | HO | 7 |
| 3 | $\overline{SD}$ | $V_S$ | 6 |
| 4 | COM | LO | 5 |

(a) (b)
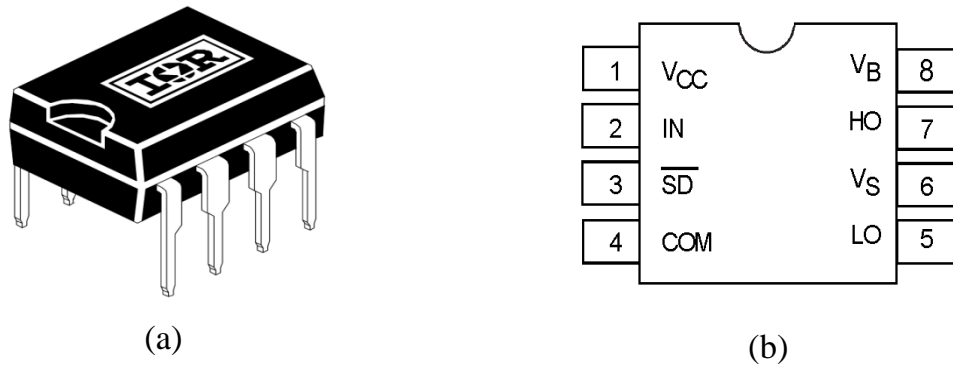
Fig. 5.3 (a) MOSFET driver (b) Pin layout of MOSFET driver

## 5.2.2 MOSFET Driver

A MOSFET driver allows a low current digital output signal from a Microcontroller to drive the gate of a MOSFET. 5 volt digital signal can switch a high voltage MOSFET using the driver. A MOSFET has a gate capacitance that need to charge so that the MOSFET can turn on and discharge it to switch off, the more current provide to the gate the faster switching on/off the MOSFET will be occur, that is why driver should be used. For this design IR2104 Half Bridge MOSFET driver is used. Fig. 5.3 (a) and (b) shows the driver IC and its pin layout respectively. The IC takes the incoming PWM signal from the microcontroller, and then drives two outputs for a high and a low side MOSFET.



(a) (b)
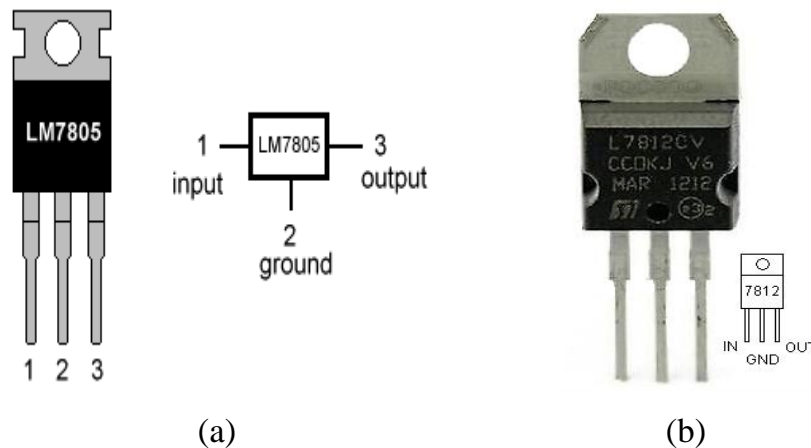
Fig. 5.4 Voltage regulator (a) LM7805, (b) LM7812

## 5.2.3 Voltage Regulator

Two possible voltage regulators have been identified for the design. Fig. 5.4 (a) is shown LM7805 voltage regulator that used before the microcontroller and it regulates

minimal voltage 7.3 V to 5.00 V. And Fig. 5.4 (b) shows the other LM7812 voltage regulator that can operates at minimum voltage of 14.6 to output as 12.0 V.
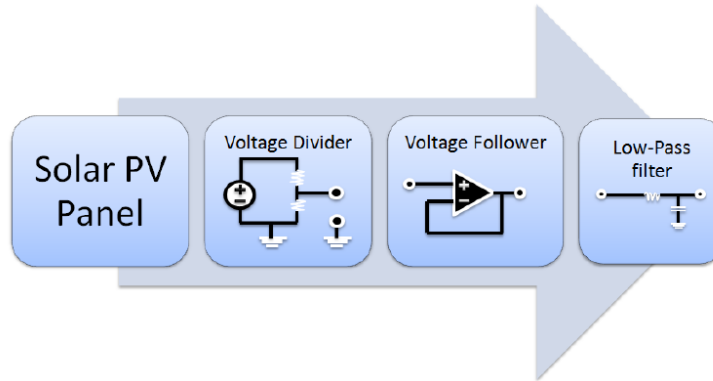


Fig. 5.5 Voltage sensor flowchart [33]
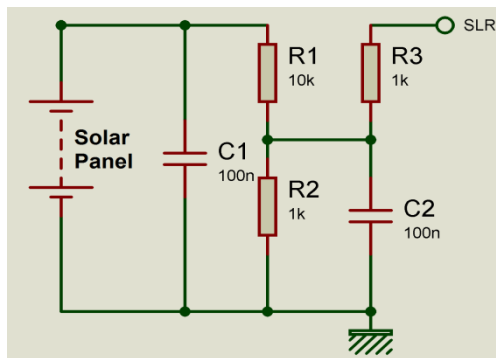


| (a) | (b) |

Fig. 5.6 (a) Voltage divider circuit, (b) ACS712 current sensor

### 5.2.4 Voltage Sensor

Fig. 5.5 is a flow chart describing the different parts that the voltage sensor circuit is going to be composed of. This sensor is responsible for calculating the voltage in real-time of the operating solar PV panel which is depicted to the left of the flow chart. Fig. 5.6 (a) shows a voltage divider circuit that acts as voltage sensor. The output terminal of the panel will run into the voltage divider circuit where the voltage will be distributed across resistors $R_1$ and $R_2$. This sensor is responsible for calculating the voltage of the operating solar PV panel in real-time. In order to monitor and calculate the voltage output, the properties of a voltage divider circuit configuration are used. Two resistors ($R_1$ and $R_2$) are placed in series with each other

and in parallel with the PV panel. The values given to the resistors are determined by the power specifications of the solar panel and the input specifications of the microcontroller ports. Ideally, $R_1$ would have a high resistance value, around the Mega ohms range. This high resistance value will keep the sensor circuit from receiving high flows of current, which would result in energy loss and could potentially damage the circuit. The voltage across $R_2$, denoted as $V_2$, is the output voltage that is going to be monitored to detect any variance in the voltage generated by the panel.
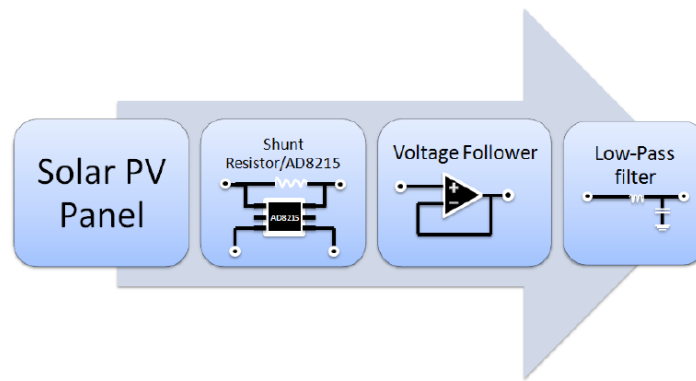


Fig. 5.7 Current sensor flowchart [33]

Before feeding this analog voltage into the microcontroller, it needs to go through some filtering to maintain an accurate reading. $V_2$ is first fed into unit amplifier or voltage follower circuit. This helps isolate the circuit so that no further implementation of electric components would affect the voltage across resistor $R_2$. After the voltage follower, the output is then fed into a low-pass filter in order to prevent noise spikes in the signal resulting in false readings. Once the signal has gone through the low-pass filter, it is finally fed into the A-to-D converter in the microcontroller to later be implemented in the algorithm used to find the MPP.

### 5.2.5 Current Sensor

The flow chart for the current sensor shown in Fig. 5.7 follows a similar path as the voltage sensor but this time the current that is output by the solar panel is what needs to be measured, and therefore it is done a little differently. The output of the panel is connected in series with a shunt resistor. These resistors will typical have a low

resistance that is around the milli-ohms. The purpose here is not to block the flow of current coming out the solar panel by placing a higher resistor value; instead, it is important that the current flows as freely as possible so that an accurate reading can be recorded. The focus is to let as much as current through as possible with a very little resistance so that just a small voltage drop is generated across the shunt resistor and then monitored by the AD8215. Since the voltage across the shunt resistor is too small to be use for actual measurements in a device, this voltage is amplified by the AD8215 by about twenty times. Once the voltage has being amplified, the output generated by the AD8215 chip is now useful for actually readings purposes. From this point on, the way the signal is treated is similar to that of the voltage sensor. First, the output is isolated from the rest of the circuit by a voltage follower, and then it is finally fed into a low-pass filter where any noise spikes are rejected. Once the signal has been filter out from potential noise, it can finally be fed into the AD converter pin of the microcontroller to be implemented in the MPPT.

The use of an electric sensor is essential in the design in order to get the maximum power output from the solar panel array. The electric sensor will be in charge of keeping track of the current that the panel outputs at all times. These readings will be fed into the microcontroller in order to provide the user with real-time values of the current by displaying them on the LCD screen. Most importantly, the current sensor will play a significant role in the realization of the MPPT in order to achieve the maximum output power from the panel. Two possible sensors have been identified for the design, one is an AD8215 current shunt monitor from Analog Devices which and the other is an ACS712 current sensor produced by Allegro Microsystems.

### 5.2.5.1 ACS712 Current Sensor

The ACS712 is a very cheap, accurate and easy to implement electric sensor chip available from Allegro Microsystems. It is a fully integrated current sensor that gives precise current measurement for both AC and DC signals. The great precision and accuracy of the sensor is due to factory trimming. The sensor comes mounted in a PCB board that is nearly the size of a quarter. Because it comes pre-soldered on a

PCB as shown in Fig. 5.6 (b), the sensor can be easily soldered to other parts in the circuit [34]. The device bandwidth can be easily set via the "FILTER" pin shown in Fig. 5.6 (b).



**40-Pin PDIP**

| | | | | |
|---|---|---|---|---|
| $\overline{MCLR}/V_{PP}$ → | 1 | | 40 | ← RB7/PGD |
| RA0/AN0 ↔ | 2 | | 39 | ← RB6/PGC |
| RA1/AN1 ↔ | 3 | | 38 | ← RB5 |
| RA2/AN2/$V_{REF}$-/$CV_{REF}$ ↔ | 4 | | 37 | ← RB4 |
| RA3/AN3/$V_{REF}$+ ↔ | 5 | | 36 | ← RB3/PGM |
| RA4/T0CKI/C1OUT ↔ | 6 | | 35 | ← RB2 |
| RA5/AN4/$\overline{SS}$/C2OUT ↔ | 7 | | 34 | ← RB1 |
| RE0/$\overline{RD}$/AN5 ↔ | 8 | PIC16F874A/877A | 33 | ← RB0/INT |
| RE1/$\overline{WR}$/AN6 ↔ | 9 | | 32 | ← $V_{DD}$ |
| RE2/$\overline{CS}$/AN7 ↔ | 10 | | 31 | ← $V_{SS}$ |
| $V_{DD}$ → | 11 | | 30 | ← RD7/PSP7 |
| $V_{SS}$ → | 12 | | 29 | ← RD6/PSP6 |
| OSC1/CLKI → | 13 | | 28 | ← RD5/PSP5 |
| OSC2/CLKO ← | 14 | | 27 | ← RD4/PSP4 |
| RC0/T1OSO/T1CKI ↔ | 15 | | 26 | ← RC7/RX/DT |
| RC1/T1OSI/CCP2 ↔ | 16 | | 25 | ← RC6/TX/CK |
| RC2/CCP1 ↔ | 17 | | 24 | ← RC5/SDO |
| RC3/SCK/SCL ↔ | 18 | | 23 | ← RC4/SDI/SDA |
| RD0/PSP0 ↔ | 19 | | 22 | ← RD3/PSP3 |
| RD1/PSP1 ↔ | 20 | | 21 | ← RD2/PSP2 |

Fig. 5.8 Wireless data transfer by Bluetooth module JU-MCU

### 5.2.6 Wireless Data Transfer

Bluetooth module is popular in short range wireless data transmission. It is a type of wireless communication protocol that is used to send and receive data between two devices. Although its range is lower than other wireless communication protocols like WiFi and ZigBee. But it is still suitable for many low range applications. Bluetooth wireless protocol lies in the same range of frequency of WiFi and ZigBee. This module operates on 2.41 GHz frequency. Fig. 5.8 shows a connection diagram of Bluetooth module JU-MCU with the microcontroller. This module has four output pin RXD, TXD, GND and VCC. RXD and TXD pin directly connected to the pin RC7 and RC6 respectively to the PIC-16F874A/877A microcontroller.

### 5.2.7 External Device Charging Unit

External device or mobile charger unit is designed by Proteus software, shown in Fig. 5.9. This circuit allowed to convert 12 V battery voltage to 5.3 V mobile charging voltage.
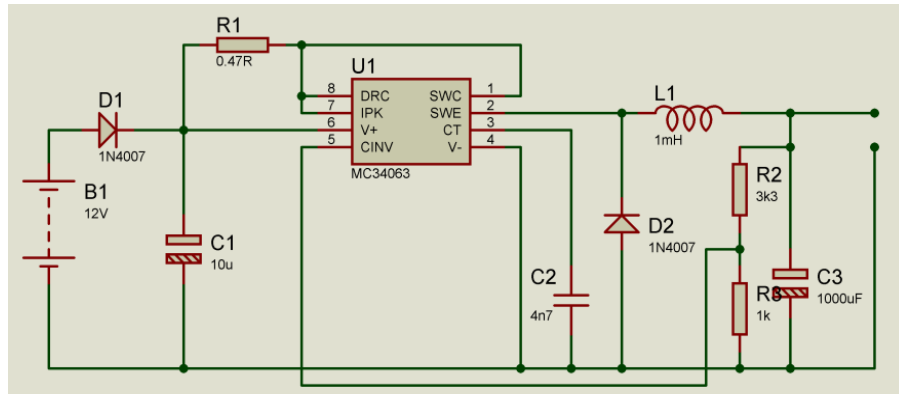
Fig. 5.9 Mobile charger unit by Proteus

### 5.2.8 Liquid Crystal Display (LCD)

A character LCD display is chosen that can consume less than 100 mA when fully backlit.  In addition, character LCD screen would provide the right balance of power consumption and image size/quality making it the most viable option. Based on these considerations a $20 \times 4$ character LCD was chosen for implementation into the charge controller design. This should provide ample space to display several quantitative values as well as any status indicators that need to be included. The specific display chosen is the serial enabled LCD-204A from JHD, shown in Fig. 5.10.



Fig. 5.10 LCD display from JHD

### 5.2.9 LED Indication

A manual indicator circuit also used to indicates system condition. Green, Blue and Red LEDs are used to indicate the battery voltage level.

- Bulk Charge: Green LED
- Float Charge: Blue LED
- Low Charge: Red LED
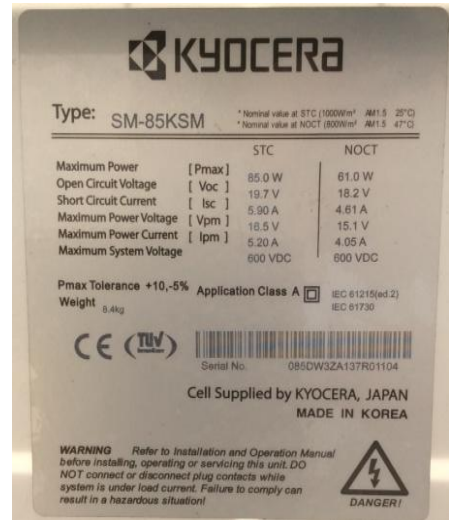
<div align="center">(a)                 (b)</div>

Fig. 5.11 (a) Solar panel of SM-85KSM by KYOCERA (b) Specification label

## 5.3 Solar Panel

Although there are many options for solar panel technologies, for this design a mono-crystalline solar panel is used. Polycrystalline silicon panels are not far behind in efficiency but they are not much cheaper than mono-crystalline panels. The panel that has been chosen for use in this project is the KYOCERA SM-85KSM. Fig. 5.11 (a) and (b) shows the panel and the specific label respectively. Table 5.2 is showing the electrical performance under standard test condition, Table 5.3 shows the module characteristics.

**Table 5.2 Electrical Performance under Standard Test Conditions (*STC)**

| | |
|---|---|
| Maximum Power (Pmax) | 85W (+10%, -5%) |
| Maximum Power Voltage (Vpm) | 16.5V |
| Maximum Power Current (Ipm) | 5.20A |
| Open Circuit Voltage (Voc) | 19.7V |
| Short Circuit Current (Isc) | 5.90A |
| Max System Voltage | 600VDC |
| Temperature Coefficient of Voc | $-0.70 \times 10^{-1}$ V/℃ |
| Temperature Coefficient of Isc | $1.66 \times 10^{-3}$ A/℃ |
| *STC : Irradiance 1000W/㎡, AM 1.5 spectrum, cell temperature 25℃ | |

**Table 5.3 Module Characteristics**

| Number of Cells | 36 Cells |
|---|---|
| Cell Technology | Multi Crystalline |
| Length × Width × Depth without box | 1030×680×38mm |
| Weight | 9.4 Kg |
| Cable | 1000mm (+/-) |
| * NOCT (Nominal Operating Cell Temperature) : 47℃ ||

## 5.4 Battery or Storage

Batteries are divided into two main categories: primary or disposable and secondary or rechargeable. The most prevalent materials used in batteries today are lithium, lead, and nickel. Primary batteries have higher energy densities than secondary and are typically used when recharging is unfeasible. Lithium-metal and alkaline are among the most common primary battery types and are found in numerous applications from remote controls, watches, and toys. However, off-grid photovoltaic systems require recharging so the focus will be on secondary battery types. Some of the chemistries used in secondary batteries are: lead-acid, nickel-cadmium (NiCd), nickel-metal-hydride (NiMH), and lithium-ion.

### 5.4.1 Lead-Acid Batteries

Though numerous rechargeable batteries exist, the most commonly used battery in PV systems is the deep-cycle lead-acid battery. There are three types of lead-acid batteries.

- Starting,
- Deep-cycle and
- Marine.

The starting lead-acid is typical automotive battery used to start a car. This type of battery has many thin plates of lead which allows for a high current output. The deep-cycle lead-acid battery has thicker lead plates which allow this type of battery to be discharged and recharged many times without degradation. One drawback is the fact

that there is lower surface area between the lead plates and the acid electrolyte meaning smaller current. A marine lead-acid battery falls somewhere in between the automotive and deep-cycle. The lead plates are thinner than deep-cycle yet thicker than a starting battery which gives it better current output and shorter lifetime when used in deep-cycle applications. In the domain of deep-cycle lead-acid batteries there are three types of battery construction.

- Flooded

- Gel and

- Absorbed glass mat (AGM).

Flooded lead acids are the cheapest and most common construction type. The electrolyte in this type of battery (30% sulfuric acid, 70% water) is in a liquid form [35]. The gel type batteries use a thickening agent to hold the electrolyte in place. This prevents leakage in the event that the case is damaged. This type of battery is sealed, which means that in the event that a significant amount of electrolyte is evaporated, it cannot be re-filled. Absorbed glass mat lead-acid batteries are by far the most advantageous of the three types of construction. These batteries have a very slow self-discharge rate and are resistant to shock and vibration damage. The main disadvantage to AGMs is that they usually cost two to three times that of a flooded lead-acid of the same capacity.
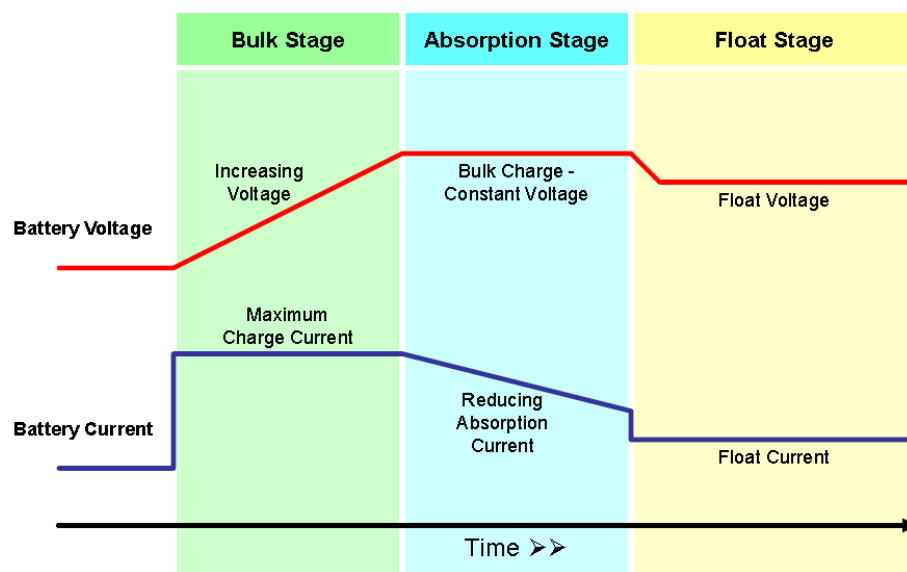


Fig. 5.12 Charging process for a typical lead-acid battery

### 5.4.2  Battery Charging Algorithms

Though the charging algorithms for each battery are different but they have same general charge stages in common. Fig. 5.12 represents three stages of battery charging process graphically.

- **Bulk Charging**

  In the first stage, **bulk charging** a constant current is applied to the battery. The charging voltage can range from about 11V to 15V for a 12V battery. The only requirement being that the charging voltage must be set higher than the current battery voltage.  A typical battery can be considered "fully discharged" when the voltage reaches 10.5V. The MPPT charge controller will contribute to improved efficiency primarily in the bulk charging stage.

- **Absorption Charging**

  The second stage is **absorption charging** begins immediately after the bulk charging stage (when the battery voltage reaches a pre-determined limit). In this stage, the charging voltage is held at a constant value and current decreases as the internal resistance of the battery increases.

- **Float Charging**

  The final stage in a typical three-stage charging process is called the **float charging** stage. In this stage the charging voltage is set to a constant value but at a lower level than the absorption stage. The float stage compensates for self-discharge or gradual loss of voltage over time, which plagues all battery chemistries.

One crucial parameter to battery charging is temperature. The temperature should be monitored and charge voltage and current values should take the temperature into account. High current and environmental factors can cause battery temperature to rise and voltage decreases with increased battery temperature. The algorithms executed by the microcontroller will factor in battery temperature when calculating current and voltage values to both maximize efficiency and provide emergency cutoff in the event that the temperature reaches an unsafe level.

## 5.5 Hardware Schematic

Fig. 5.13 presents the block diagram of the designed charge controller system. Generated voltage and current from the PV module enter through the voltage and current sensor respectively. A voltage divider circuit acts as voltage sensor and ACS712 current sensor is used to detect over current. Output of the voltage and current sensor fed to the input of PIC16F877A microcontroller as analog input. In the same time, same voltage and current fed to the buck converter. Buck converter maintenance the voltage required to charging up the battery. Simply, it converts the nonlinear panel voltage to 12 volt. To control over voltage or current, converter is also connected to sensor that can detect and protect the battery from over charge, deep discharge etc. A Bluetooth device is connected to microcontroller, which is interfaced by a mobile phone. An app helps to monitor overall system status through the phone. A 20×4 character display will continuously show the system status including voltage, current and power of both panel and battery, charging percentage of battery, load condition etc.
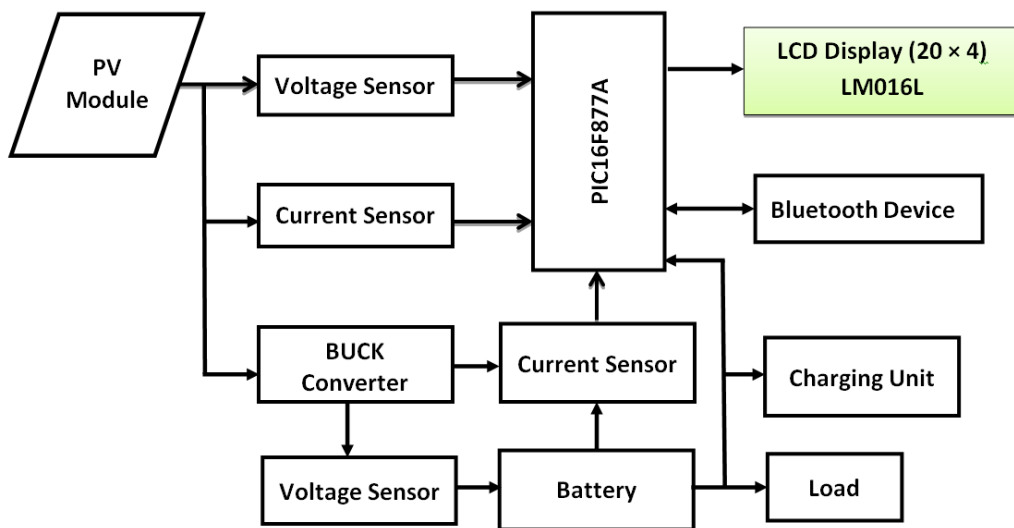
Fig. 5.13 Block diagram of the researched charge controller system

The schematic diagram of the designed charge controller is shown in Fig. 5.14, designed by Proteus software. Top right side shows the Microcontroller and LCD display interfacing connection. The input power connector to the solar panels is the screw terminal JP1 and JP2 is the output screw terminal connector to the battery. The third connector JP3 is connection for the load. FU1, FU3 are 8A and FU2 is the 25A

safety fuses. The buck converter is made with synchronous MOSFET switches Q2 and Q3 and the energy storage devices inductor L1 and capacitors C8. Inductor smoothes the switching current. Along with capacitor C8 smoothes the output voltage. Capacitor C8 and R6 are a snubber network, used to cut down on the ringing of the inductor voltage generated by the switching current in the inductor. The third MOSFET Q1 is added to allow the system to block the battery power from flowing back into the solar panels at night. As all diodes have a voltage drop a MOSFET is much more efficient than diodes. Q1 turns on when Q2 is on from voltage through D1. R1 drains the voltage off the gate of Q1 so it turns off when Q2 turns off. The diode D3 (UF4007) is an ultra fast diode that will start conducting current before Q3 turns on. It is supposed to make the converter more efficient. The IC IR2104 is a half bridge MOSFET gate driver. It drives the high and the low side MOSFETs using the PWM signal from the microcontroller. The IR2104 can also be shut down with the control signal from the microcontroller.
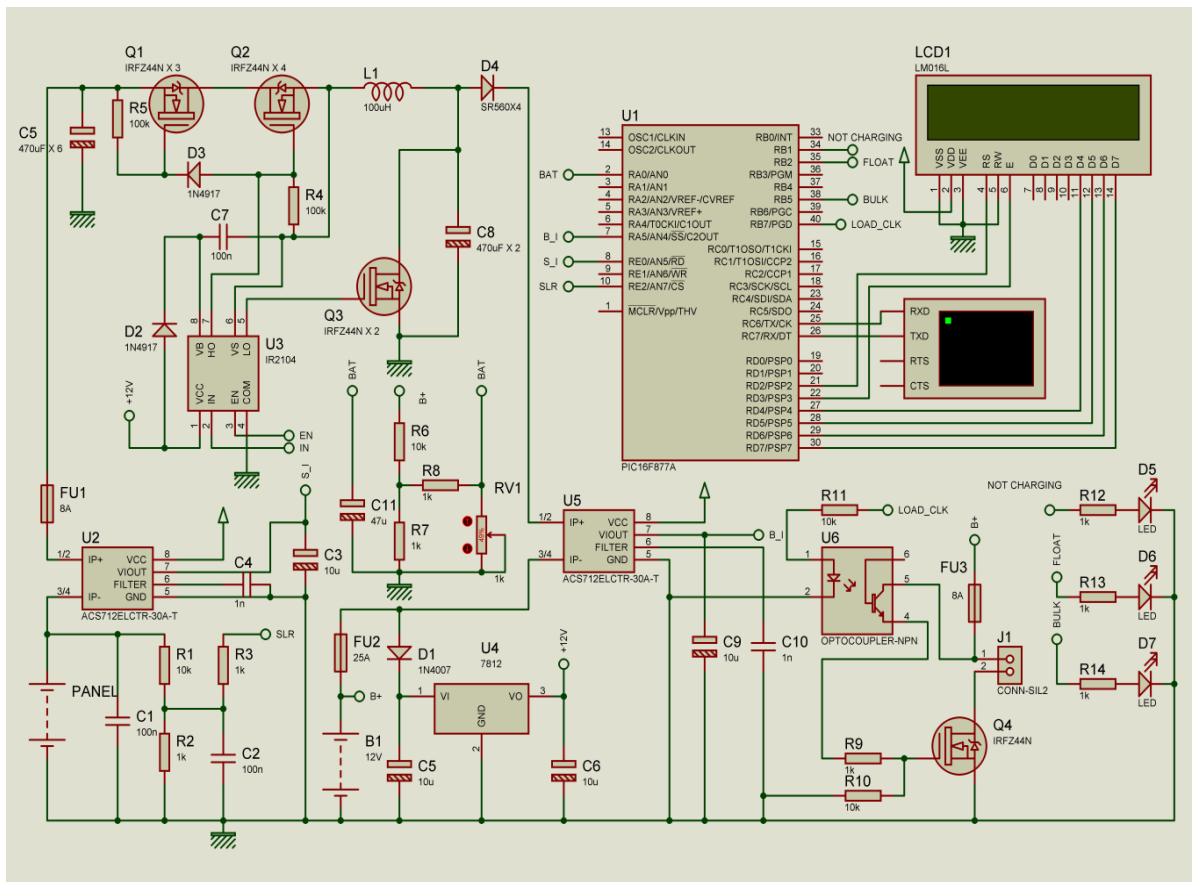


Fig. 5.14 Schematic circuit layout of designed solar charge controller

D2 and C7 are part of the bootstrap circuit that generates the high side gate drive voltage for Q1 and Q2. The software keeps track of the PWM duty cycle and never allows 100% or always on. It caps the PWM duty cycle at 99.9% to keep the charge pump working. In this circuit layout, two voltage divider circuits (R1, R2 and R3, R4) are to measure the solar panel and battery voltages. The output from the dividers are feeds the voltage signal to Analog pin-0 and Analog pin-2. The ceramic capacitors C3 and C4 are used to remove high frequency spikes. The MOSFET Q4 is used to control the load. The driver for this MOSFET is consists of a transistor and resistors R9, R10. The diode D4 and D5 are TVS diodes used for over voltage protection from solar panel and load side. The current sensor ACS712 senses the current from the solar panel and feeds to the microcontroller pin-1. The 3 LEDs are connected to the digital pins of the microcontroller and serve as an output interface to display the charging state. Reset switch is helpful if the code gets stuck. The back light switch is to control the back light of LCD display.
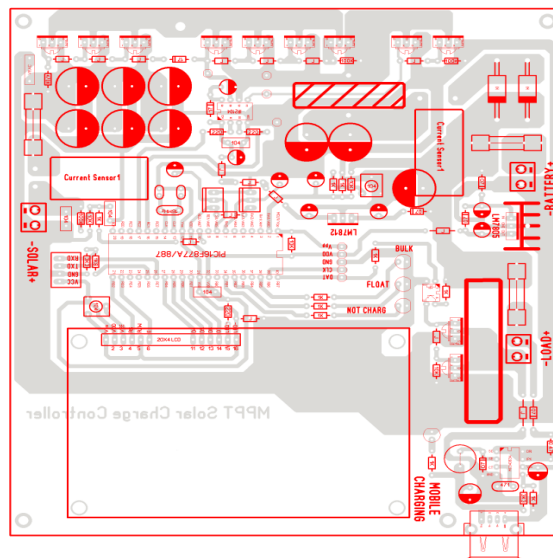


Fig. 5.15 PCB design of solar MPPT charge controller

## 5.6 PCB Design

A custom printed circuit board (PCB) will be designed for hardware implementation of the solar MPPT charge controller that is shown in Fig. 5.15. The board is designed using circuit board design software, CadSoft's Eagle PCB Design. A designed PCB allows for the best performance and optimization, along with a nice clean look.

## 5.7 Final Design

Fig. 5.16 presents the designed hardware device, indicating all the specific parts integrated to work it as a MPPT solar charge controller. Input as the solar panel output connected through the left side of the device. Output as the load and external device charging USB unit in the right side of the device, battery connector is also the same side. Two current sensors make sure high excessive current protection of the total system. Two fuses used both the panel and battery sides, 10A fuse in the panel side and 25A fuse in the battery side.
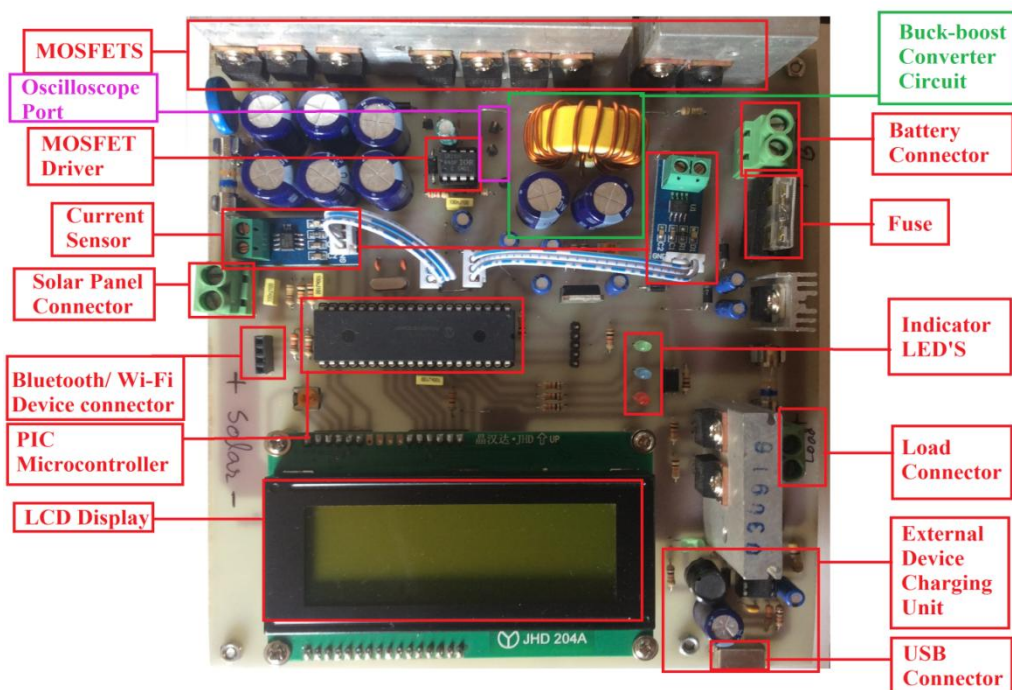


Fig. 5.16 Designed MPPT solar charge controller

## 5.8 Cost Analysis

Parts are bought in December 2015 and the price list is shown in Table 5.4. This price may vary with current price. Total unit price of the parts is BDT 2047 (USD 26). Highest value among the parts is the LCD display (BDT 450), current sensor (BDT 250) and the Bluetooth device (BDT 270). By neglecting these costly features, this MPPT solar charge controller can be industrialized within only BDT 800 (approx) only.

**Table 5.4 Component List with Unit Price**

| Sl. No. | Product | Model | Quantity | Unit price (BDT) | Total Price (BDT) |
|---|---|---|---|---|---|
| MPPT solar charge controller, 12 V, 10 A | | | | |
| 01 | Microcontroller | PIC16F877A | 01 | 200 | 200 |
| 02 | Capacitor | 0.1 µF | 04 | 0.50 | 02 |
| | | 10 µF-50 V (Electrolyte) | 09 | 1.25 | 11.25 |
| | | 470 µF-50 V (Electrolyte) | 08 | 8 | 64 |
| | | 1000 µF-16 V (Electrolyte) | 01 | 12 | 12 |
| 03 | Inductor | 100 µH | 02 | 5 | 1.00 |
| 04 | MOSFET | IRFZ44N | 11 | 26 | 286 |
| 05 | MOSFET Driver | IR2104 | 01 | 120 | 120 |
| 06 | Voltage Regulator | LM7805 | 01 | 15 | 15 |
| | | LM7812 | 01 | 15 | 15 |
| 07 | Inverting Switching Regulator | MC34063A | 01 | 10 | 10 |
| 08 | Diode | 1N4917 | 07 | 1.00 | 7.00 |
| 09 | Current sensor | ACS712ELCTR-30A-T | 02 | 250 | 500 |
| 10 | LED | Green | 02 | 0.50 | 1.00 |
| | | Red | 01 | 0.50 | 0.50 |
| | | Blue | 01 | 0.50 | 0.50 |
| 11 | LCD Display | JHD204A | 01 | 450 | 450 |
| 12 | Bluetooth Module | - | 01 | 270 | 270 |
| 13 | Opto-coupler | PC817 | 01 | 5 | 5.00 |
| 14 | Resistor | 220 Ω | 03 | 0.50 | 1.50 |
| | | 1 KΩ | 12 | 0.50 | 6.00 |
| | | 3.3 KΩ | 02 | 0.50 | 1.00 |
| | | 10 KΩ | 05 | 0.50 | 2.50 |
| | | 100 KΩ | 02 | 0.50 | 1.00 |
| 15 | Fuse | T8AL250 V | 02 | 5 | 10 |
| | | 25 A | 01 | 15 | 15 |
| 16 | Wire socket | - | 03 | 10 | 30 |
| 17 | USB port | - | 01 | 10 | 10 |
| | **Total Product Cost** | | | | **2047** |

## 5.9 Experimental Setup

Fig.5.17 shows the experimental set up and testing of the charge controller. A solar panel of 85W is installed in the rooftop, Battery and other testing device including the charge controller are set up in the laboratory room. A battery of 12V, 100Ah is used to store the charges, oscilloscope to visualize the MOSFET pulses and the digital multimeter are used to check the buck-boost voltages. Analog meter helps to compare the related value displaying in the LCD display. It's clearly evident that the system is working very well and it has been continuously tested for two months.



Fig. 5.17 Experimental setup of the designed solar charge controller

## 5.10 Experimented Data

The designed charge controller has been tested for eight (08) days. Among the experimented day's data of 24 February 2016 are shown in Table 5.7. This data is recorded from 8.55 AM to 5.00 PM. Table 5.5 is showing the both panel and batteries voltage, current and power. Efficiencies are also determined from this Table. Average efficiency is 96.03%. Fig. 5.18 shows the efficiency recorded from the designed charge controller. In the beginning of the day at 8.55 AM panel power was 22.75W, battery power was

**Table 5.5 Experimented Data with Efficiency of the Designed Charge Controller**

| Sr. No | Time | Panel | | | Load | | | Efficiency (%) |
|---|---|---|---|---|---|---|---|---|
| | | Voltage (V) | Current (A) | Power (W) | Voltage (V) | Current (A) | Power (W) | |
| 1 | 08.55AM | 14.4 | 1.58 | 22.75 | 12.6 | 1.76 | 22.18 | 97.47 |
| 2 | 09.25AM | 13.9 | 2.89 | 40.17 | 13.4 | 2.83 | 37.92 | 94.40 |
| 3 | 09.55AM | 14.2 | 1.99 | 28.26 | 13.0 | 1.74 | 22.62 | 80.05 |
| 4 | 10.25AM | 13.6 | 1.89 | 25.70 | 13.3 | 1.92 | 25.54 | 99.35 |
| 5 | 10.55AM | 14.0 | 2.45 | 34.30 | 13.6 | 2.51 | 34.14 | 99.52 |
| 6 | 11.25AM | 14.1 | 2.58 | 36.39 | 13.9 | 2.61 | 36.27 | 99.73 |
| 7 | 11.55AM | 14.2 | 0.26 | 03.69 | 12.2 | 0.25 | 03.05 | 82.61 |
| 8 | 12.25PM | 14.2 | 2.78 | 39.48 | 13.9 | 2.82 | 39.19 | 99.30 |
| 9 | 12.55PM | 13.8 | 1.92 | 26.49 | 13.5 | 1.95 | 26.33 | 99.35 |
| 10 | 01.22PM | 14.0 | 2.59 | 36.26 | 14.1 | 2.53 | 35.68 | 98.38 |
| 11 | 01.52PM | 14.3 | 1.77 | 25.31 | 13.5 | 1.87 | 25.25 | 99.74 |
| 12 | 02.10PM | 13.9 | 0.47 | 06.53 | 12.8 | 0.47 | 06.02 | 92.09 |
| 13 | 02.30PM | 14.0 | 1.79 | 25.06 | 13.5 | 1.80 | 24.30 | 96.97 |
| 14 | 02.55PM | 14.5 | 2.64 | 38.28 | 14.1 | 2.68 | 37.78 | 98.71 |
| 15 | 03.25PM | 13.4 | 0.51 | 06.83 | 12.9 | 0.52 | 06.71 | 98.16 |
| 16 | 04.00PM | 13.4 | 0.47 | 06.29 | 12.9 | 0.47 | 06.06 | 96.27 |
| 17 | 04.25PM | 13.3 | 0.45 | 05.98 | 12.9 | 0.46 | 05.93 | 99.15 |
| 18 | 04.55PM | 13.3 | 0.55 | 07.32 | 12.9 | 0.55 | 07.09 | 96.99 |
| 19 | 05.00PM | 13.3 | 0.47 | 06.25 | 12.8 | 0.47 | 06.02 | 96.24 |
| | **Average** | | | | | | | **96.03** |
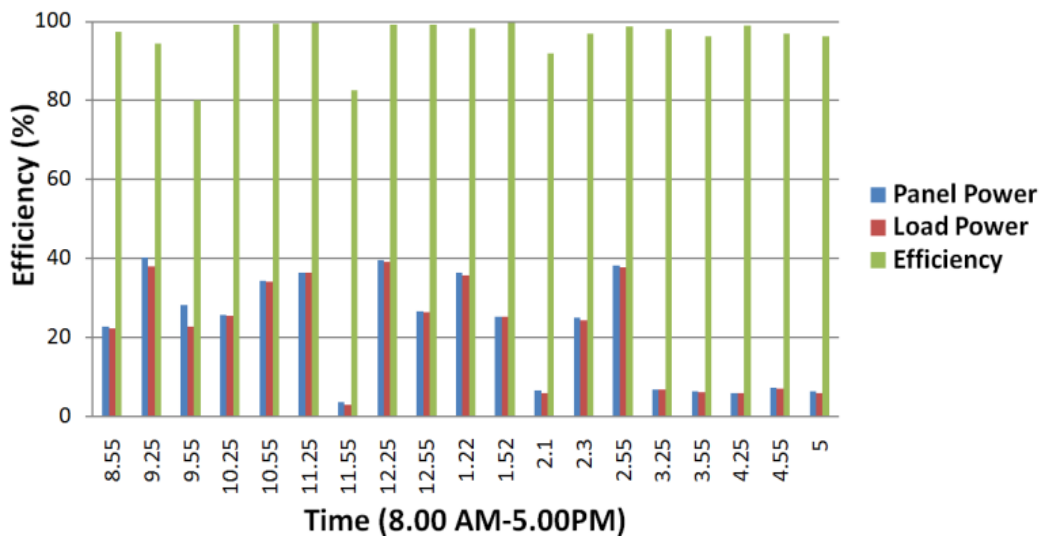


Fig. 5.18 Graphical representation of the charge controller efficiency

22.18W and charge controller efficiency was 97.47%. At the end of the day, at 5.00PM panel and battery power is recorded 6.25W and 6.02W respectively, and the efficiency measured 96.24%. Experiment shows that the efficiency level is almost

over than 95%. It is also evident that due to low sunlight does not affect the efficiency of the CC and it works properly. Additionally, reverse power protection also works good due to night or less sunlight. In the same time, excessive current flow due to over load system is protects perfectly, due to low voltage control unit disconnect the load side as well as protect due to over voltage. The total eight days experimented average efficiency of the designed solar MPPT charge controller is 96.52%. Table 5.6 shows average efficiency of the charge controller of eight days.

**Table 5.6 Average Efficiency for Experimented Days**

| Date of Experiment | Time | Average Efficiency (%) |
|---|---|---|
| 18.2.16 | 8.56AM-2.46PM | 98.50 |
| 23.2.16 | 9.50AM-3.18PM | 97.87 |
| 24.2.16 | 8.55AM-5.05PM | 97.49 |
| 25.2.16 | 8.52AM-3.52PM | 98.21 |
| 26.2.16 | 8.17AM-11.06PM | 91.49 |
| 28.2.16 | 8.22AM-5.38PM | 93.74 |
| 29.2.16 | 8.23AM-3.10PM | 97.68 |
| 01.3.16 | 8.04AM-3.04PM | 97.16 |
| **08 Days** | 44 Hour 42 Minute | **96.52** |

## 5.11  Testing Results

Features are added to this device are implemented well and working properly. Field test of some special features like LCD display, wireless data transfer and external device charging unit are discussed below.

### 5.11.1 LCD Display

Fig. 5.19 shows the full hardware system in testing period and the LCD display that represent the full system status. There are three columns of data. First column shows the solar panel voltage, current and power condition. Second column shows the battery voltage, current and charging state condition. Third column shows pulse width status with load on or off condition.
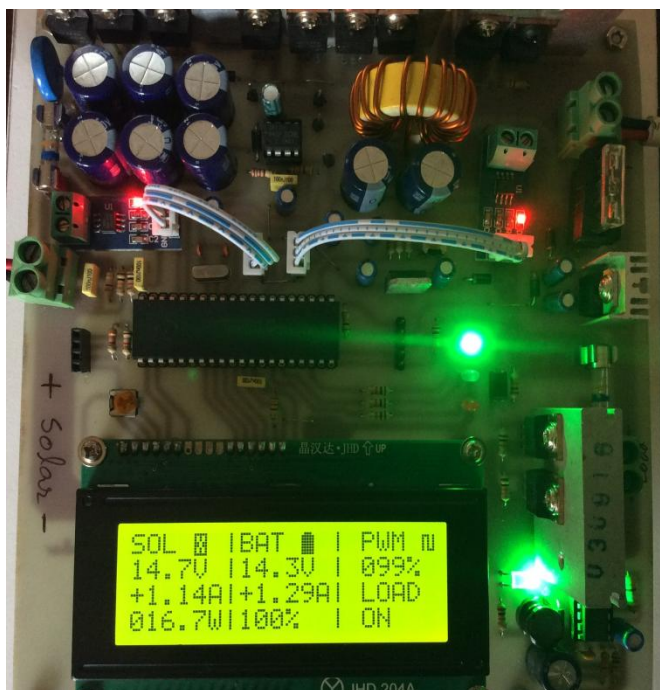
Fig. 5.19 LCD display is working properly
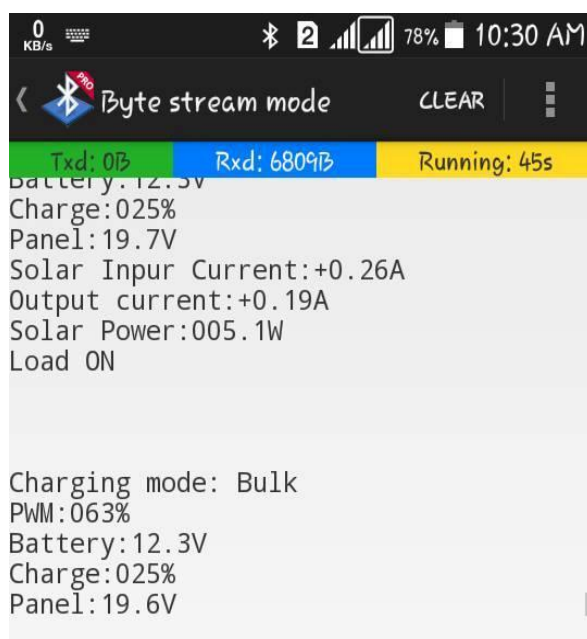


Fig. 5.20 Wireless data transfer to smart phone

### 5.11.2 Wireless Data Transfer

The same data displaying the LCD monitor is directly transferable to a handset or laptop through a Wi-Fi or Bluetooth module. This enables an advantage to maintain or observe the system from any place connected with internet. For the convenience a

Bluetooth device is used and "Bluetooth SPP Pro" android open source application is used to receive and monitor the system status. Fig. 5.20 shows the receiving data from the Bluetooth device through android applications. This data are proven with LCD display and analog meters used in the testing time.



Fig. 5.21 External device charging unit

## 5.11.3 External Device Charging

To test the external device charging unit, a mobile phone is used and tested very well. Fig. 5.21 shows the charging test period. The mobile is showing its charging up 45%.

## 5.12    Conclusion

Finally, an efficient MPPT solar charge controller is designed and tested. The controller is designed with several smart features that have been added to increase the ease of use and make this device more users friendly. In order to quick view the system status an LCD screen has been attached to the charge controller to display several values such as current, voltage, power, load and state of charge of the battery. In addition, this information will be transmitted wirelessly to a separate Bluetooth module that is attached to a smart phone or computer. An external charging unit added to charge up any electronic gadgets like mobile phone or laptop. Experimented average efficiency of the designed charge controller is 96.52% and total cost is around BDT 2047 (Approximate USD 26).

# CHAPTER 6
# CONCLUSIONS AND FUTURE WORK

## 6.1 Summary

The concept for the design has been developed to make a solar charge controller more relevant to home system, industrial practices and needs. The most significant change would be the addition of the display system, external device charging unit, wireless data transfer for monitoring or remote control and customized programmable control unit. This adjustment is the main contributions presented in the thesis.

Live and past data is of great value to both industrial and research entities. Over time both could benefit from learning about how atmospheric conditions affect the efficiency of the photovoltaic system. Meanwhile, live monitoring would be inherently useful for maintenance and alerting the user of any status issues, significantly reducing down time and unnecessary field surveys. This thesis intends to give a contribution for the solar system including battery charging process by implementing a MPPT control system that allows a safe and fast charging process using a duty cycle ratio control. By doing this, it is attended to achieve better performance and efficiency for the charging process. Experiments prove that the designed charge controller has an average efficiency of 96.52%. The MPPT algorithm was used and allowed to simulate the system behaviour for different conditions. For the theoretical analysis, Matlab/Simulink environment are employed.

In Chapter 2, a detail description of the PV system has been given including electrical models for each of the components namely for the photovoltaic solar cell and for the Lead-Acid battery. The charge controller unit (DC/DC converter and the MPPT algorithm) and the control unit (microcontroller PIC18F4585 and IC SG3524) are presented. Throughout this chapter the MPPT technique implemented is explained and the interconnection of the different elements is set in a clear way. Chapter 3 describes about the charge controller in details starting from the evolution, operating

principle, switching mechanism, classifications of charge controller. Relating this sequence PWM and MPPT techniques are discussed briefly, Pros and cons of this both popular techniques are also shown. In addition, the charge regulation set points, selection of a charge controller are narrated here. The simulation of the system in MATLAB/SIMULINK environment, made in Chapter 4, allowed a better understanding of the system behaviour when in the presence of different irradiance and temperature. The system dynamics is affected for different loads and as a consequence the duty cycle ratio control, that allows the implementation of the MPPT algorithm. Using MATLAB/SIMULINK tool it is possible to conclude that the theoretical assumptions made. The results achieved are in good agreement which is an indicator that the system is properly dimensioned and correctly interconnected. The system is always controlling and seeking for the MPPT. It was also possible to obtain an estimate for the charging process, approximately seven hours for a Lead-Acid battery to fully discharge.

From the theoretical and simulation experiences designed hardware implementation, experiments set up and results of the charge controller are described in Chapter 5. All the components are interconnected and the solar MPPT charge controller prototype was tested. The close agreement between simulation and experimental work shows that the electrical models and the sizing of the entire system accurately predict the system behaviour. The experimental work allowed seeing the real implementation of the MPPT and the functioning of the microcontroller. The controller allowed to correctly charging the Lead-Acid battery and during this process it is possible to see, through measurements in real time, the permanent adjustment in order to achieve always the maximum power transfer from the PV to the battery. The field test occurred in a sunny day and allowed to charge the battery in approximately seven hours. Average charging efficiency 96.52% is determined and cost analysis show the approximate cost around BDT 2047 (USD 26).

Finally, the main goal for this thesis has achieved. The construction of a solar charge controller prototype using a microcontroller, which is based on a MPPT algorithm,

was implemented and tested in a real life possible usage. The final prototype allows verifying the utility and efficiency of the MPPT algorithm in order to constantly transfer the maximum power from the PV to the load. Beyond the practical advantage of getting a real solar charge controller this thesis also allowed to understand the system dynamics and behaviour for different conditions on the load and even for environmental issues.

## 6.2 Future Work

Future work could include simplifying the design to create the most cost effective charge controller possible. This would be necessary to reach a competitive price point that would allow the expense to be justified through energy savings. A significant savings could be achieved through the elimination of the LCD screen. The budgeted cost of the LCD in this system is BDT 450 (approximately $6) and would not be necessary to implement at each charge controller in a solar panel field. For an industrial or consumer application the LCD screen is redundant with the wireless data that is being transferred to the computer so it would be easily removed without losses in functionality.

Depending on the need, wireless capability could be removed as well. Wireless capability would provide unique insight into the system status, MPPT efficiency, as well as allow for remote distress alerts. However, if these benefits are not necessary for the given application, the removal of the wireless Bluetooth modules and the supporting circuitry would equate to a substantial savings BDT 280 (approximately $3.5). Oppositely, in order to investigate a more robust system, additional features could be added that would increase the system performance and allow for advanced operations. One concept that could be applied might be a charge controller with memory so that it could save relevant data and establish good starting points for calculating the maximum power point. This would enable faster acquisition of the MPP therefore making the system more efficient. This would in turn require a faster and more capable microcontroller as well as the addition of memory to the system as previously stated. A different direction to pursue would be to adapt the maximum

power point tracker for use with other renewable energy sources. This tracking technique can be applied to sources such as small water turbines and fixed-pitch-rotor wind-power turbines.

## 6.3 Industrial Scaling

This maximum power point tracking device will serve as a proof of concept and has the potential to be scaled to industrial implementation. Research is being conducted into the concept of implementing a microcontroller based customized solution that would be installed at each solar system. As previously discussed, this research work could act as a precursor to a type of charge controller that could be realized at individual PV or grid connected solar systems. In order to do so, the competitive price point would need to be determined through a rigorous study of the cost of implementation and market research. Once this number is identified, the features could be scaled down appropriately to reach this goal. Consequently, if a charge controller of this type is to be produced at an industrial scale, it would drive down the cost of the parts and manufacturing significantly and should be considered in the initial research into the feasibility of producing such a system.

For industrialization and remote control facility of this charge controller Bluetooth device could replace with WiFi or GSM module that enables the data to be transferred over much larger distances. Alternative would be to incorporate a Wi-Fi (ESP 8266) transceiver or Xbee wireless GSM module which also has a larger range than the current design. This device was not used in the current research because although it transfers data at a high rate, it consumes more power.

This research for solar MPPT charge controller designed for an off-grid system and uses a battery to store its power. And it would be beneficial to develop an MPPT charge controller to interface with a grid tied system in industrial purposes.

# REFERENCES

[1] Mohamad A. S. Masoum, Seyed Mahdi Mousavi and Ewald F. Fuchs, "Microprocessor-Controlled New Class of Optimal Battery Chargers for Photovoltaic Applications", *IEEE Transactions on Energy Conversion*, vol. 19, no. 3, Sep. 2004.

[2] J. Appelbaum, "Starting and steady state characteristics of DC motors powered by solar cell generators", *IEEE Trans. Energy Conversion*, vol. EC-1, pp. 17-25, Mar. 1986.

[3] K. Tanaka, E. Sakoguchi, Y. Fukuda, A. Takeoka, and H. Tokizaki, "Residential solar powered air conditioner", in *Proc. Eur. Power Electronics Conf.,* Brighton, U. K., pp. 127-132, Apr. 1993.

[4] S. Rahman and K. Tam, "A Feasibility Study of Photovoltaic Fuel Cell Hybrid Energy System", *IEEE Trans. Energy Conversion*, vol. 3, pp. 50-55, Mar. 1988.

[5] E. Koutroulis and K. Kalitzakis, "Novel Battery Charging Regulation System for Photovoltaic Applications", *IEE Proc.-Electr. Power Appl,* vol. 151, no. 2, Mar. 2004.

[6] Md Hossam-E-Haider and Md. Rokonuzzaman "Design of an Efficient Energy Generating Systems Using Speed Breaker for Bangladesh" The 5th National Symposium on Information Technology: Towards Smart World from 17-19 February, 2015, King Saud University (KSU), Riyadh, Saudi Arabia.

[7] N. Femia, D. Granozio, G. Petrone, G. Spagnuolo, and M. Vitelli, "Optimized One-Cycle Control in Photovoltaic Grid Connected Applications," IEEE Transactions on Aerospace and Electronic Systems, vol. 42, no. 3, pp. 954–972, 2006.

[8] K. S. Tey and S. Mekhilef, "Modified Incremental Conductance Algorithm for Photovoltaic System Under Partial Shading Conditions and Load Variation", IEEE Transactions on Industrial Electronics, vol. 61, no. 10, pp. 5384–5392, 2014.

[9] G. Yu, Y. Jung, J. Choi, and G. Kim, "A Novel Two-Mode MPPT Control Algorithm Based on Comparative Study of Existing Algorithms," Solar Energy, vol. 76, no. 4, pp. 455–463, 2004.

[10] T. Noguchi, S. Togashi, and R. Nakamoto, "Short-Current Pulse-Based Maximum-Power-Point Tracking Method for Multiple Photovoltaic and Converter Module System", IEEE Transactions on Industrial Electronics, vol. 49, no. 1, pp. 217–223, 2002.

[11] R. B. Roy, E. Basher, R. Yasmin, and M. Rokonuzzaman, "Fuzzy Logic Based MPPT Approach in A Grid Connected Photovoltaic System", in 8th International Conference

on Software, Knowledge, Information Management and Applications (SKIMA 2014). IEEE, 2014, pp. 1–6.

[12] T. L. Kottas, Y. S. Boutalis, and A. D. Karlis, "New Maximum Power Point Tracker for PV Arrays Using Fuzzy Controller in Close Cooperation with Fuzzy Cognitive Networks", IEEE Transactions on Energy conversion, vol. 21, no. 3, pp. 793–803, 2006.

[13] M. Lin, C. M. Hong, and C.-H. Chen, "Neural-Network-Based MPPT Control of A Stand-Alone Hybrid Power Generation System," IEEE Transactions on Power Electronics, vol. 26, no. 12, pp. 3571–3581, 2011.

[14] A. N. A. Ali, M. H. Saied, M. Mostafa and T. Abdel-Moneim, "A Survey of Maximum PPT Techniques of PV Systems" in IEEE Energytech, 2012.

[15] T. Esram, P. L. Chapman et al., "Comparison of Photovoltaic Array Maximum Power Point Tracking Techniques", IEEE Transactions on Energy Conversion EC, vol. 22, no. 2, p. 439, 2007.

[16] B. Subudhi and R. Pradhan, "A Comparative Study on Maximum Power Point Tracking Techniques for Photovoltaic Power Systems," IEEE transactions on Sustainable Energy, vol. 4, no. 1, pp. 89–98, 2013.

[17] B. Scrosati, "Power Sources for Portable Electronics and Hybrid Cars: Lithium Batteries and Fuel Cells", The Chemical Record, vol. 5, no. 5. Pp. 286-297, 2005.

[18] B. Kennedy, D. Patterson and S. Camilleri, "Use of Lithium-Ion Batteries in Electric Vehicles", *J. Power Sources*, vol. 90, pp. 156-162, 2000.

[19] T. Horiba, K. Hironaka, T. Matsumura, T. Kai, M. Koseki, and Y. Muranaka, "Manganese Type Lithium Ion Battery for Pure and Hybrid Electric Vehicles", *J. Power Sources*, vol. 97-98, pp. 719-721, 2001.

[20] Min Chen and Gabriel A. Rincón-Mora, "Accurate Electrical Battery Model Capable of Predicting Runtime and I-V Performance", *IEEE Transactions on Energy Conversion*, vol. 21, no.2, June 2006.

[21] M. Boxwell, "*Solar electricity handbook: a simple, practical guide to solar energy: how to design and install photovoltaic solar electric systems.*" Greenstream Publishing, 2012.

[22] Mann Kin (Eddie) Lee, *Implementation of Photovoltaic Maximum Power Tracking using a Microcontroller*, Ph. D. Thesis, Curtin University of Technology, Curtin, September 2004.

[23] Md. Saifur Rahman, S Shanawaz Ahmed, S.I. Khan et al., "Solar Home System", German Technical Cooperation (GIZ), March 2013.

[24] P. Fran, *Report on Power Electronics, DC/DC Buck Converter*, University of Massachusetts, USA, Oct. 2007.

[25] Mann Kin Lee, *Implementation of Photovoltaic Maximum Power Point Tracking using a Micro controller*, Bachelor, Curtin University of Technology, 2004.

[26] J. R. Fisher and Carla Beaudet, "Functional Description of PIC 16F877A Function and Interfaced to GBT RFI Monitor Station Electronics Division Technical Note No 208", 2005.

[27] M. Berrera, A. Dolara, R. Faranda, and S. Leva, "Experimental test of seven widely-adopted MPPT algorithm," IEEE Bucharest Power Tech Conference 2009, pp. 1 - 8.

[28] Steve Harrington and James Dunlop. "Battery charge controller characteristics in photovoltaic systems." *IEEE Aerospace and Electronic Systems Magazine* 7.8 (1992): 15-21.

[29] Report IEA PVPS T3-05:1998: "Recommended Practices for Charge Controllers"; August, 1998.

[30] O. Wasynczuk, "Dynamic behavior of a class of photovoltaic power systems," *IEEE Trans. Power App. Syst.*, vol. 102, no. 9, pp. 3031–3037, Sep. 1983.

[31] Brigitte Hauke, "Basic calculation of a buck converter's power stage." *Texas Instruments, Dallas, Texas, Tech. Rep. SLVA477,* 2011.

[32] Muhammad H. Rashid. *Power electronics handbook: devices, circuits and applications*. Academic press, 2010.

[33] Amber Scheurer, et al. "Photovoltaic MPPT charge controller." *Mentor Alan Shaffer Lakeland Electric, Sponsored by Workforce Central Florida, Spring* 2012.

[34] SparkFun Hall-Effect Current Sensor Breakout - ACS712. Accessed on: 10 November 2016, Retrieved from https://www.sparkfun.com/products/8882

**// LCD module connections**

sbit LCD_RS at RD2_bit;
sbit LCD_EN at RD3_bit;
sbit LCD_D4 at RD4_bit;
sbit LCD_D5 at RD5_bit;
sbit LCD_D6 at RD6_bit;
sbit LCD_D7 at RD7_bit;
sbit LCD_RS_Direction at TRISD2_bit;
sbit LCD_EN_Direction at TRISD3_bit;
sbit LCD_D4_Direction at TRISD4_bit;
sbit LCD_D5_Direction at TRISD5_bit;
sbit LCD_D6_Direction at TRISD6_bit;
sbit LCD_D7_Direction at TRISD7_bit;

// End of LCD module connections

```
void Lcd_COut(char row, char col, const char *cptr)
{
  char chr = 0;                              //1st, it is used as empty string
  Lcd_Out(row, col, &chr);                   //set position.
  for ( ; chr = *cptr ; ++cptr ) Lcd_Chr_CP(chr);   //out in loop
  asm CLRWDT;
}
void UART_Write_CText(const char *cptr)
{
   char chr;
   for ( ; chr = *cptr ; ++cptr ) UART1_Write(chr);
}
const char character6[] = {0,29,21,21,21,21,23,0};
const char character5[] = {31,21,21,27,27,21,21,31};
const char character4[] = {14,17,17,17,17,17,17,31};
const char character3[] = {14,17,17,17,17,17,31,31};
const char character2[] = {14,17,17,17,17,31,31,31};
const char character1[] = {14,17,17,31,31,31,31,31};
const char character[] = {14,31,31,31,31,31,31,31};
void CustomChar(char pos_row, char pos_char,char num)
{
   char i;
   switch(num)
   {
    Case 0:
       {
          Lcd_Cmd(64);
```

```
        for (i = 0; i<=7; i++)Lcd_Chr_CP(character[i]);
        Lcd_Cmd(_LCD_RETURN_HOME);
        Lcd_Chr(pos_row, pos_char, num);
      }
Case 1:
    {
      Lcd_Cmd(72);
      for (i = 0; i<=7; i++)Lcd_Chr_CP(character1[i]);
      Lcd_Cmd(_LCD_RETURN_HOME);
      Lcd_Chr(pos_row, pos_char, num);
    }
Case 2:
    {
      Lcd_Cmd(80);
      for (i = 0; i<=7; i++)Lcd_Chr_CP(character2[i]);
      Lcd_Cmd(_LCD_RETURN_HOME);
      Lcd_Chr(pos_row, pos_char, num);
    }
Case 3:
    {
      Lcd_Cmd(88);
      for (i = 0; i<=7; i++)Lcd_Chr_CP(character3[i]);
      Lcd_Cmd(_LCD_RETURN_HOME);
      Lcd_Chr(pos_row, pos_char, num);
    }
Case 4:
    {
      Lcd_Cmd(96);
      for (i = 0; i<=7; i++)Lcd_Chr_CP(character4[i]);
      Lcd_Cmd(_LCD_RETURN_HOME);
      Lcd_Chr(pos_row, pos_char, num);
    }
Case 5:
    {
      Lcd_Cmd(104);
      for (i = 0; i<=7; i++)Lcd_Chr_CP(character5[i]);
      Lcd_Cmd(_LCD_RETURN_HOME);
      Lcd_Chr(pos_row, pos_char, num);
    }
Case 6:
    {
      Lcd_Cmd(112);
      for (i = 0; i<=7; i++)Lcd_Chr_CP(character6[i]);
      Lcd_Cmd(_LCD_RETURN_HOME);
      Lcd_Chr(pos_row, pos_char, num);
    }
```

```
    }
}
void Background()
{
  Lcd_COut(1,7,"|");Lcd_COut(2,7,"|");Lcd_COut(3,7,"|");Lcd_COut(4,7,"|");
  Lcd_COut(1,14,"|");Lcd_COut(2,14,"|");Lcd_COut(3,14,"|");Lcd_COut(4,14,"|");
  Lcd_COut(1,1,"SOL"); Lcd_COut(1,8,"BAT");Lcd_COut(3,15," LOAD");
 Lcd_COut(1,15," PWM");
 CustomChar(1,12,0);                                    // Battery
 CustomChar(1,5,5);                                     // Panel
 CustomChar(1,20,6);                                    // PWM
}
long adc_rd=0;
unsigned int Battery=0,Solar=0,i;
unsigned int Battery1=0,Solar1=0;
unsigned int Charging_current=0,Battery_Current=0;
unsigned int Charging_Current1=0,Battery_Current1=0;
unsigned int Solar_Power = 0,Solar_Power1=0;
unsigned int Previous_power=0,Recent_power=0;
unsigned int parcentage=0,parcentage1=0;
int duty=0,duty1=0;
int d_prcnt=0,d_prcnt1=0;
short charging_mode=0;                                  //0 = bulk by default bit load;

void Get_Battery();
void Get_Solar();
void Get_Charging_Current();
void Get_Battery_Current();
void Get_Solar_power();
void Load_Control();
void Charging_Control();

#define    load_clk   RB7_bit
#define    Clock_EN   RC1_bit
#define    Bulk_LED   RB5_bit
#define    Float_LED  RB2_bit
#define    NoChar_LED RB1_bit
#define    ON         1
#define    OFF        0
```

**//Main Function**

```c
void main()
{
 TRISA = 0xFF;                          //all input
 TRISE0_bit = 1;                        //set as input
 TRISE2_bit = 1;                        //set as input
 TRISC = 0x00;                          //all output
 TRISB = 0x00;                          //all output
 ADCON1 = 0x00;                         //all Analog ing
 Delay_ms(100);
 Lcd_Init();                            //initialize LCD
 Lcd_Cmd(_LCD_CLEAR);                   //clear display
 Lcd_Cmd(_LCD_CURSOR_OFF);              //cursor off
 Lcd_COut(1,1,"MPPT Solar Charger");
 PWM1_Init(22500);                      //initialize PWM at 22.5 KHz
 PWM1_Start();                          //start PWM
 PWM1_Set_Duty(duty);                   //duty cycle=(duty/255) X 100 %
 UART1_Init(9600);
 Delay_ms(2000);
 Lcd_Cmd(_LCD_CLEAR);                   //clear display
 Background();
 load = 1;
 OPTION_REG = 0x0F;                     //enable WDT
 while(1)
 {
   asm CLRWDT;
   Get_Battery();
   Get_Solar();
   Get_Charging_Current();
   Get_Battery_Current();
   Get_Solar_power();
   Load_Control();
   Charging_Control();

 }                                      //while(1)
}                                       //void main

void Charging_Control()
{
   char pwm_prcnt[]="000%";
   if(Solar>125)
   {
     Clock_EN = ON;                     //enable clock
     NoChar_LED = OFF;
      if(Battery>143)
```

```
        {
          charging_mode = 1;                    // go to float mode
          Float_LED = ON;
          Bulk_LED = OFF;
          UART_Write_CText("Charging mode: Float \r\n");
        }
        if(Battery<126)
        {
          charging_mode = 0;
          Float_LED = OFF;
          Bulk_LED = ON;
          UART_Write_CText("Charging mode: Bulk \r\n");
        }
        if(Solar>200)
        {
          if(duty<244)duty+=10;
        }
        else if(Solar<Battery)
        {
          if(duty>10)duty-=10;
        }
        else
        {
          Recent_power = Solar_Power;
          if(Recent_power>Previous_power)
          {
            if(duty<254)duty+=1;
            //Delay_ms(10);
          }
          else
          {
            if(duty>0)duty-=1;
            //Delay_ms(10);
          }
          Previous_power = Recent_power;
        }
      }
      else if(Solar<105)
      {
        Clock_EN = OFF;                         //Disable clock when solar not available
        NoChar_LED = ON;
        Float_LED = OFF;
        Bulk_LED = OFF;
        duty = 0;
        UART_Write_CText("Solar not available. \r\n");
      }
```

```
      PWM1_Set_Duty(duty);
      d_prcnt = duty*100/255;
      pwm_prcnt[0] = d_prcnt/100 + 48;
      pwm_prcnt[1] = (d_prcnt/10)%10 + 48;
      pwm_prcnt[2] = d_prcnt%10 + 48;
      Lcd_Out(2,16,pwm_prcnt);
      UART_Write_CText("PWM:");
      UART1_Write_Text(pwm_prcnt);
      UART_Write_CText("\r\n");
  asm CLRWDT;
  Delay_ms(2);
 }
 void Get_Battery()
 {
    char Bat[]="00.0V";
    char parcen[] = "000%";
    adc_rd = 0;                                        //clear previous data
    ADCON0 = 0x01;                                     //select channel 0
    for(i=0;i<100;i++)
    {
        adc_rd += ADC_Read(0);
        asm CLRWDT;
    }
    adc_rd/=100;
    Battery = (int)adc_rd*0.644922871516105;
    Bat[0] = Battery/100 + 48;
    Bat[1] = (Battery/10)%10 + 48;
    Bat[3] = Battery%10 + 48;
    Lcd_Out(2,8,Bat);
    UART_Write_CText("Battery:");
    UART1_Write_Text(Bat);
    UART_Write_CText("\r\n");
    asm CLRWDT;
    Delay_ms(2);
    adc_rd = 0;                                        //clear all data
    if(Solar>120)                                      //solar is available
    {
        if(Battery>116)parcentage = (Battery-116)*3.71;
        else parcentage = 0;
        if(parcentage>100)parcentage=100;
        if(parcentage<0)parcentage = 0;
    }
    else
    {
        if(Battery>116)parcentage = (Battery-116)*10;
        else parcentage = 0;
```

```c
        if(parcentage>100)parcentage=100;
        if(parcentage<0)parcentage = 0;
    }
    parcen[0] = parcentage/100 + 48;
    parcen[1] = (parcentage/10)%10 + 48;
    parcen[2] = parcentage%10 + 48;
    Lcd_Out(4,8,parcen);
        UART_Write_CText("Charge:");
        UART1_Write_Text(parcen);
        UART_Write_CText("\r\n");
    asm CLRWDT;
    Delay_ms(2);
    if(parcentage>85)CustomChar(1,12,0);                            // Battery 100%
    else if(parcentage>65 && parcentage<=85)CustomChar(1,12,1);   // Battery 75%
    else if(parcentage>35 && parcentage<=65)CustomChar(1,12,2);   // Battery 75%
    else if(parcentage>25 && parcentage<=35)CustomChar(1,12,3);   // Battery 75%
    else CustomChar(1,12,4);// Battery 75%
}
void Get_Solar()
{
    char Sol[]="00.0V";
    adc_rd = 0;                                           //clear previous data
    ADCON0 = 0x39;                                        //select channel 7
    for(i=0;i<500;i++)
    {
        adc_rd += ADC_Read(7);
        asm CLRWDT;
    }
    adc_rd/=500;
    Solar = (int)adc_rd*0.537634408602151;
    Sol[0] = Solar/100 + 48;
    Sol[1] = (Solar/10)%10 + 48;
    Sol[3] = Solar%10 + 48;
    Lcd_Out(2,1,Sol);
    UART_Write_CText("Panel:");
    UART1_Write_Text(Sol);
    UART_Write_CText("\r\n");
    asm CLRWDT;
    adc_rd = 0;                                           //clear all data
}
void Get_Charging_Current()
{
    char Ccurr[]="0.00A";
    unsigned int crnt1=0;
    int k=0;
    adc_rd = 0;                                           //clear previous data
```

```
    ADCON0 = 0x29;                              //select channel 5
    for(k=0;k<80;k++)
    {
        for(i=0;i<50;i++)
        {
            adc_rd += ADC_Read(5);
            asm CLRWDT;
        }
        adc_rd/=50;
        crnt1 = adc_rd*4.78515625;              //convert into mV
        Charging_current += abs(crnt1-2500)/0.66;   //convert into A
    }
    Charging_current/=80;                       //get average value again
    UART_Write_CText("Solar Inpur Current:");
    if(crnt1>2500)
    {
        Lcd_COut(3,1,"-");
        UART_Write_CText("-");
    }
    else if(crnt1<2500)
    {
        Lcd_COut(3,1,"+");
        UART_Write_CText("+");
    }
    else Lcd_COut(3,1," ");
    Ccurr[0] = Charging_current/100 + 48;
    Ccurr[2] = (Charging_current/10)%10 + 48;
    Ccurr[3] = (Charging_current)%10 + 48;
    Lcd_Out(3,2,Ccurr);
    UART1_Write_Text(Ccurr);
    UART_Write_CText("\r\n");
    asm CLRWDT;
    Delay_ms(2);
    adc_rd = 0;                                 //clear all data
}
void Get_Battery_Current()
{
    char Bcurr[]="0.00A";
    unsigned int crnt2=0;
    int b;
    adc_rd = 0;                                 //clear previous data
    ADCON0 = 0x21;                              //select channel 4
    for(b=0;b<80;b++)
    {
        for(i=0;i<50;i++)
        {
```

```c
        adc_rd += ADC_Read(4);
        asm CLRWDT;
      }
      adc_rd/=50;
      crnt2 = adc_rd*4.78515625;                    //convert into mV
      Battery_Current += abs(crnt2-2500)/0.66;      //convert into A
  }
  Battery_Current/=80;                              //get average value
  UART_Write_CText("Output current:");
  if(crnt2>2500)
  {
    Lcd_COut(3,8,"-");
    UART_Write_CText("-");
  }
  else if(crnt2<2500)
  {
    Lcd_COut(3,8,"+");
    UART_Write_CText("+");
  }
  else Lcd_COut(3,8," ");
  Bcurr[0] = Battery_Current/100 + 48;
  Bcurr[2] = (Battery_Current/10)%10 + 48;
  Bcurr[3] = (Battery_Current)%10 + 48;
  Lcd_Out(3,9,Bcurr);
  UART1_Write_Text(Bcurr);
  UART_Write_CText("\r\n");
  asm CLRWDT;
  Delay_ms(2);
  adc_rd = 0;                                       //clear all data
}
void Get_Solar_power()
{
  char slpwr[]= "000.0W";
  Solar_Power = Solar*Charging_current/100;
  slpwr[0] = Solar_Power/1000 + 48;
  slpwr[1] = (Solar_Power/100)%10 + 48;
  slpwr[2] = (Solar_Power/10)%10 + 48;
  slpwr[4] = (Solar_Power)%10 + 48;
  Lcd_Out(4,1,slpwr);
  UART_Write_CText("Solar Power:");
  UART1_Write_Text(slpwr);
  UART_Write_CText("\r\n");
  asm CLRWDT;
  Delay_ms(2);
}
void Load_Control()
```

```
{
  if(Battery>126)load=1;                                    //battery is over 12.6V
  if(Battery<116)load = 0;



// Load Control

  if(load)
  {
    load_clk = ON;
    Lcd_COut(4,15," ON ");
    UART_Write_CText("Load ON");
    UART_Write_CText("\r\n");
  }
  else
  {
    load_clk = OFF;
    Lcd_COut(4,15," OFF");
    UART_Write_CText("Load OFF");
    UART_Write_CText("\r\n");
  }
  UART_Write_CText("\r\n");
  UART_Write_CText("\r\n");
  UART_Write_CText("\r\n");
}
//End
```